ERDC/GSL TR-02-12

Geotechnical and Structures Laboratory

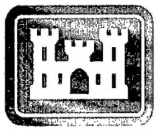

US Army Corps
of Engineers®
Engineer Research and
Development Center

Rapid Strengthening of Full-Sized Concrete Beams with Powder-Actuated Fastening Systems and Fiber-Reinforced Polymer (FRP) Composite Materials

Lawrence C. Bank, David T. Borowicz,
Anthony J. Lamanna, James C. Ray,
and Gerardo I. Velázquez

July 2002

The contents of this report are not to be used for advertising, publication, or promotional purposes. Citation of trade names does not constitute an official endorsement or approval of the use of such commercial products.

The findings of this report are not to be construed as an official Department of the Army position, unless so designated by other authorized documents.

PRINTED ON RECYCLED PAPER

ERDC/GSL TR-02-12
July 2002

Rapid Strengthening of Full-Sized Concrete Beams with Powder-Actuated Fastening Systems and Fiber-Reinforced Polymer (FRP) Composite Materials

by Lawrence C. Bank, David T. Borowicz, Anthony J. Lamanna

Department of Civil and Environmental Engineering
University of Wisconsin-Madison
Madison, WI 53706

James C. Ray, Gerardo I. Velázquez
Geotechnical and Structures Laboratory
U.S. Army Engineer Research and Development Center
3909 Halls Ferry Road
Vicksburg, MS 39180-6199

Final report

Prepared for U.S. Army Corps of Engineers
Washington, DC 20314-1000

Contents

List of Figures

List of Tables

Preface

This study was conducted by personnel of the Department of Civil and Environmental Engineering, University of Wisconsin-Madison, under contract No. DACA42-00-P-0364, and the U.S. Army Engineer Research and Development Center (ERDC), Geotechnical and Structures Laboratory (GSL), Vicksburg, MS. The study was part of the Department of the Army Project No. 4A162784AT40, Work Package 1259B, "Bridge Assessment and Repair," Work Unit BR002, "Rapid Bridge Repair and Retrofit," which is sponsored by Headquarters, U.S. Army Corps of Engineers.

The experimental work was accomplished in GSL during December through November 2001 under the general supervision of Dr. Michael J. O'Connor, Director, Dr. David W. Pittman, Deputy Director, Dr. Robert L. Hall, Chief, Geosciences and Structures Division (GSD), and Mr. James S. Shore, Chief, Structural Engineering Branch (StEB). Messrs. James C. Ray and Gerardo I. Velázquez, StEB, were the project investigators for this effort. Professor Lawrence C. Bank was the Principal Investigator, and Mr. Anthony Lamanna and U.S. Army CPT David Borowicz were research assistants for the University of Wisconsin. The authors were assisted in the construction and testing phase by Mr. Jesse B. Blalack, Ms. Laura R. Hyde, and Messrs. Michael W. Keene, GSD; Cliff R. Gill, Brian H. Green, and Dan E. Wilson, Engineering Systems & Materials Division; Messrs. Jerome Carter and Leroy Peeples, Instrumentation Systems Development Division, Information Technology Laboratory; and Messrs. Gerald Black, Donald Harris, Michael B. Sims, James C. Stephens, George Walls, Directorate of Public Works. Ms. Corine E. Pugh, Graphics Specialist, DynTel Corporation, also assisted the authors in the preparation of this report.

At the time of publication of this report, Dr. James R. Houston was Director of ERDC, and COL John W. Morris III, EN, was Commander and Executive Director.

Conversion Factors, Non-SI to SI Units of Measurement

Non-SI units of measurement used in this report can be converted to SI units as follows:

Multiply	By	To Obtain
cubic feet	0.028317	cubic meters
degrees Fahrenheit	(f-32)/1.8	degrees Celsius
feet	0.304800	meters
grams	0.001	kilograms
gallons	0.00378	cubic meters
inches	0.025400	meters
inches	25.4	millimeters
miles (U.S. statute)	1.609	kilometers
ounces (U.S. fluid)	0.00002957	cubic meters
pint	0.00004731	cubic meters
pounds (force) per square inch	0.006894757	megapascals
pounds per cubic foot	16.0	kilograms per cubic meter
square inches	0.000645	square meters

1 Introduction

Over the past decade, industry has utilized lightweight, non-metallic fiber reinforced composite materials to repair and strengthen concrete structures. Current fastening techniques require the use of two-part epoxies to adhere composite strips to concrete surfaces (Emmons et al. 1998). This method is labor-intensive, time consuming, and quite dependent on environmental factors to include ambient temperature and relative humidity.

This research study continues to investigate an attachment procedure that utilizes powder actuated fastening systems to attach composite materials to concrete members (Bank et al. 2000; Ray et al. 2001a). This repair method is rapid, utilizes readily available materials, and requires minimal training (Lamanna et al. 2001a). Further, the installation procedure is not sensitive to environmental factors; personnel can utilize the procedure in any climate or condition. To be sure, this method is suited for military applications and can meet the Army's need for a versatile and dependable repair package.

The first year of the research study focused on analytical models of the system, materials testing, and small-scale modeling (Bank and Lamanna 1999). Year two activities included small scale testing of retrofitted (composite strip attached with powder actuated fasteners) beams and comparison to epoxy-bonded specimens (Bank et al. 2000; Ray et al. 2001b). Overall, the results from the first two years of research indicated that the powder-actuated procedure was viable and should be tested on full-scale members (Lamanna et al. 2001b).

Year three studies discussed herein apply the powder actuated fastening process to full-scale concrete beams of varying steel reinforcement and investigate their performance under increasing load. The T-beam pictured in Figure 1 was chosen as the large-scale test specimen: (Full construction drawings are provided in Appendix A.) This T-beam is representative of those used on highway bridges around the United States.

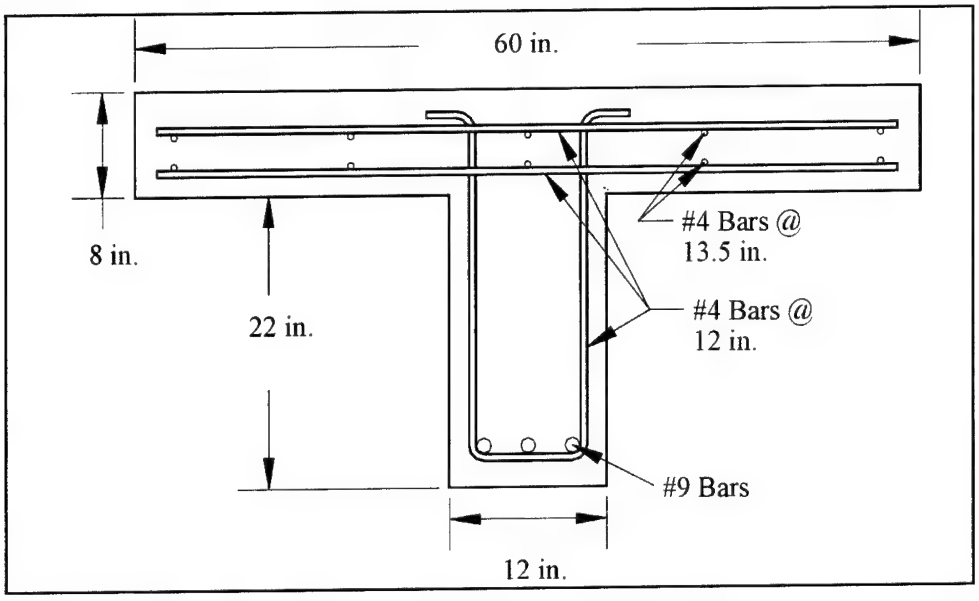

Figure 1. Example construction drawing (A table of contents for converting non-SI units of measurement to SI units is presented on page xi.)

2 Technical Objective and Scope

The objective of this research study was to test the powder actuated fastening system on large-scale concrete beams (representative of typical bridge components) to determine its viability for military applications. The report is focused on the design, construction, testing, and analysis of results of an experimental investigation of full-size bridge T-beams strengthened with composite strips and powder-actuated fasteners.

The scope of work for the research reported is as follows:

a. *Design a Test Plan for Full-Sized Beams.* This plan included not only testing the beams, but also developing an application procedure for the strengthening method. The test plan focused on loading the beams in displacement control to their ultimate capacity and recording modes of failure.

b. *Test Full-Sized Beams.* Testing was carried out at the U.S. Army Corps of Engineers Research and Development Center in Vicksburg, Mississippi. The beams were tested in four-point bending utilizing two 110 kip actuators. Data acquired included actuator load, actuator stroke, beam displacement (via LVDT), and strains in both the composite strip and concrete.

c. *Analyze Results of Full-Sized Beam Tests.* Analysis of the data recorded during testing consisted of comparing the strengthened beams to the control (unstrengthened) beams. Moment capacity, strain in the composite strip, strain in the concrete, and midspan deflection were the key data sets used to determine the effectiveness of the strengthening system.

d. *Conduct Parametric Studies of Different Models.* Analytical models, to include moment-curvature and moment-deflection, were investigated and compared to experimental results. A moment-deflection model was automated to determine if accurately predicted the behavior of the large-scale beams.

e. *Conduct Small-Scale Tests to Investigate Failure Modes Seen in Large-Scale Beam Tests.* Ten small-scale beams were constructed to continue

testing the strengthening method. Termination lengths, short shear spans, and cyclic loading were all tested in an effort to determine their effects on the strengthening method.

3 Materials Used in T-Beams

Concrete

The ERDC construction personnel used a nominal 2500 psi mix (Mix ID V-2610251) supplied by a local vendor for the construction of the nine T-beams. The mix design, based on 1 cu yd of concrete, is shown in Table 1.

Table 1. Concrete Mix Design

Component	Quantity Per Cubic Yard
ASTM Type I Cement	352 lb
ASTM Class C Fly Ash	88 lb
Natural Fine Aggregate	1,415 lb (SSD)
ASTM No. 57 Natural Course Aggregate	1,797 lb (SSD)
Water	217 lb
Air Entrainment Agent	1 fluid oz
Water Reducing Agent	13 fluid oz
HRWR Agent	1 – 3.7 lb per yd

The large aggregate was chert, a very hard river-washed stone, and had a maximum size of 2 in. The slump of the mix was 1 to 3 in., and cylinder tests revealed the compressive strengths listed in Table 2.

Table 2. Concrete Compressive Strengths

Beam Number	28-Day Strength (psi)	Age at Testing (days)	Strength at Testing (psi)
Beam A3_Control	4,643	44	5,133
Beam A3_Test1	4,297	48	4,913
Beam A3_Test2	4,757	41	4,920
Beam A5_Control	4,343	54	5,213
Beam A5_Test1	4,823	58	5,827
Beam A5_Test2	4,290	61	5,227
Beam A8_Control	4,060	43	4,650
Beam A8_Test1	4,577	49	5,323
Beam A8_Test2	4,970	51	5,720
Average	4,335	50	5,214

Steel Reinforcing

Beams were designed in accordance with ACI 318-99, but steel reinforcement ratios were varied to see how the differences impacted the effectiveness of the strengthening method. Full construction details are provided in Appendix A, while Table 3 is a summary of the reinforcement details.

Table 3. Steel Reinforcement Details

Beam Type	Type Reinforcement	Size Rebar	Area of Steel ($in.^2$)	A_s/A_{bal}	Yield Strength of Steel (ksi)
A3 Family	Tension	3 No. 9's	3.00	0.38	60
A5 Family	Tension	5 No. 9's	5.00	0.55	60
A8 Family	Tension	8 No. 9's	8.00	0.81	60
All	Compression	10 No. 4's	5.00	NA	60
All	Shear	No. 4 open stirrups @ 12 in. OC	NA	NA	60

Composite Strengthening Strips

Both the Year 1 and Year 2 reports describe the composite material in detail (Bank and Lamanna 1999, 2000). The strip is a glass and carbon hybrid pultruded strip with a vinylester resin. The strip properties were determined through tensile testing of the composite. Table 4 lists the results of the tensile testing. The ultimate strength is the material stress at rupture of a 1-in.-wide by 10-in.-long coupon. Open-hole strength is the stress at rupture of the same coupon with a 3/16-in. hole drilled in the center.

Table 4. Composite Material Properties

Type Strength	No. of Tests	Average Failure Strength (ksi)	Standard Deviation (ksi)	Coeff of Variance (%)	Modulus of Elasticity (ksi)	Standard Deviation (ksi)	Coeff of Variance (%)
Ultimate	10	107.80	12.70	11.80	8,200	700	8.70
Open-Hole	10	5.00	6.20	6.50	8,200	600	7.80

From the data in Table 4, one can calculate the maximum possible strain in the strip. Using the open-hole strength and the material constitutive relations, the failure strain is 0.0116 or 1.16 percent. Based on the net strength, the failure strain is predicted to be 0.0131 or 1.31 percent.

Fasteners

The Hilti DX A41 Powder Actuated Fastening system was used to attach the composite strips to the concrete T-beams (Hilti 2001). The A41 system utilizes a small powder charge to "fire" fasteners into the desired media. The purple number six, or extra heavy, charge was used in conjunction with X-AL-H fasteners during the attachment procedure. Hilti produces the X-AL-H fasteners with heat-treated high-strength steel for difficult applications. These fasteners are also corrosion resistant due to their zinc plating. An 18 mm (0.7 in.) steel washer with a neoprene backing was used in conjunction with the steel fasteners. These washers provided clamping pressure and prevented the fastener head from penetrating and damaging the composite strip. Table 5 summarizes all of the pertinent fastener data used in the T-beam tests.

Table 5. Fastener Properties

Nomenclature	Intended Use	Length, in.	Shank Diameter, in.
X-ALH 47	High Strength Concrete & High Grade Steel	1.83	0.175
X-ALH 52	High Strength Concrete & High Grade Steel	2.02	0.175

4 Fabrication of T-Beams

The test plan called for beams of varying reinforcement ratios with dimensions representative of those found in bridge construction within the continental United States. The area of tensile steel (A_s) in the three sets of beams was based on these typical designs.

The ERDC fabricated the test specimens utilizing in-house expertise and labor. All told, ERDC personnel used 52 cu yd of concrete to construct nine beams (three beams of each reinforcement ratio) for testing. Table 6 is a summary of the nine beams, their characteristics, and their intended purpose for testing.

Table 6. Specimen Details

Beam Name	A_s/A_{bal}	Specimen Purpose
A3_Control	0.38	Determine Flexural Capacity of Unstrengthened Beam
A3_Test1	0.38	Test Attachment Method and Determine Flexural Capacity of Beam Strengthened with One Strip
A3_Test2	0.38	Test Attachment Method and Determine Flexural Capacity of Beam Strengthened with Two Strips
A5_Control	0.55	Determine Flexural Capacity of Unstrengthened Beam
A5_Test1	0.55	Test Attachment Method and Determine Flexural Capacity of Beam Strengthened with One Strip
A5_Test2	0.55	Test Attachment Method and Determine Flexural Capacity of Beam Strengthened with Two Strips
A8_Control	0.81	Determine Flexural Capacity of Unstrengthened Beam
A8_Test1	0.81	Test Attachment Method and Determine Flexural Capacity of Beam Strengthened with One Strip
A8_Test2	0.81	Test Attachment Method and Determine Flexural Capacity of Beam Strengthened with Two Strips

Formwork

Technicians used 3/4 in. plywood and 2 in. x 4 in. lumber to create three forms for the large scale T-beams (Figure 2). They utilized modular construction and wood screws at all the joints to facilitate the reuse of the formwork. As such, the same forms were used on all three sets (nine beams total) of test specimens.

Figure 2. Formwork for test beams

Reinforcing Bar Cages

In order to allow for ample workspace, technicians built the reinforcing bar cages outside of the forms. They began the fabrication process by laying out the bottom layer of tension steel across a pair of sawhorses.

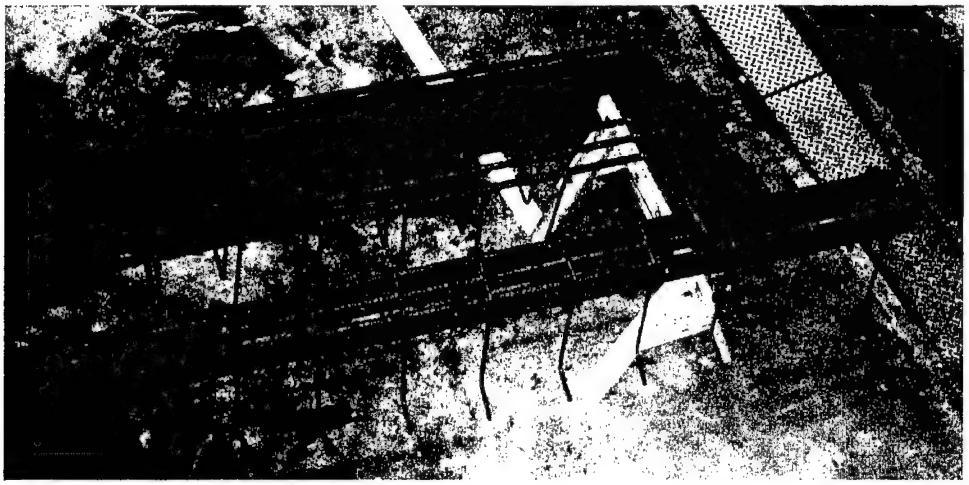

Figure 3. Fabricating the reinforcing bar cages

From there, they tied on both vertical stirrups and additional tension reinforcement at the required intervals with 10-gauge tie wire (Figure 3). The result was an upside down (tension steel on top) steel cage that was sturdy and met all construction specifications. Technicians then flipped the cages with an overhead crane and positioned them into their respective forms as shown in Figure 4. Technicians utilized 2-in. chairs (continuous high chair upper) along the bottom of the forms to maintain the required cover over the tension steel (Figure 5). These chairs, triangular in shape, were 2 ft in length and located at

both ends and at midspan of the beam. Once the cages were in the forms, technicians completed the steel reinforcement by securing the compression steel (flange reinforcement) to the vertical stirrups.

Figure 4. Reinforcing bar cages inside formwork

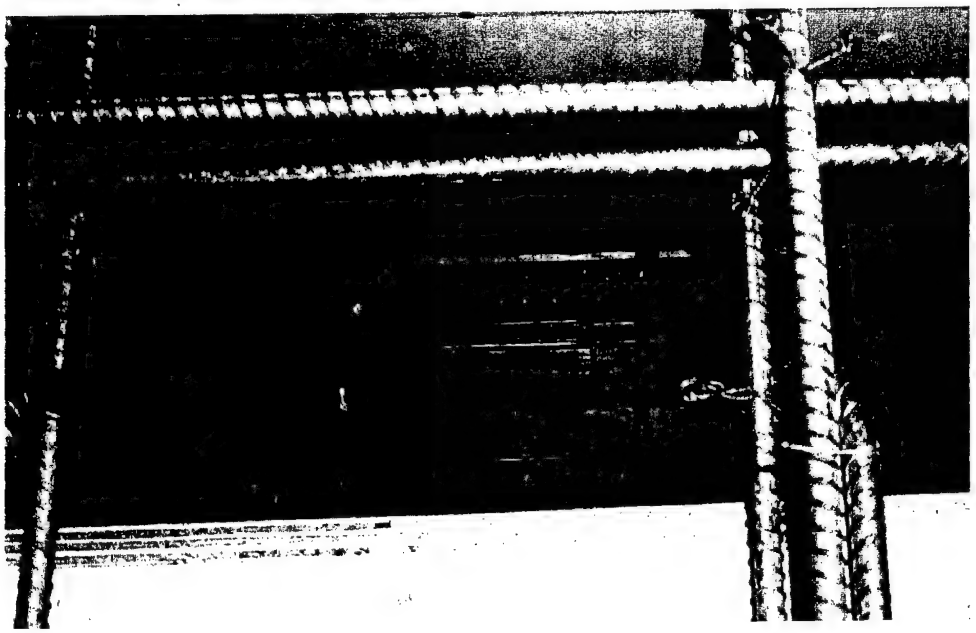

Figure 5. First set of T-beams ready for concrete reinforcing bar cage resting on 2 in. continuous high chair upper

Placing Concrete

It took 5.5 cu yd of concrete to construct each beam. Technicians tested the material properties of the batch when it arrived on site from a commercial vendor. Once they determined the mix to be satisfactory, technicians utilized the overhead crane and bucket to place the concrete into the forms (Figures 6 and 7). They consolidated the concrete via an electric concrete vibrator and finished the beams with a float. Technicians removed the forms after the beams cured for seven days, repositioned the forms, and prepared to place another set of beams.

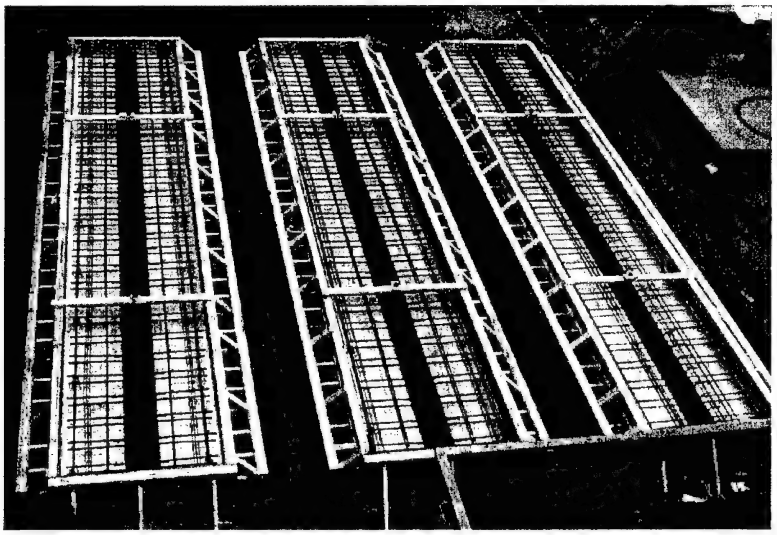

Figure 6. First set of T-beams ready for concrete

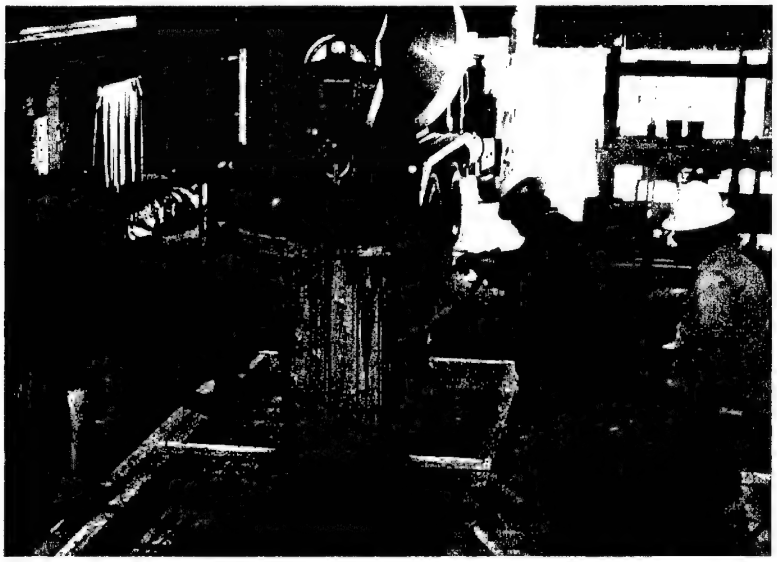

Figure 7. ERDC personnel placing concrete

5 Attachment of FRP Composite

Once support personnel moved the beams into the testing bay (Figure 8) and placed the large-scale beam into position upon its simple supports, the composite strip was then attached to the bottom of the beam. This was significant in that it marked the first time a strip was attached from underneath a beam. Previously, the beam was "flipped" upside down to provide a stable work area and ease attachment. While the T-beams were not under live load, they were supporting their self-weight (dead load) and producing tension in the bottom of the beam's web.

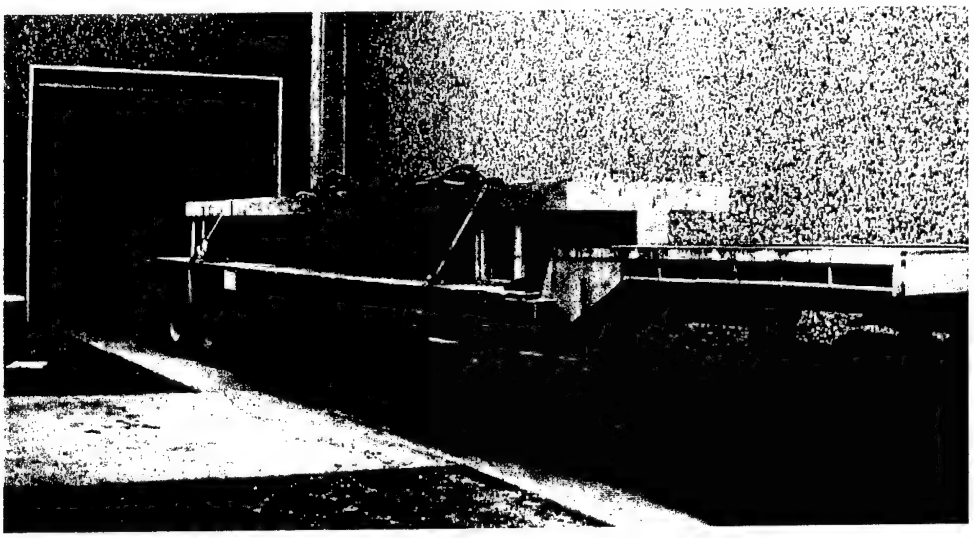

Figure 8. Moving specimen into the testing bay

Attachment Procedure

a. *Measure and mark composite strip.* The desired fastener spacing for the study was 2 in. As such, tape measures and indelible markers were used to lay out the grid over the 28-ft long by 4-in. wide by 0.125-in. thick strip pictured in Figure 9.

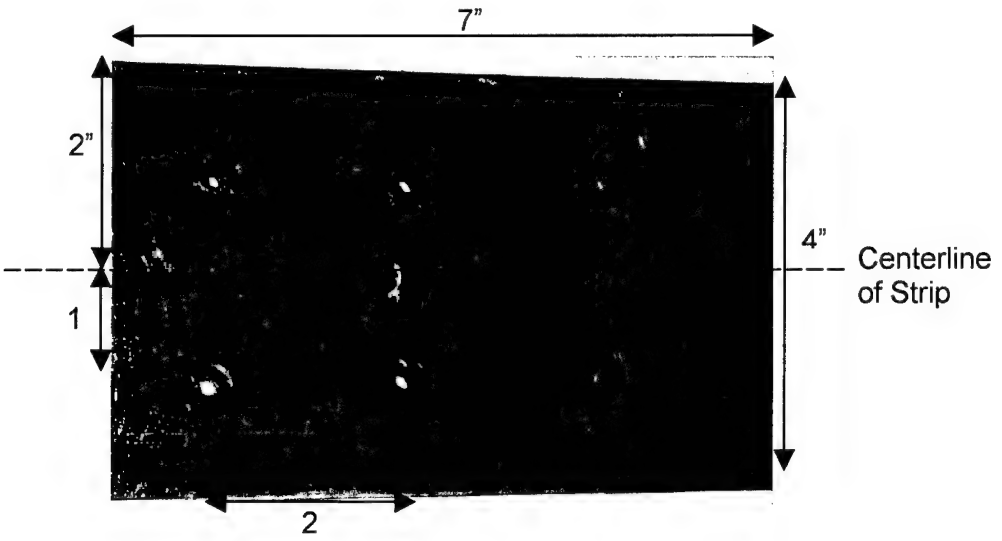

Figure 9. Grid spacing

b. Suspend Strip along Beam. The strip was suspended along the underside of the beam with large carpenter's clamps (Figure 10). The clamps allowed the positioning of the strip near the desired edge distances and individuals hands were free to work.

c. Position Strip on Beam. Working from midspan of the beam towards one support, the strip was adjusted to its proper position (centered across beam width leaving 4 in. edge distance) and secured to the beam by tightening the clamps and bolstering with duct tape. Upon finishing one side, the remaining strip was adjusted to its proper position from midspan and worked toward the remaining support.

d. Secure Strip at Midspan. A rotary hammer drill was used with 3/16-in. masonry drill bit to drill four holes through the composite strip at marked locations nearest the strip midspan. The holes extended through the 1/8-in. strip and 1/2 in. into the concrete beam. After drilling, the powder actuated fastening system was used with appropriate charges and fasteners to attach the strip at the predrilled locations (four holes closest to strip centerline). The drilling and fastening procedure is shown in Figures 10 and 11.

Figure 10. Predrilling the composite strip and concrete member

Figure 11. Fastening the composite strip using powder actuated fasteners

e. *Fasten Strip.* Working from the midspan towards one support, a set of four holes were alternately drilled and fastened (drill four, fasten at those four holes) until one half of the strip was secure. A similar process was applied to the remaining half of the support. In total, it took five man-hours to attach a strip with 318 fasteners. Figure 12 shows an example of the strip fastened to the beam.

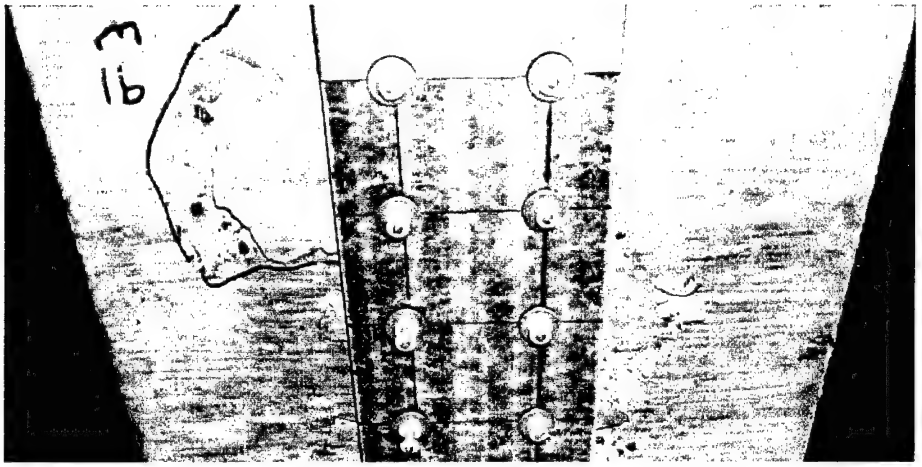

Figure 12. Composite strip positioned on the beam

When using a double strip, the procedure was slightly adjusted. First, a double strip was created by placing the two strips together, lining up all four edges, and securing the two strips to each other every 24 in. with a 2 in. piece of duct tape. Also, the double strip was predrilled prior to suspending and positioning. Taking such action allowed them to ensure that the holes were accurate and perpendicular to the face of the strip. Figure 13 shows the predrilled double strip.

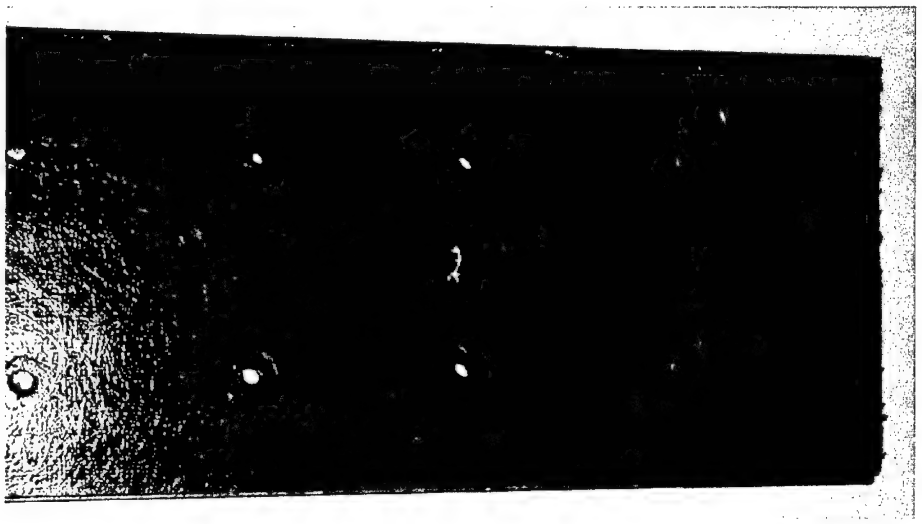

Figure 13. Predrilled double strip

Spalling of Concrete

During the attachment procedure, significant spalling was encountered despite predrilling of both the composite strip and the concrete beam. As the fasteners were "shot" into the concrete, cracks formed and chunks of concrete broke away from the surrounding area. Figure 14 shows an example of typical spalling.

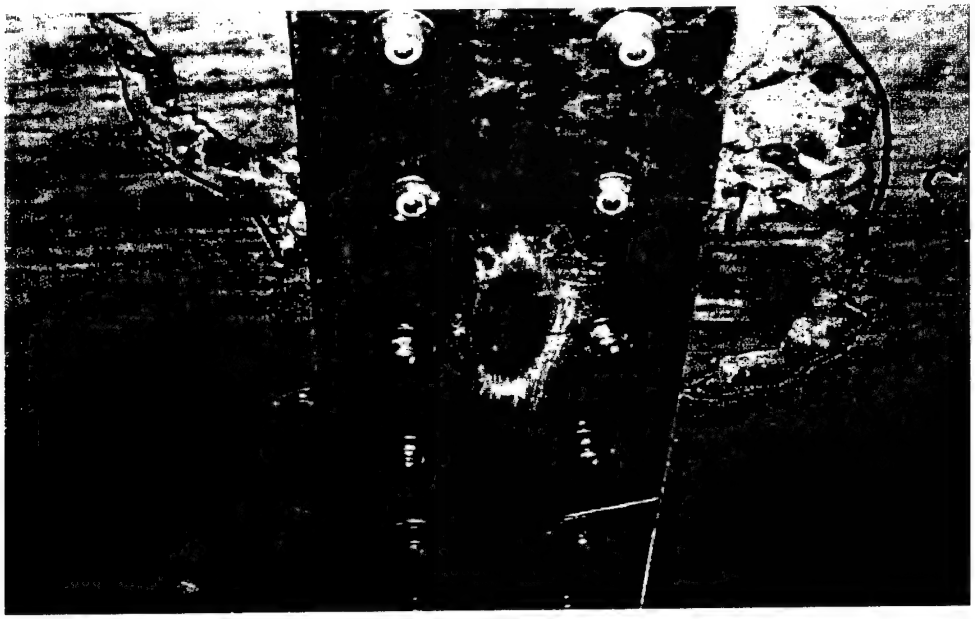

Figure 14. Typical concrete spalling created while attaching composite strip

In addition to typical spalling, local spalling was encountered while attaching the composite strip. This local spalling occurred under one of the three following conditions:

a. *Fastener Struck Reinforcing Bar Chair.* Construction personnel used 2-in. bolster beam type chairs to maintain proper concrete cover for the reinforcing bar cages. When a fastener struck one of the chairs, the fastener would either stop and not fully penetrate the member or bend into a "J" and angle away from the chair. This condition resulted in the formation of deeper cracks and caused the concrete surrounding the fastener to break into chunks (up to 2 in. in length) and fall away from the beam. Figure 15 shows the spalling created after striking a chair with a powder-actuated fastener. Note that the fasteners are not flush with the concrete (penetration stopped) and the concrete has broken away from the area that borders the strip.

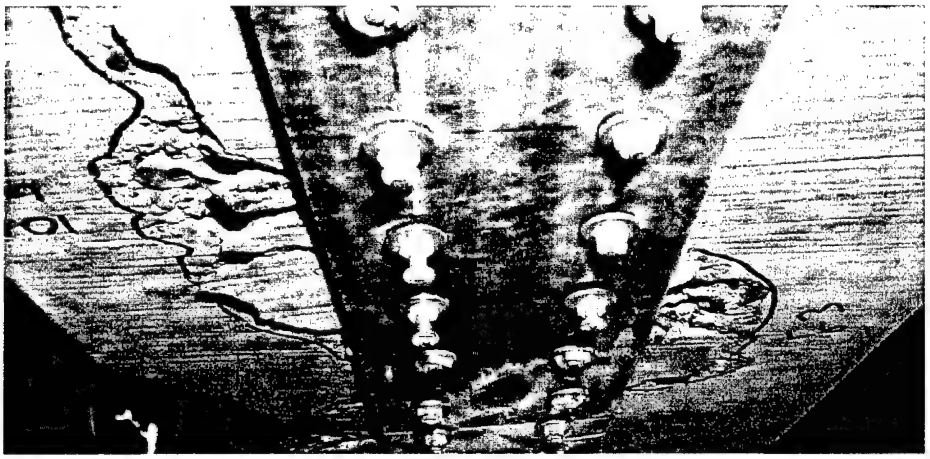

Figure 15. Spalling created after striking a chair

b. *Fastener Encountered a Large Aggregate.* Large aggregates stopped the fastener from penetrating fully and produced spalling identical to the spalling seen when a fastener struck a reinforcing bar chair. It should be noted that attempting to "redrive" (applying a second charge) to a fastener that is not flush with the strip is not recommended. Doing so will damage the fastener, the washer, and quite possibly the composite strip, so leave the fastener protruding from the concrete.

c. *Fastener Driven into a Pocket of Poor Consolidation.* When a fastener penetrated an area of poor consolidation, the surrounding concrete would turn to powder and leave a considerable void in between the strip and the concrete (Figure 16). This condition was significant for two reasons. First, it caused some fasteners to be over-driven. That is, the fastener penetrated too deep and crushed the neoprene-backed washer. Second, a pocket of poor consolidation did not provide sufficient concrete for a fastener to take hold. Consequently, some fasteners fell right out of the member prior to testing.

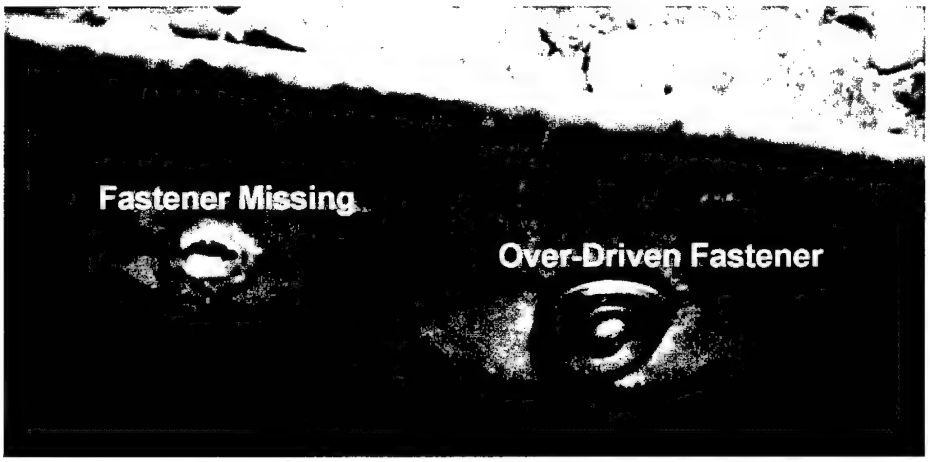

Figure 16. Effects of driving a fastener into a pocket of poor consolidation

6 Testing of Full Scale T-Beams

The experimental setup, as seen in Figure 17, placed the simply supported beam into four-point bending through the use of two load points equally spaced from the ends of the beams. The constant moment span was 60 in., the shear spans equaled 138 in. each, and the total span length reached 336 in.

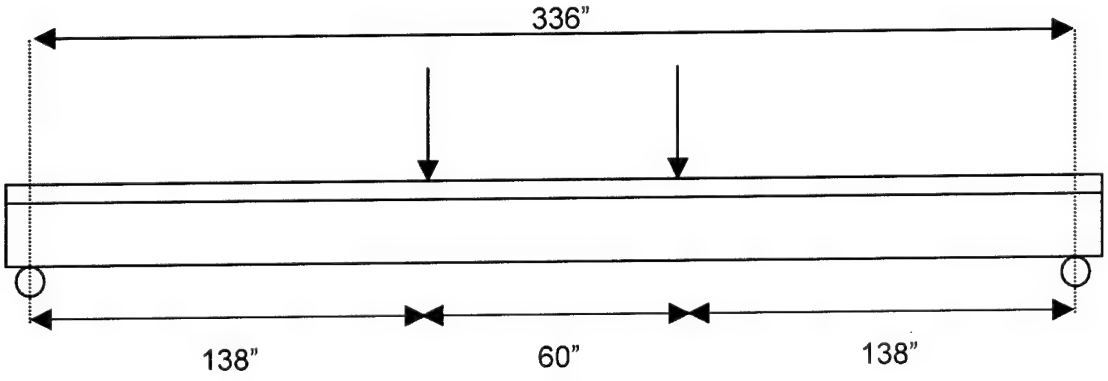

Figure 17. Experimental setup

A MTS Testar system was used to control two 110 kip actuators (each point load was a separate actuator) at a rate of deflection at 0.1 in./min. The data acquisition system consisted of an Optimum Megadac reading and recording data from the following inputs:

a. *Concrete Strain Gages:* seven 120 ohm gages along top flange spaced at 8 in. along the length of the beam.

b. *Internal Steel Strain Gages:* three 120 ohm gages placed at the centroid of tensile steel.

c. *Composite Strip Strain Gages:* varying number of 350 ohm gages placed at various locations along length of strip.

d. Free-standing LVDTs : three LVDTs measuring the deflection of the web at midspan and under each load point, and two LVDTs measuring the deflection of the flange at midspan.

e. Load: both actuators registered separate readings.

f. Stroke: measured stroke of each actuator separately.

The stroke data were chosen instead of LVDT data in all graphical and theoretical comparisons for two reasons. First, the average difference in the two readings was less than 1.00 percent. Second, since technicians removed the LVDTs prior to strip delamination/beam failure, the stroke data was more complete and therefore more useful. Figure 18 shows a plot of moment vs displacement for both the actuator stroke and LVDT measurements. The plot shows the close correlation of the two sets of data.

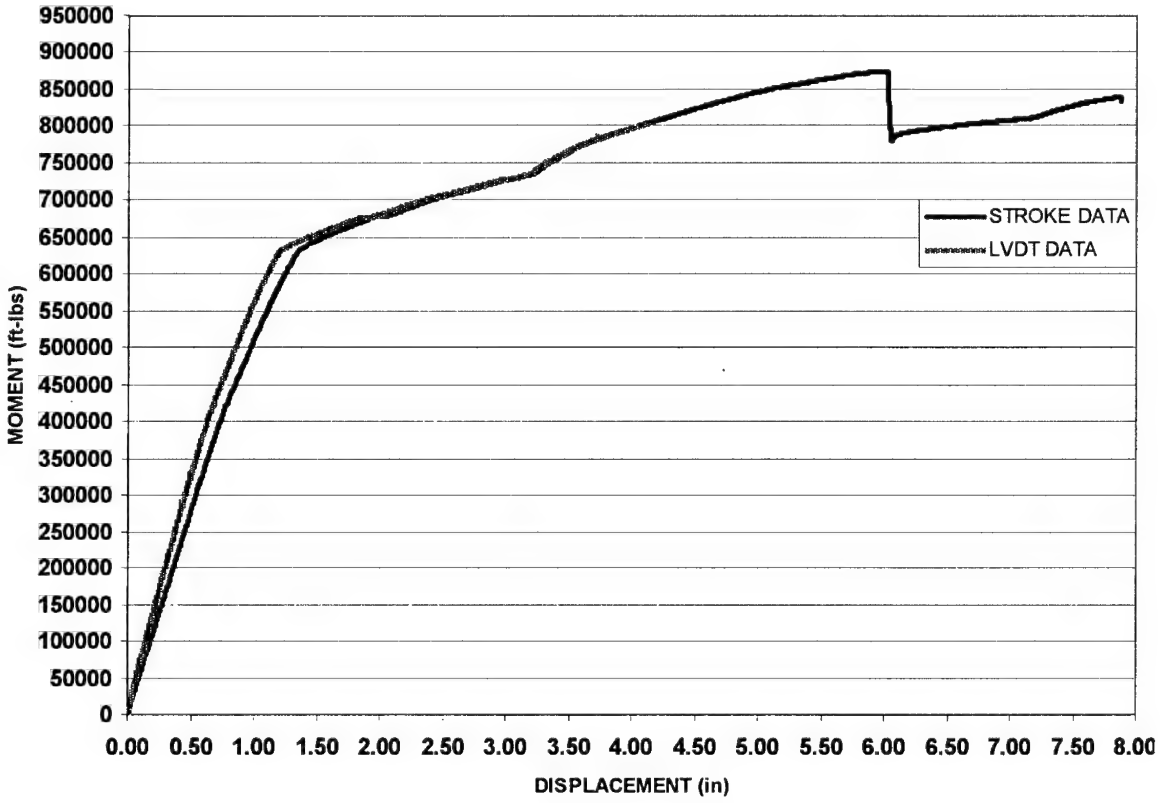

Figure 18. Comparison of stroke and LVDT data for Beam A5_Test1

Figure 19 shows an overhead view of the actual experimental setup. Note the size of the load frame and the positioning of the LVDTs along the bottom of the specimen.

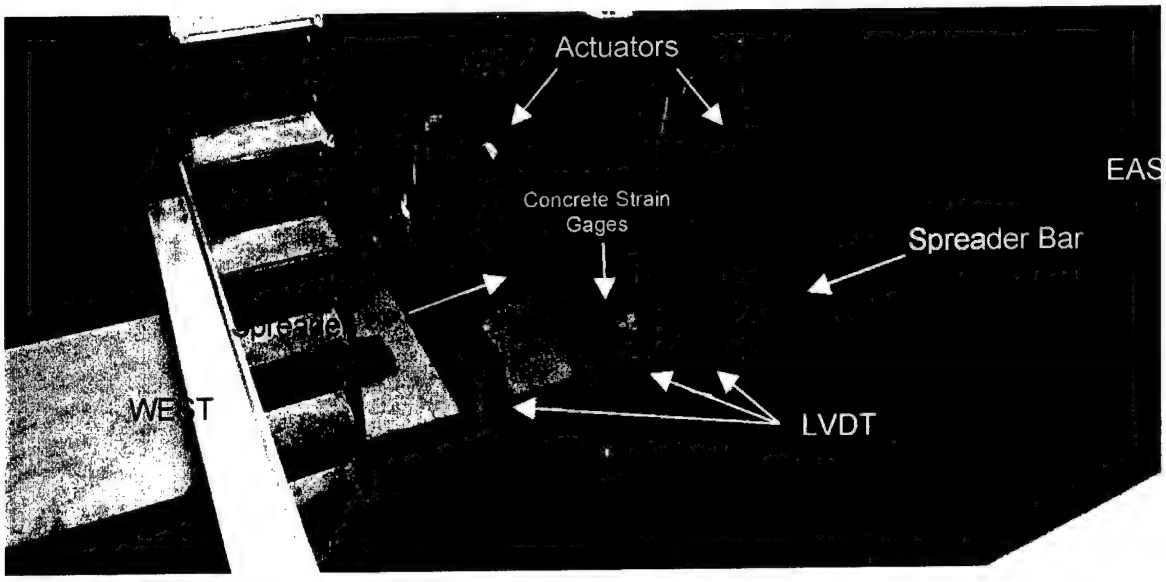

Figure 19. Large-scale T-beam ready for testing

Control Beam Testing

The control beams were tested first. The testing started with five cycles of loading to 342.5 ft-kips (load = 29.78 kips/actuator) and unloading to zero. This was done for two purposes. The cyclic loading not only cracked the specimens, but also afforded additional ERDC personnel the opportunity to conduct concurrent research on deflections and their relationship to reinforcement ratios. The control beams were then loaded under displacement control at 0.1 in./min until the beam achieved its ultimate capacity (concrete crushing in the compression zone) or the actuators reached their mechanical stroke limit of 6 in. The tests of beam A3_Control and beam A5_Control ended when the actuators reached their limits (no concrete crushing), while the test on beam A8_Control ended in a compression failure in the flange.

Strengthened Beam Testing

Prior to attaching the composite strip, the unstrengthened beam was loaded until it cracked while keeping the specimen below its yield capacity. The loading consisted of five cycles of loading to 342.5 ft-kips (load = 29.78 kips/actuator) and unloading to zero. Researchers then attached the composite strip (five man-hours to install) and proceeded to load the beam at a rate of 0.1 in./min. Researchers continued to load the beam until either the concrete crushed or the actuators reached their stroke limits. Figure 20 provides an overall view of the testing to include the load frame and actuators.

Figure 20. End view of beam during testing

7 Results of Full-Scale T-Beam Tests

Table 7 provides a summary of the critical variables in the full-scale beam tests. Some constants not listed in the table are fastener spacing (2 in. for all tests), test control (displacement control except for Beam A8_Control as described in what follows), and test rate (0.1 in./min for all trials). Termination length is defined as the distance from the support at the ends of the span to the first row of fasteners attaching the composite strip.

Table 7. Specimen Summary

Beam Number	Main Reinfor	A_s/A_{bal}	Strip Width (in.)	Strip Length (in.)	Strip Thick (in.)	Type Fastener	No. Fastener	Term Length (in.)
A3_Control	3 No. 9's	0.38	-	-	-	-	-	-
A3_Test1	3 No. 9's	0.38	4	300	.125	AL-47	300	19
A3_Test2	3 No. 9's	0.38	4	330	.250	AL-52	328	3
A5_Control	5 No. 9's	0.55	-	-	-	-	-	-
A5_Test1	5 No. 9's	0.55	4	300	.125	AL-47	300	19
A5_Test2	5 No. 9's	0.55	4	332	.250	AL-52	332	2
A8_Control	8 No. 9's	0.81	-	-	-	-	-	-
A8_Test1	8 No. 9's	0.81	4	300	.125	AL-47	300	19
A8_Test2	8 No. 9's	0.81	4	332	.250	AL-52	332	2

Table 8 summarizes the results of the nine tests. Since failure was not obtained in all of the beams, the moment at 2.5 in. of stroke was chosen as the postyield comparison. Comparisons at strip detachment are provided in Table 9. The value of 2.5 in. is significant for two reasons. First, all nine tests had viable data at 2.5 in. Second, 2.5 in. of stroke equals a ductility ratio of L/135; a value well beyond typical design limits of L/360. The results in Table 8 show increases in both the yield moment and the moment at L/135 for all six strengthened beams. In addition to the gains in moment capacity, each beam displayed an increase in the postyield stiffness as described by the slope of the moment vs stroke diagram in Figure 21.

Table 8. Test Results				
Beam Number	Yield Moment (ft-kips)	% Yield Increase (%)	Moment @ 2.5" Stroke (ft-kips)	% Increase @ 2.5" Stroke (%)
A3_Control	352	-	423	-
A3_Test1	380	7.95	484	14.42
A3_Test2	393	11.65	538	27.19
A5_Control	623	-	684	-
A5_Test1	637	2.25	705	3.07
A5_Test2	660	5.94	797	16.52
A8_Control	950	-	1,030	-
A8_Test1	960	1.05	1,070	3.88
A8_Test2	993	4.53	1,110	7.77

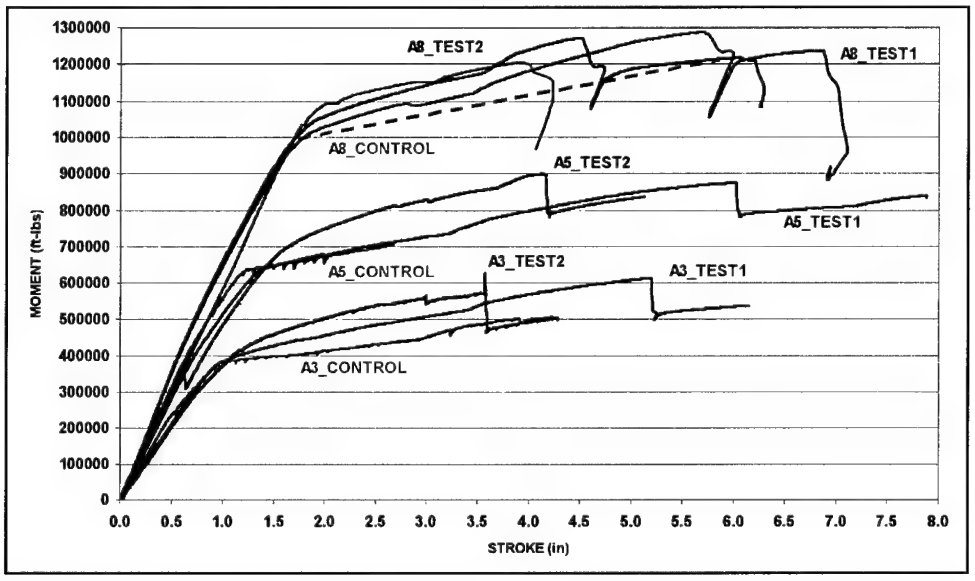

Figure 21. Cumulative moment vs stoke plot

Figures 22 through 25 graphically show both the increases in the yield moment as well as the increases in moment capacity at 2.5 in. of stroke. Two trends are visible from these graphs. First, the addition of a greater area of strip (increasing the number of strips from one to two) increased the strengthening benefit. For all three types of beams, Test 2 (the double strip) had nearly twice the yield moment and twice the moment at 2.5 in. of stroke as compared to Test 1 (single strip). Also, Figures 22 and 24 show the strengthening effect of the composite strip was greatest in the A3 family of beams and the least in the A8 family. In fact, trend in the results varied with the reinforcement ratio. That is, the lower ratio of A_s/A_{bal}, the greater the benefit of the composite strip.

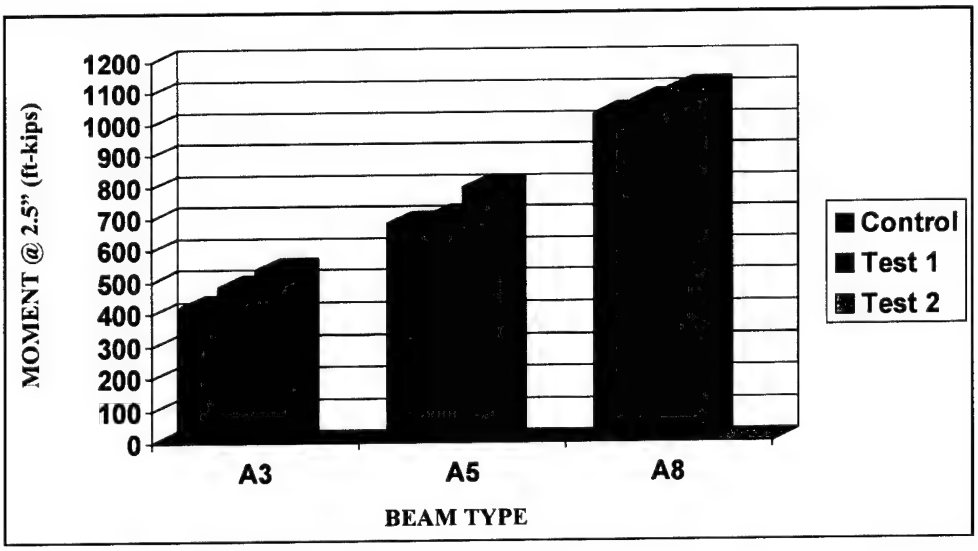

Figure 22. Moment capacity @ 2.5 in. of stroke

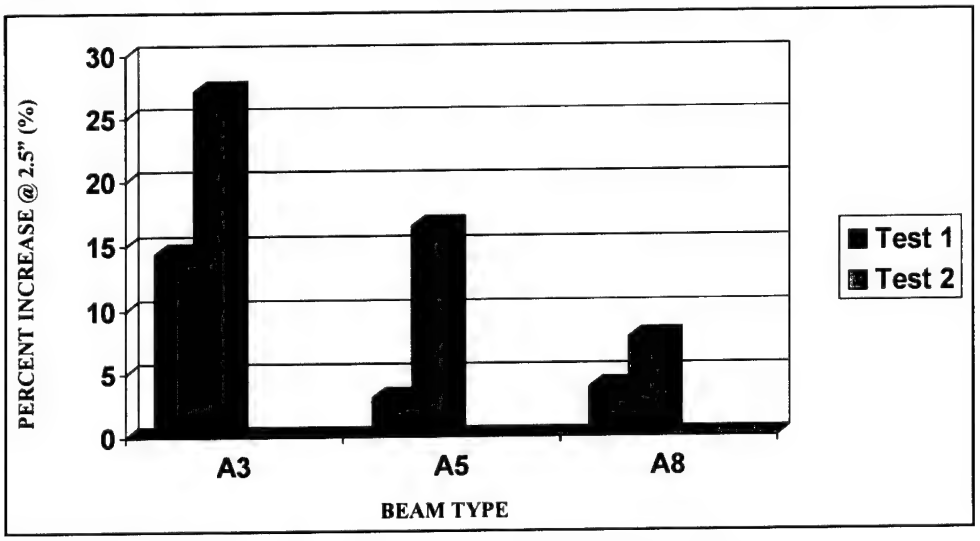

Figure 23. Percent increase in moment capacity @ 2.5 in. of stroke

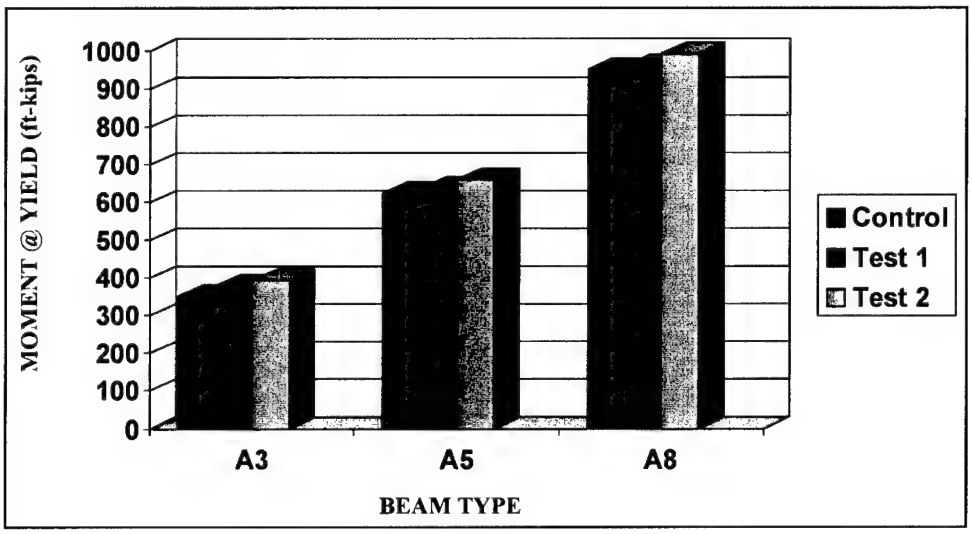

Figure 24. Moment capacity @ yield

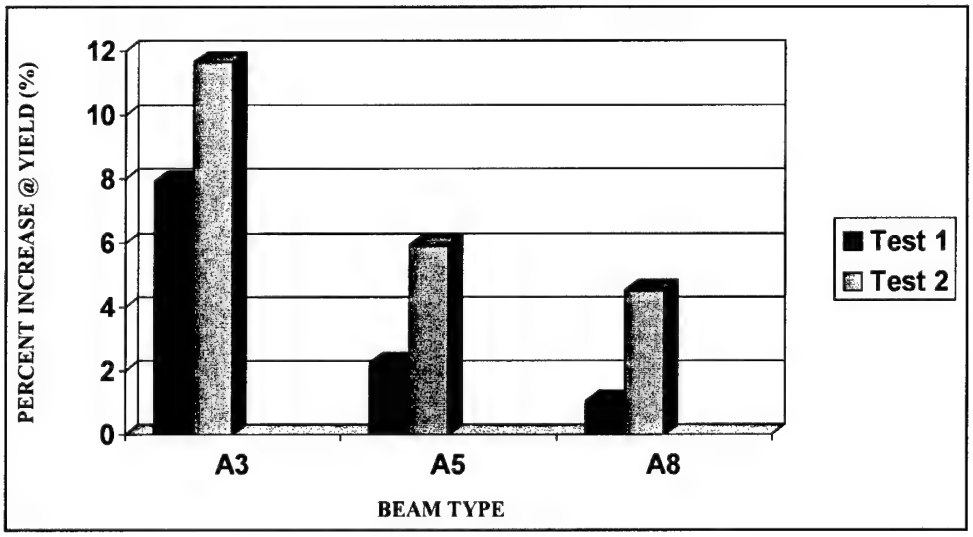

Figure 25. Percent increase in moment capacity @ yield

As discussed in what follows, the strengthened beams failed by delamination of the strengthening composite strip either from the free end (bearing) or from the interior (gross fastener). The maximum moments and displacements achieved by the strengthened beams at failure of the strengthening system are shown in Table 9. The percent increase over the unstrengthened beam was determined by measuring the drop in moment capacity at the point of delamination, as opposed to comparing the capacity to the ultimate strength of the control beam.

Table 9. T-Beam Behavior at Failure					
Beam -	Moment @ Failure (ft-kips)	% Increase Over Unstrengthened (%)	Deflection @ Max Moment (in.)	Ductility Ratio @ Failure -	Delamination Failure Mode -
A3_Test1	612	22.65	4.40	L/76	Bearing
A3_Test2	573	23.76	3.60	L/93	Gross Fastener
A5_Test1	874	11.91	6.00	L/56	Bearing
A5_Test2	899	14.96	4.15	L/81	Gross Fastener
A8_Test1	1,290	21.70	5.80	L/58	Bearing
A8_Test2	1,270	17.59	4.60	L/73	Gross Fastener

8 Description of Failure Modes of T-Beams

In addition to the importance of an increase of moment capacity, the way in which each beam failed is also of great significance. This section of the report contains a discussion of each test and a description of the mode by which each beam failed. Yield strengths were determined by an examination of the "knee" in the moment versus stoke curves, the moment versus steel strain curves, and the moment versus strip strain curves (when applicable) for each beam. Since the loads applied by each independent actuator were not identical, the testing was not truly four-point bending. The moment was computed by taking the maximum load and multiplying it by the length of the shear span.

Beam A3_Control

Beam A3_Control never achieved a concrete crushing failure because the actuators reached their maximum stroke limit forcing termination of the test. The test revealed that the lightly reinforced beam was very ductile and could achieve significant displacements. Large cracks developed under each load point (Figure 26) and horizontal splitting along the line of tensile reinforcement was evident. Flexural cracks were predominant in the moment region and extended throughout the depth of the section. Figure 27 shows the moment versus stroke plot for beam A3_Control. Steel yielding is evident at 352 ft-kips, and the shallow slope of the graph after the yield point indicates low stiffness.

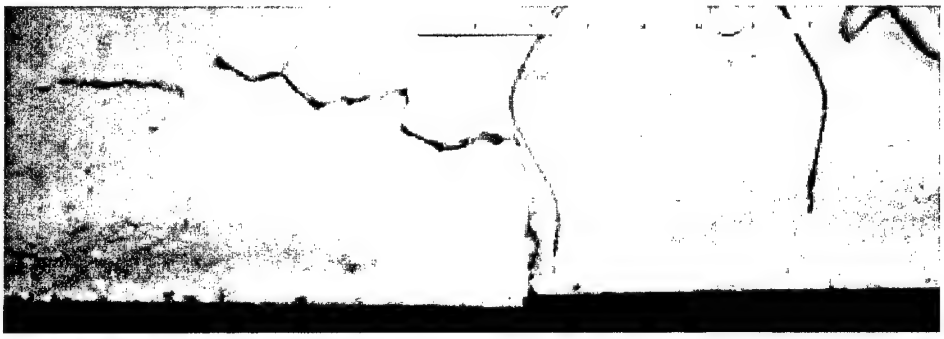

Figure 26. Large crack in web of Beam A3_Control

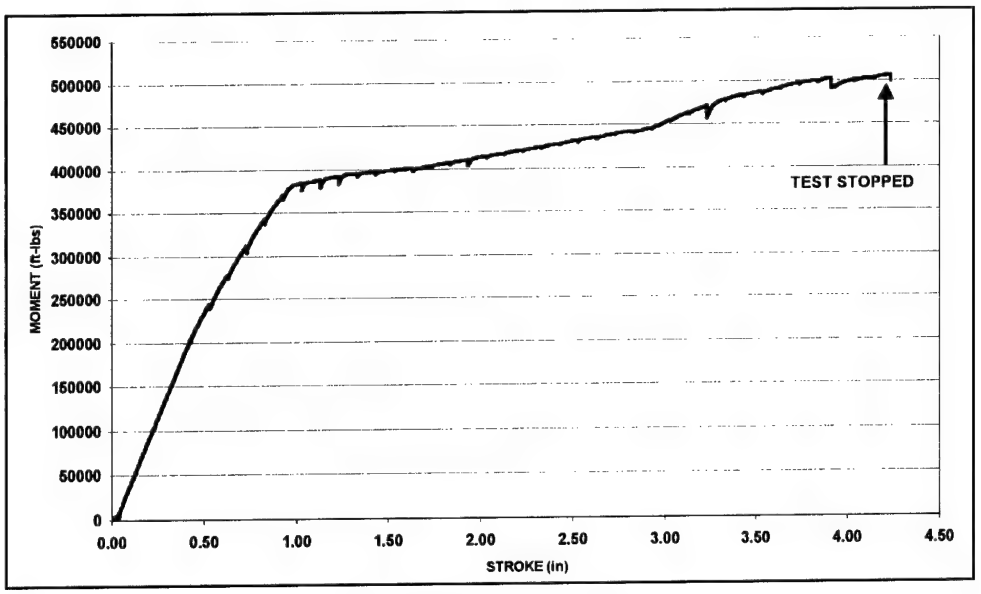

Figure 27. Plot of moment vs stroke for Beam A3_Control

Beam A3_Test1

Beam A3_Test1 failed due to a sudden strip delamination beginning from the east support and continuing all the way to the midspan of the beam. That is, the strip delamination originated at the support and propagated towards the midspan of the beam. The cause of the delamination was a bearing failure of the strip at the fastners closest to the support. As evidenced by Figures 28 and 29, the forces in the strip pulled the strip right through the fasteners and started the violent delamination. Figure 30 depicts the delamination as a sudden drop in the moment vs stroke curve for the test. After the strip delaminated, the beam returned to its unstrengthened, post-yield capacity and began to pick-up more load. Since the deflection capacity of the beam exceeded that of the actuators, the testing was terminated once the apparatus reached its stroke limit.

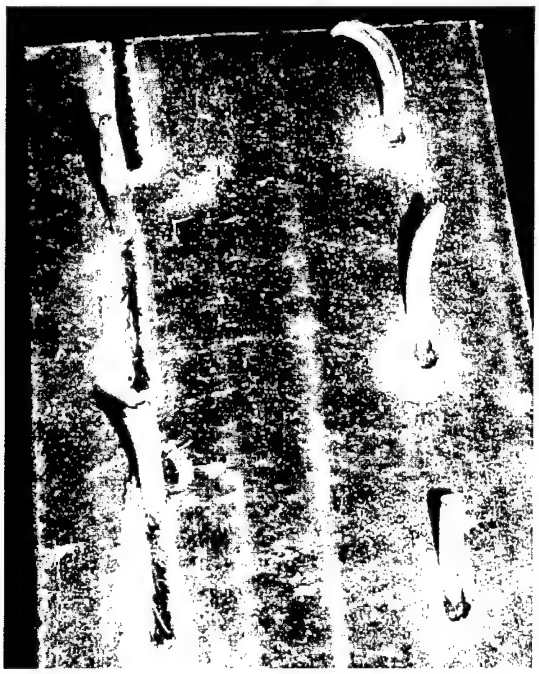

Figure 28. Bearing failure of strip attached to Beam A3_Test1

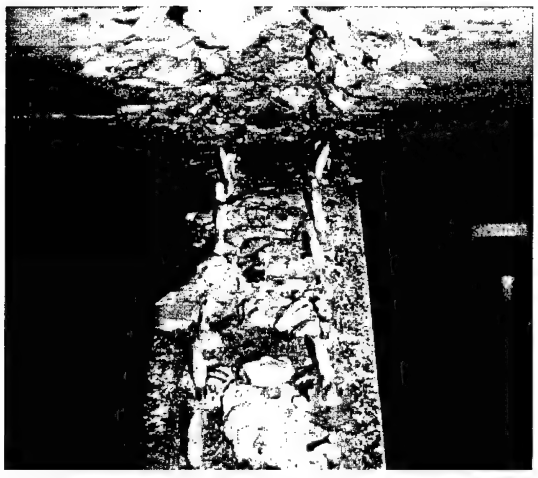

Figure 29. Effects of strip delamination on Beam A3_Test1

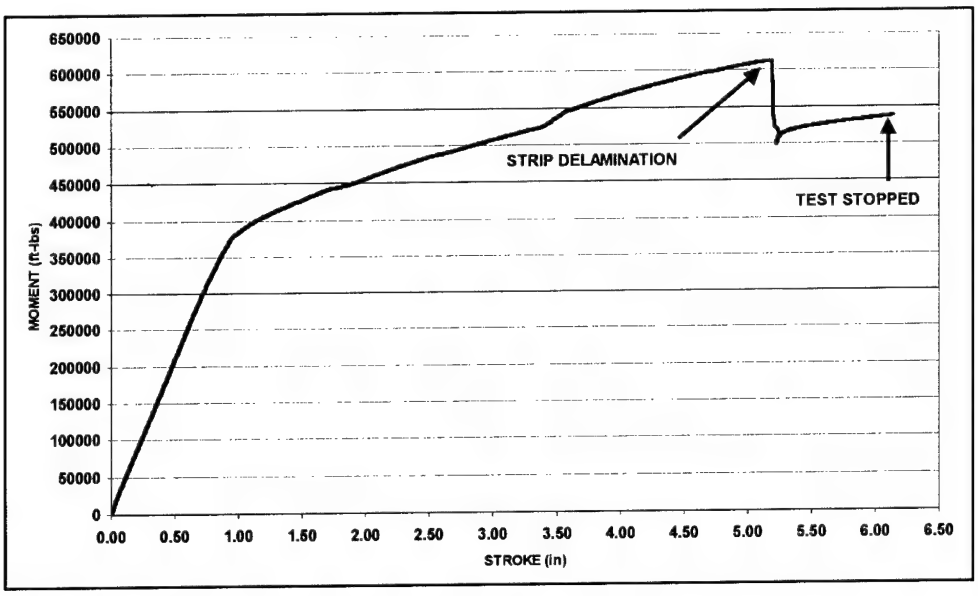

Figure 30. Plot of moment vs stroke for Beam A3_Test1

Beam A3_Test2

Beam A3_Test 2 failed due to a delamination of the strip prior to achieving the ultimate capacity of the beam. The delamination originated 12 in. west of the beam's midspan and propagated outwards toward both supports. In fact, the strip remained attached at both ends and sagged freely in the middle (Figure 32). The origin of the delamination, as seen in Figure 31, coincided with a large crack and differential displacement of the beam within the moment span. Also of note was the horizontal cracking in the beam within the moment span. This cracking added to the differential displacement and appeared to occur at the level of the internal reinforcing steel located within the web.

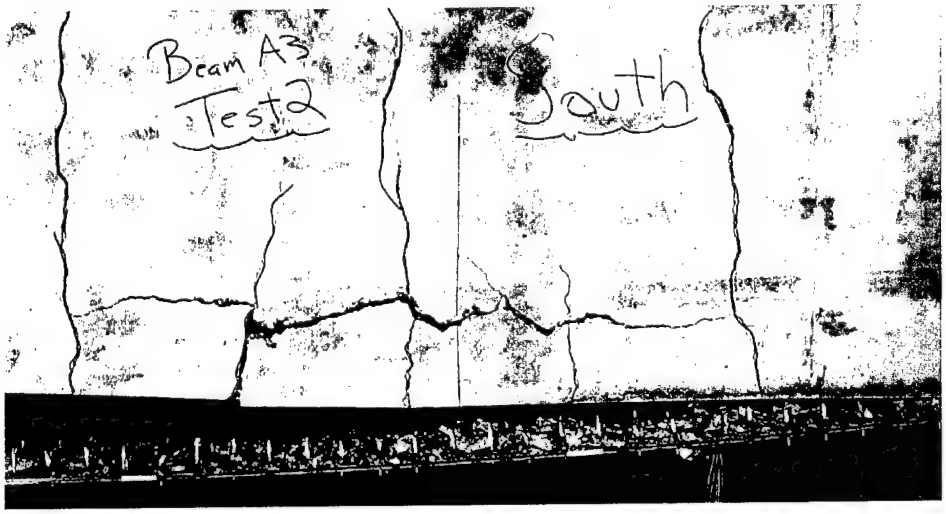

Figure 31. Severe horizontal splitting of Beam A3_Test2

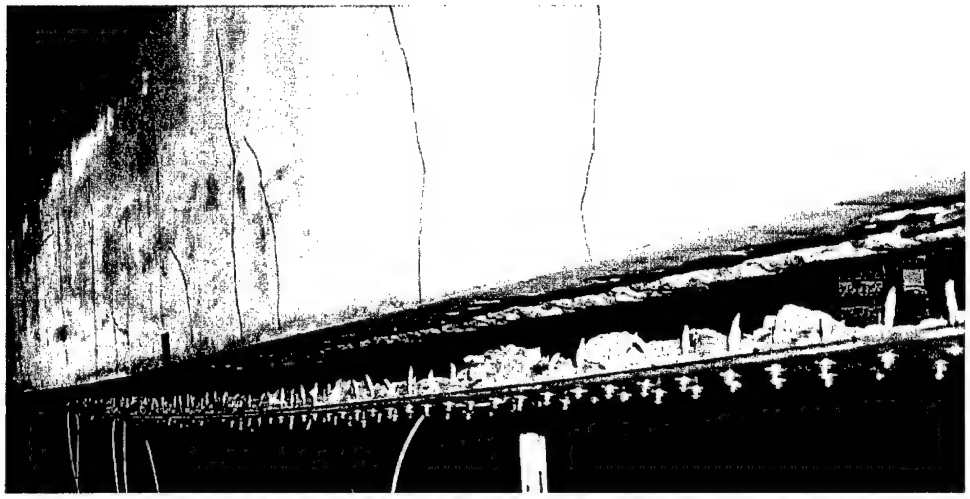

Figure 32. Delaminated strip suspended from ends

Figure 33 shows the behavior of the beam via the moment vs stroke diagram. Delamination occurred at 580 ft-kips and is evident by the sharp decline in moment capacity. Also apparent from the graph is the fact that the beam reverted to its unstrengthened postyield capacity after the delamination and accepted more load until the test was terminated.

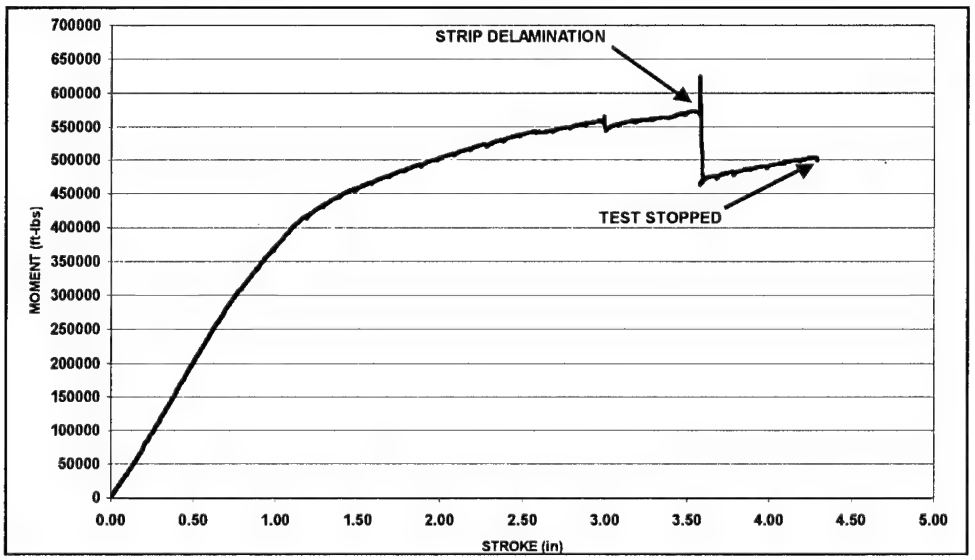

Figure 33. Plot of moment vs stroke for Beam A3_Test2

Beam A5_Control

Beam A5_Control never achieved a concrete crushing failure. The testing was terminated prematurely at a stroke of 2.75 in. The test revealed that despite the increased area of tensile steel, that the beam was ductile, capable of significant displacements, and would not achieve ultimate failure during testing. As with A3_Control, the beam developed large cracks in the web under each load point. Cracking, as seen in Figure 34, was again predominantly flexural, and the cracks extended from the base of the web up to 2 in. below the web/flange interface. Figure 35 shows that the beam yielded at 623 ft-kips and did not possess much postyield stiffness.

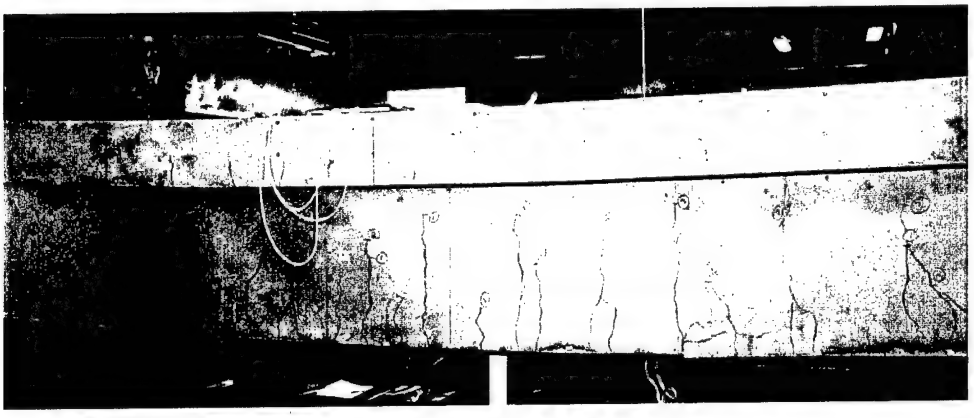

Figure 34. Cracking pattern of Beam A5_Control after testing

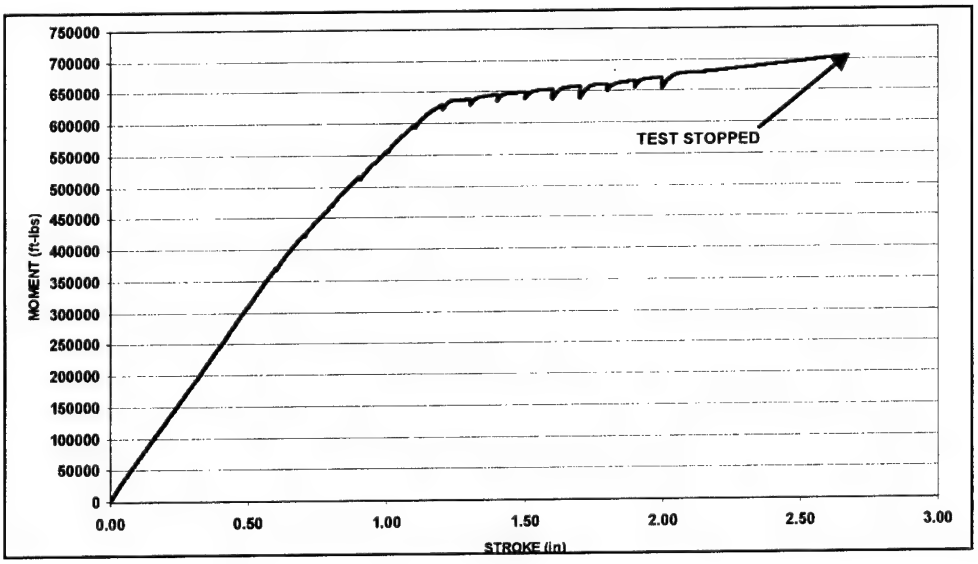

Figure 35. Plot of moment vs stroke for Beam A5_Control

Beam A5_Test1

The test on Beam A5_Test1 also resulted in a strip delamination (Figure 36) that started at the east support and propagated toward the midspan of the beam. In fact, the delamination extended from the east support to just 48 in. short of the west support. The cause of the delamination was bearing failure in the strip (Figure 37) at the fasteners closest to the east support. In fact, four fasteners remained in the beam after the strip delaminated from the beam and are shown in Figure 38.

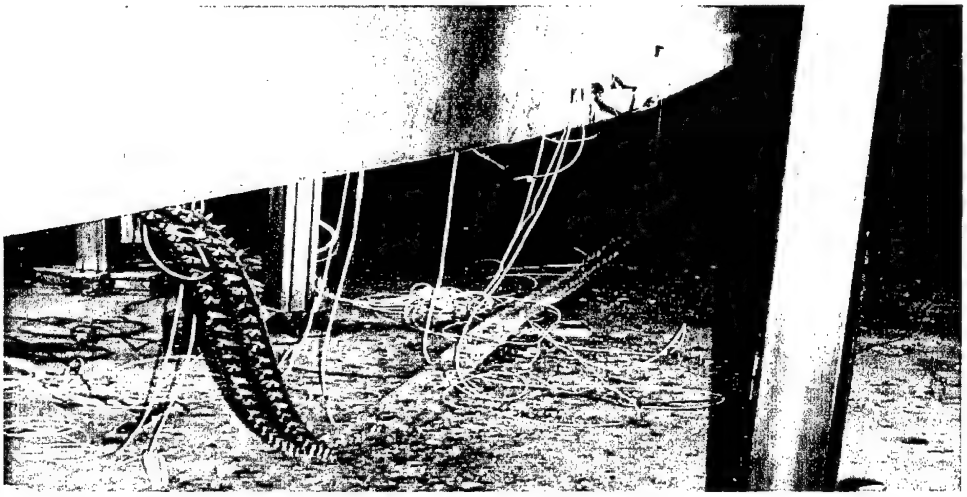

Figure 36. Delamination on Beam A5_Test1

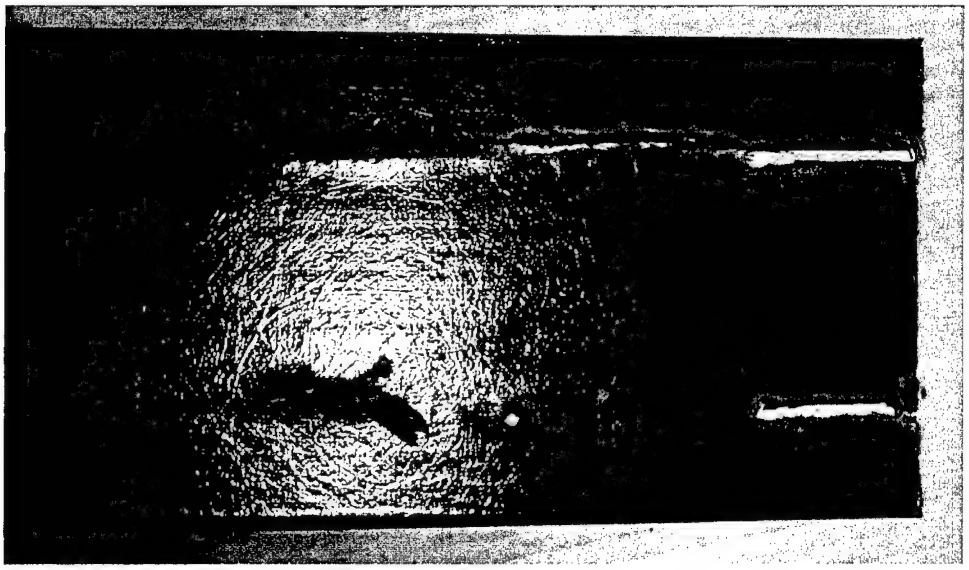

Figure 37. Slotting due to bearing failure on Beam A5_Test 1

Figure 38. Four fasteners remain on Beam A5_Test 2

Figure 39 shows the delamination at 880 ft-kips with a large drop in the moment vs deflection curve. The figure also shows that after the delamination, beam A5_Test1 began to take on more load. However, since the experimental set-up could not reach the ultimate flexural capacity of the beam, researchers had to stop the test prior to beam failure.

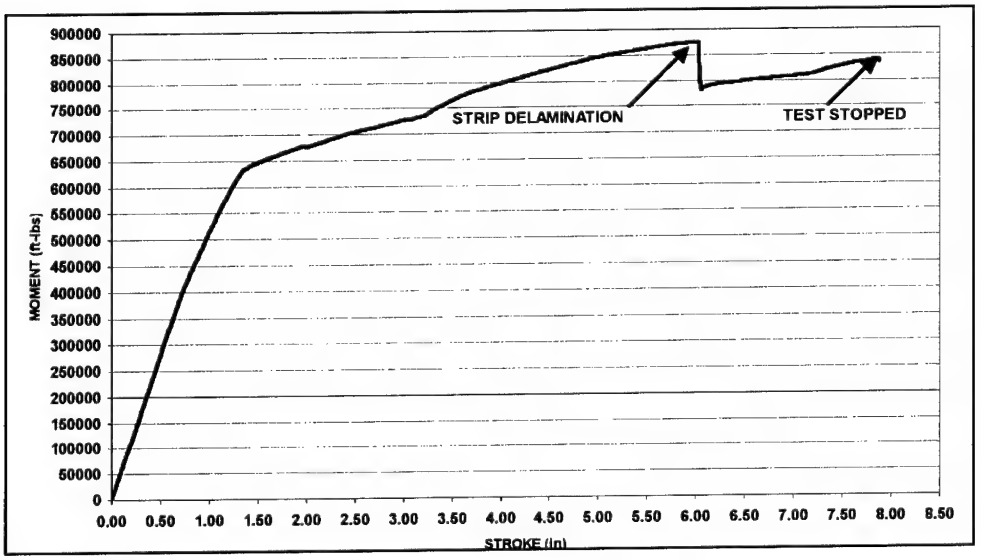

Figure 39. Plot of moment vs stroke for Beam A5_Test1

Beam A5_Test2

The test on beam A5_Test2 resulted in a strip delamination that started 30 in. east of the beam midspan and propagated outward towards both the east and west support. The origin of the delamination coincided with the large crack in the beam within the moment span shown in Figure 40. Also of note was the horizontal cracking in the beam within the moment span. This cracking added to the differential displacement and appeared to occur at the level of the internal reinforcing steel located within the web.

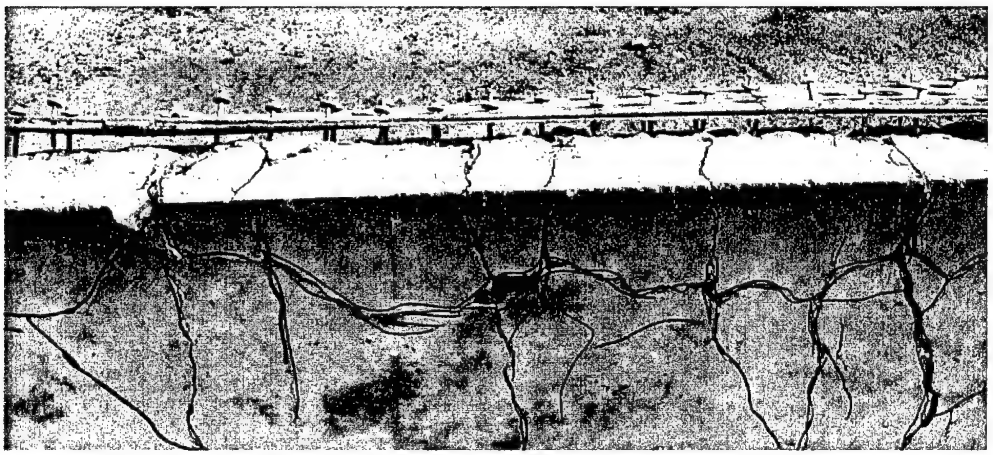

Figure 40. Large crack and origin of delamination for Beam A5_Test2 (Post-mortem of inverted beam)

Figure 41 shows the delamination at 900 ft-kips with a large decrease in moment capacity. The data has a slight jog between 300 and 350 ft-kips. This jog occurred because of a tight safety chain that made the beam appear stiffer than it actually was. Once the chain was released, the beam returned to its actual stiffness and the test ran as planned. After the strip delaminated, the beam continued to accept load and recovered to 820 ft-kips. However, the capacity of the actuators was less than the capacity of the unstrengthened beam. Consequently, researchers stopped the test prior to reaching the ultimate failure of the beam.

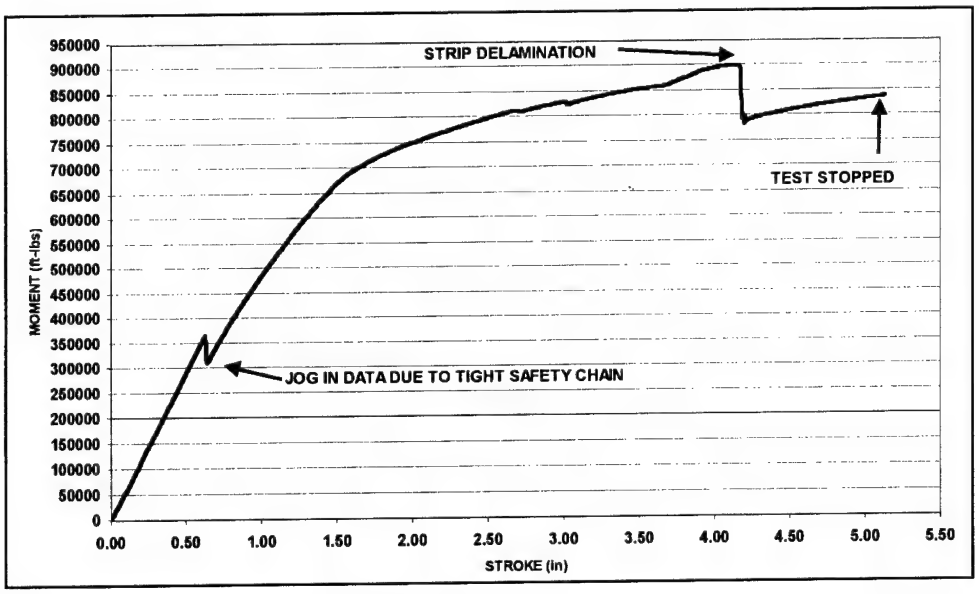

Figure 41. Plot of moment vs stroke for Beam A5_Test2

Beam A8_Control

Beam A8_Control was the only beam to be tested with the experimental apparatus in load control. While the beam did fail due to concrete crushing in the flange within the constant moment region (Figure 42), the moment vs stroke plot provided results inconsistent with the other tests. In fact, the data for this beam suggested that the control had a greater moment capacity than the strengthened beams. As such, researchers assumed a post-yield behavior consistent with the other beams in the A8 family to compare A8_Control to the strengthened beams. The assumed post-yield behavior was based on the common yield point and the values of the strengthened A8 beams after strip delamination (Figure 20).

Figure 42. Compression failure in flange of Beam A8_Control

Figure 43 shows the moment vs stroke diagram for Beam A8_Control. From the interpolated graph, the yield moment equals 1000 ft-kips, and the capacity of the beam at failure is 1150 ft-kips. The crushing failure began with a local failure in the vicinity of the east load point, and then progressed westward until the entire flange within the constant moment region was crushed.

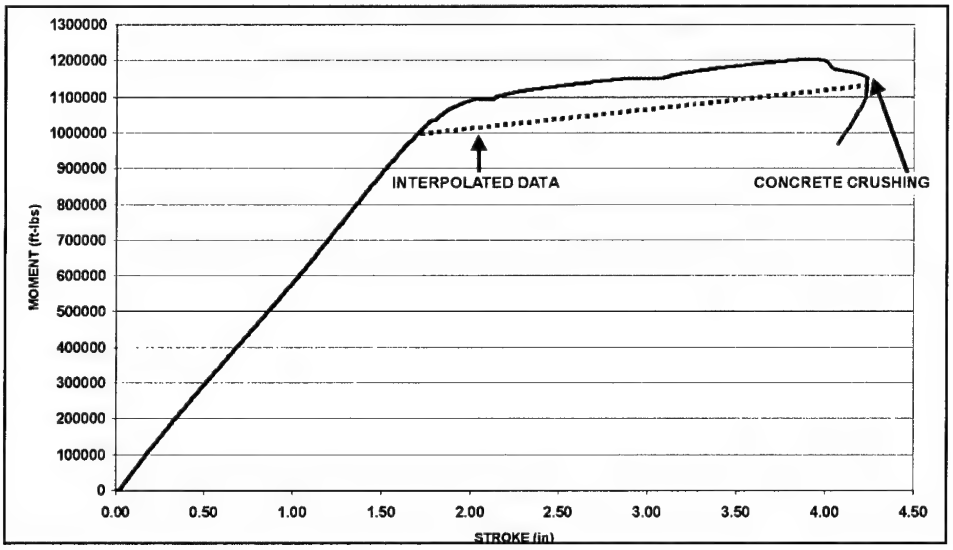

Figure 43. Moment vs stroke plot for Beam A8_Control

Beam A8_Test1

Beam A8_Test1 failed due strip delamination prior to ultimate failure of the beam. The delamination was a result of two phenomena. First, there was a bearing failure of the strip at the fasteners closest to the west support. The slotting of the strip as the fasteners "pulled through" the strip is pictured in Figure 44. Also, a large chunk of concrete, pictured in Figure 45, fell off the beam 64 in. west of the midspan of the beam. Figure 46 shows exposed reinforcing bar and provides a look at the failure plane of this chunk of concrete. While both events occurred nearly simultaneously, it was concluded that the delamination originated at the west support and propagated inward.

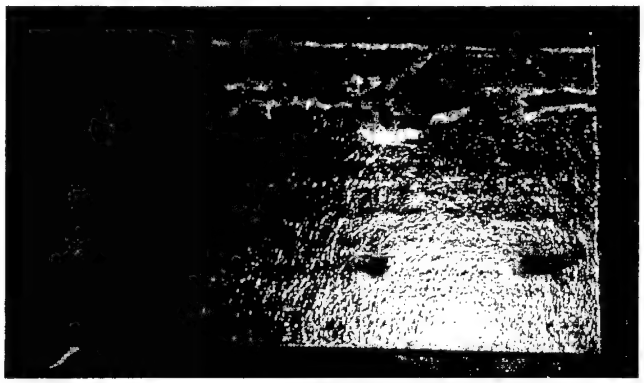

Figure 44. Bearing failure in strip on Beam A8_Test1

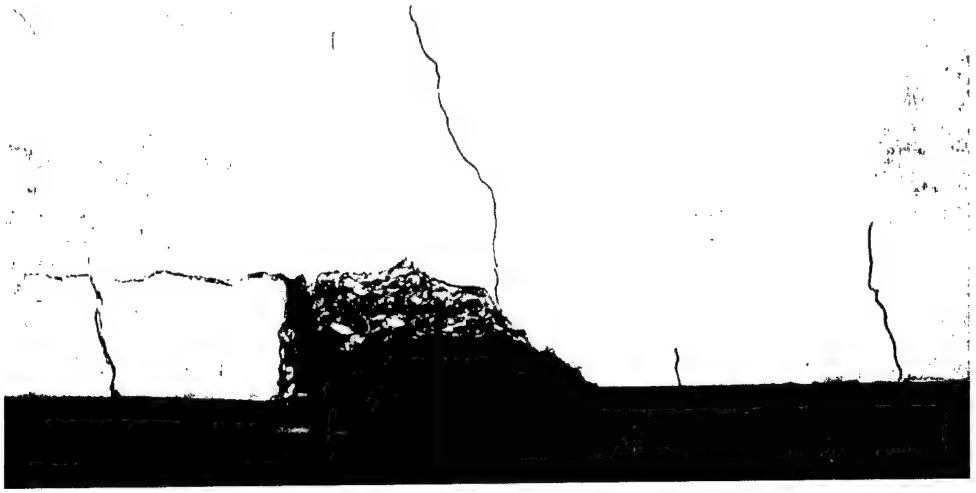

Figure 45. Large chunk missing from Beam Test1

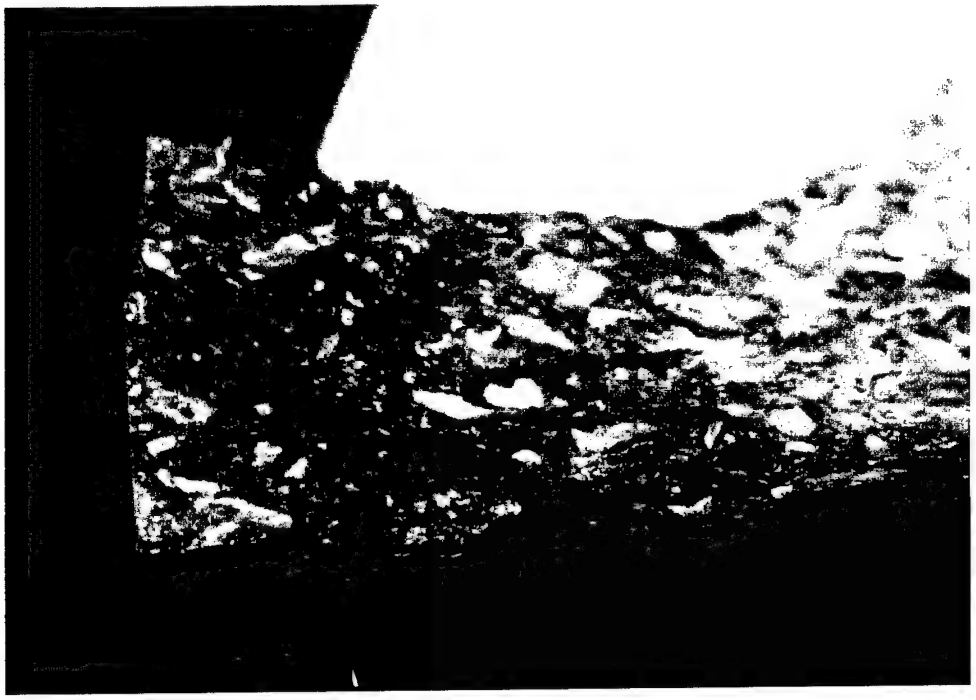

Figure 46. Close-up of missing chunk from Beam A8_Test1

Figure 47 shows the plot of moment vs stroke for Beam A8_Test1. Strip delamination is shown at 1280 ft-kips by a sharp drop in moment capacity. After delamination, the beam recovered to its unstrengthened capacity and accepted more load until it failed via concrete crushing in the flange at 1220 ft-kips.

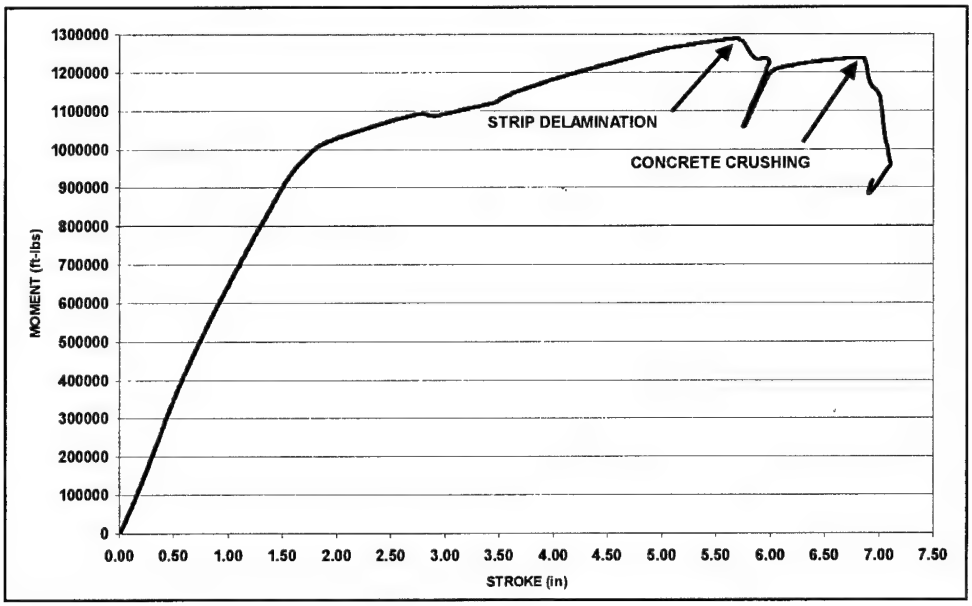

Figure 47. Plot of moment vs stroke for Beam A8_Test1

Beam A8_Test2

The test on Beam A8_Test2 resulted in a strip delamination followed by ultimate failure of the beam. The delamination began just outside the moment span at a large crack (Figures 48 and 49) located 34 in. east of the beam's midspan and propagated outward towards both supports. The violent delamination left the strip hanging by only the five pairs of fasteners closest to the west support. Concrete compression failure, shown in Figure 50, initiated at the east load point and propagated throughout the flange within the moment region.

Figure 48. Large crack in web of Beam A8_Test2 (Vic East load point)

Figure 49. Bottom view of large crack in Beam A8_Test2

Figure 50. Concrete crushing of flange at ultimate capacity of Beam A8_Test2

The strip delaminated at 1280 ft-kips of moment as seen in Figure 51. The delamination caused the moment capacity to drop to the unstrengthened beam strength. Since the beam had not yet reached its ultimate capacity, it accepted more load until the concrete compression failure in the flange at a moment of 1200 ft-kips.

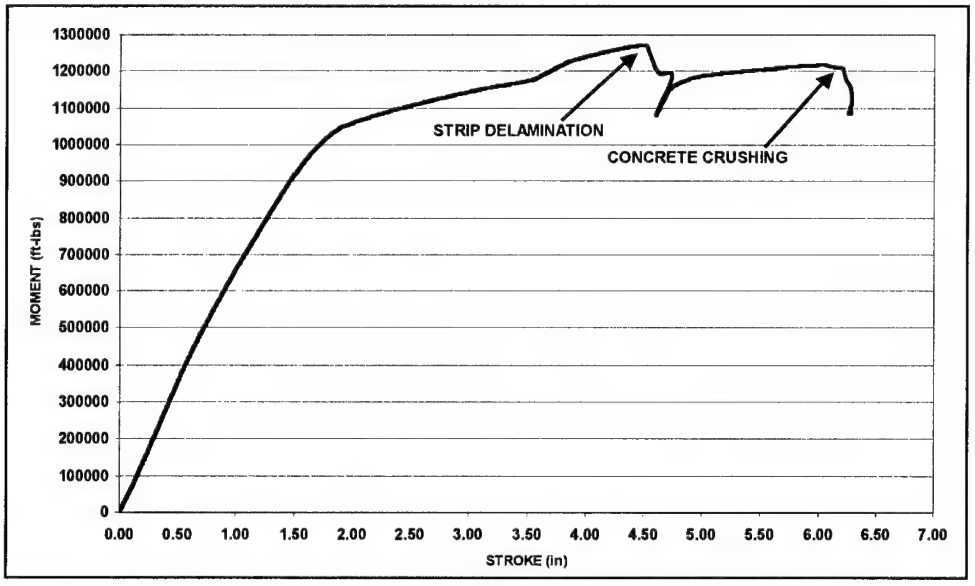

Figure 51. Plot of moment vs stroke for Beam A8_Test2

9 Strain Gage Data For T-Beams

Each beam had three different sets of strain gages. There were three gages on the internal steel reinforcement; seven gages spaced at 8 in. along the length of the beam on the top flange (concrete); and a varying number of gages along the composite strip of the retrofitted beams. The data from the internal steel gages was inconsistent at best and is not discussed or described in this report. The strip strain data and the concrete strain data, however, have been used to create two plots for each strengthened beam: a plot of moment vs strain and a plot of strain through the depth (30 in.) of the section. Each plot provides insight into the behavior of the strengthened section. The moment vs strain plot shows not only the maximum strain experienced by the strip, but also depicts the distribution of strain along the length of the specimen. Concrete strains are shown as negative, while the strain in the composite strip is positive. The plot of strain through the depth of the section shows the movement of the neutral axis as moment increases (the graph was constructed using three readings: one preyield, one near yield, and one postyield). The maximum strain expected in the composite strip was 11,600 με (based on open-hole strength), while the failure strain for the concrete is approximately 3,700 με.

Moment Vs Strain

While the strain data for each beam is unique, there are trends in the data worth investigating. First, the strain distribution along the length of the strip mirrors strain data from tests previously conducted on large-scale beams (Bank et al. 2000). The strain is greatest at the midspan of the beam, remains nearly constant into the shear span, then decreases linearly to zero at the ends of the composite strip. The point where the strain begins to transition from a constant value to zero is roughly 40 in. from the midspan of the beam. Second, in five out of the six tests the strain at the midspan of the beam exceeded the predicted ultimate strength of the composite strip (11,600 με). This indicates that the open-hole tests done on the 2-in. coupons provide conservative estimates of composite material strengths. Finally, in five out of six of the moment vs strain plots, there is a postyield "knee" in the data. The knee represents an increase in the amount of strain experienced by the strip and indicates that the strip assumes more of the moment as the internal reinforcing steel continues to yield. Refer to Figures 52-57 for the moment vs strain plots for each strengthened beam.

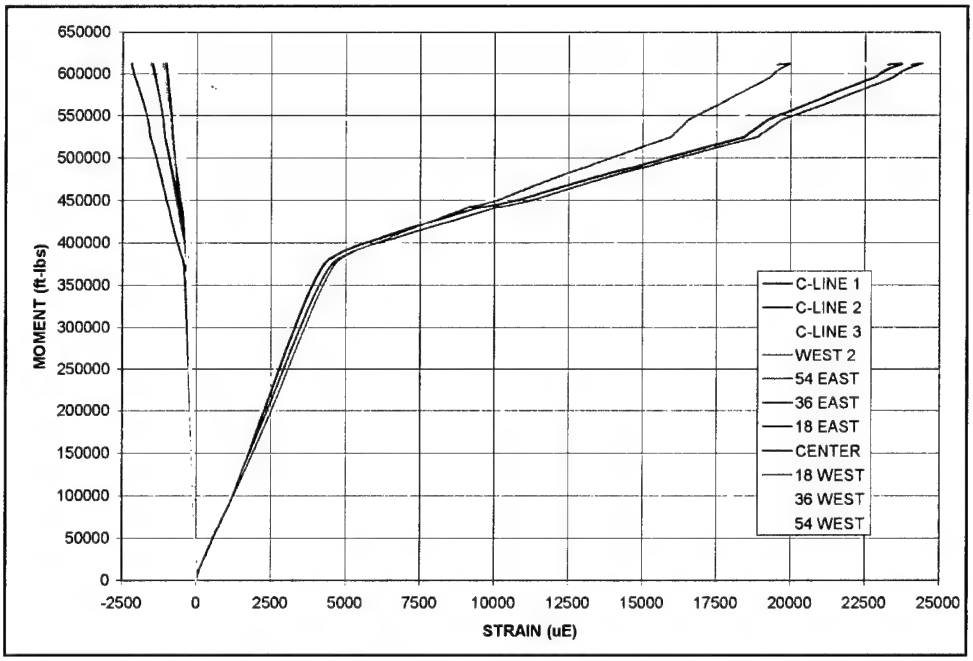

Figure 52. Plot of moment vs strain for Beam A3_Test1

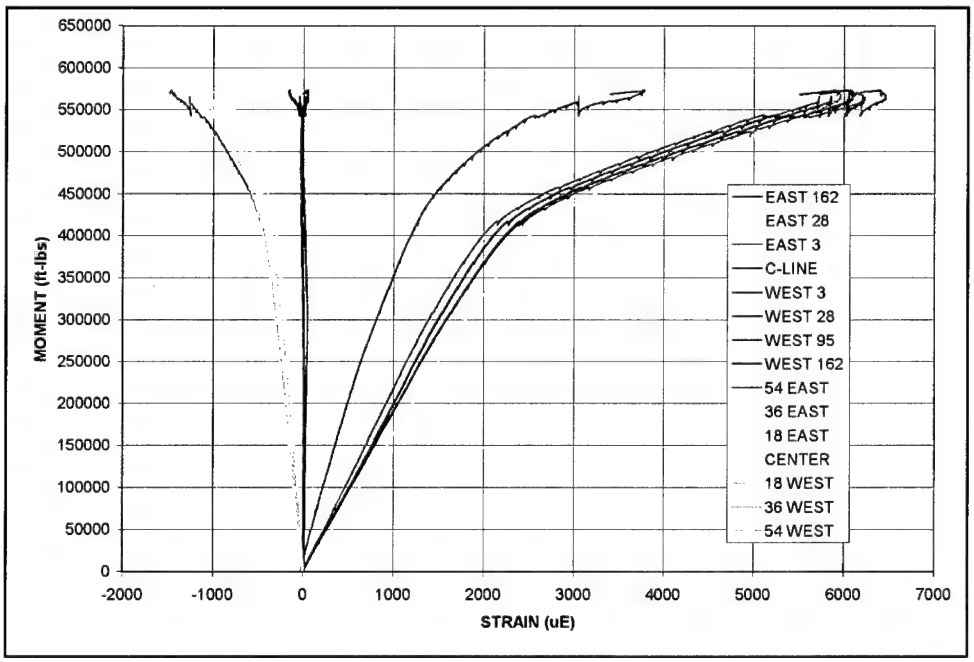

Figure 53. Plot of moment vs strain for Beam A3_Test2

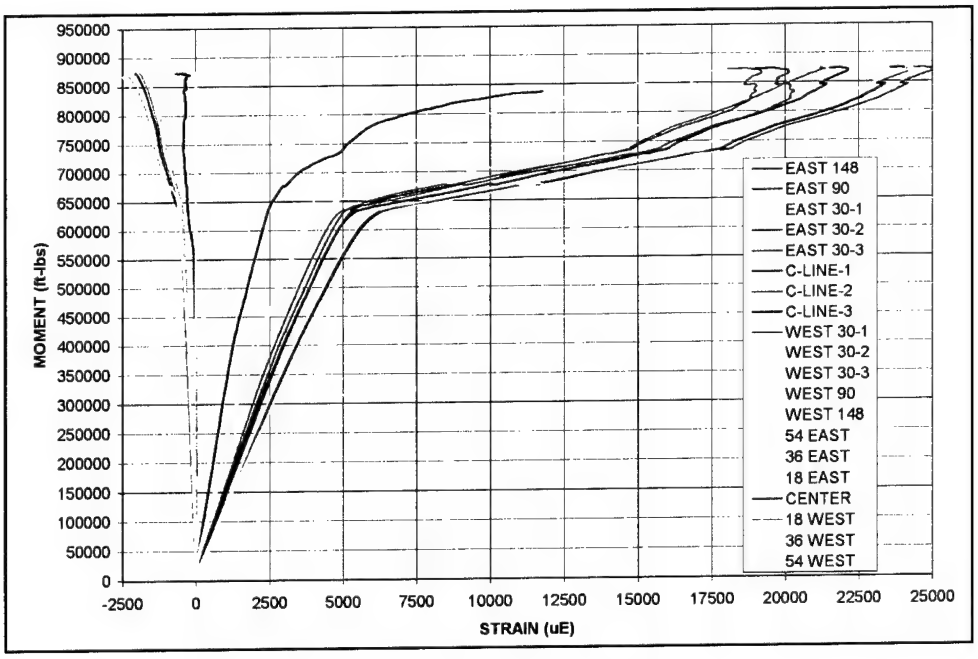

Figure 54. Plot of moment vs strain for Beam A5_Test1

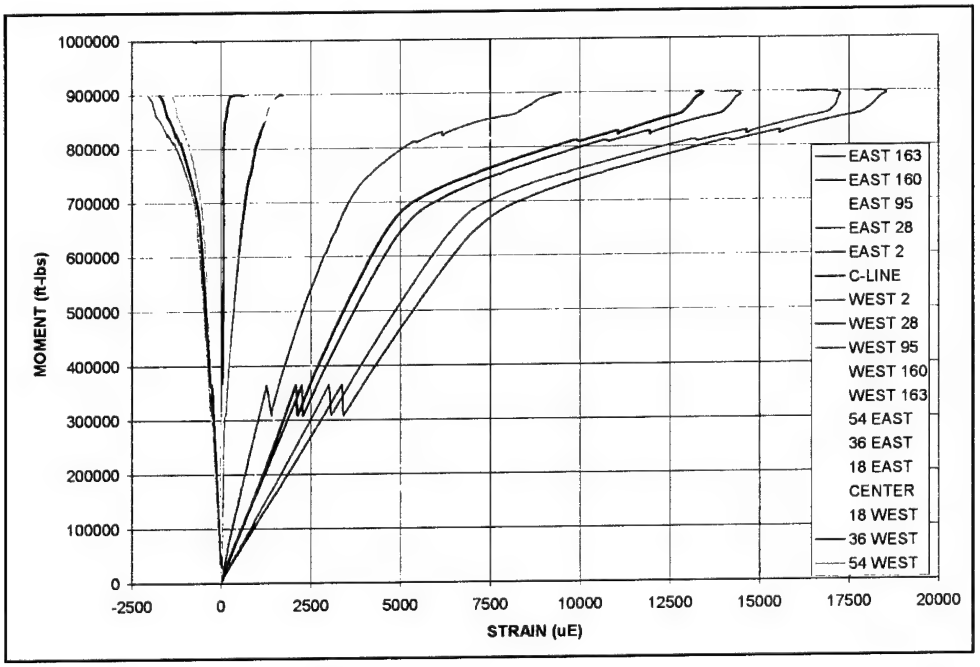

Figure 55. Plot of moment vs strain for Beam A5_Test2

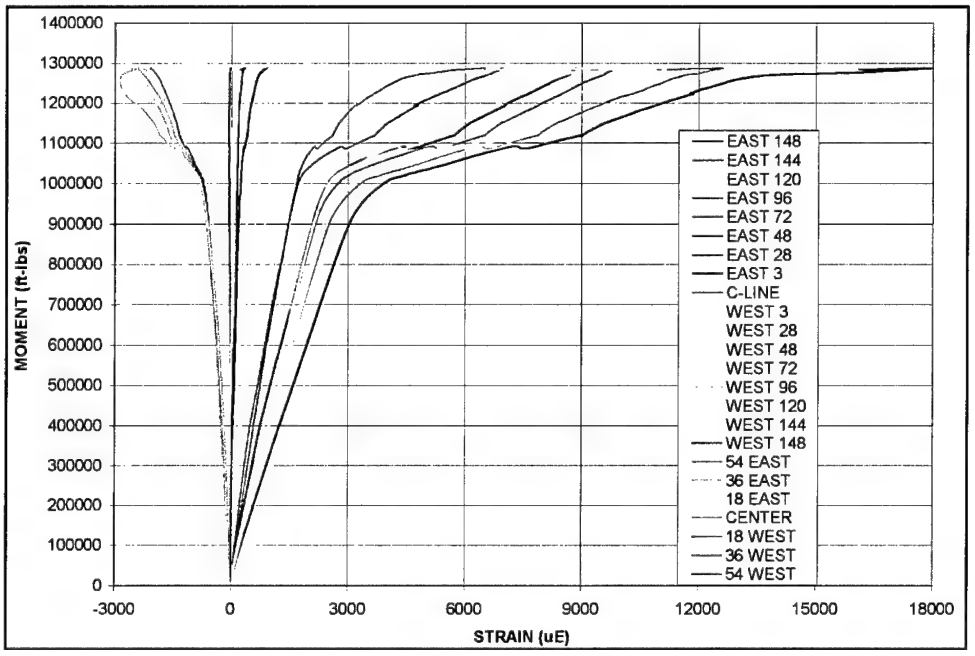

Figure 56. Plot of moment vs strain for Beam A8_Test1

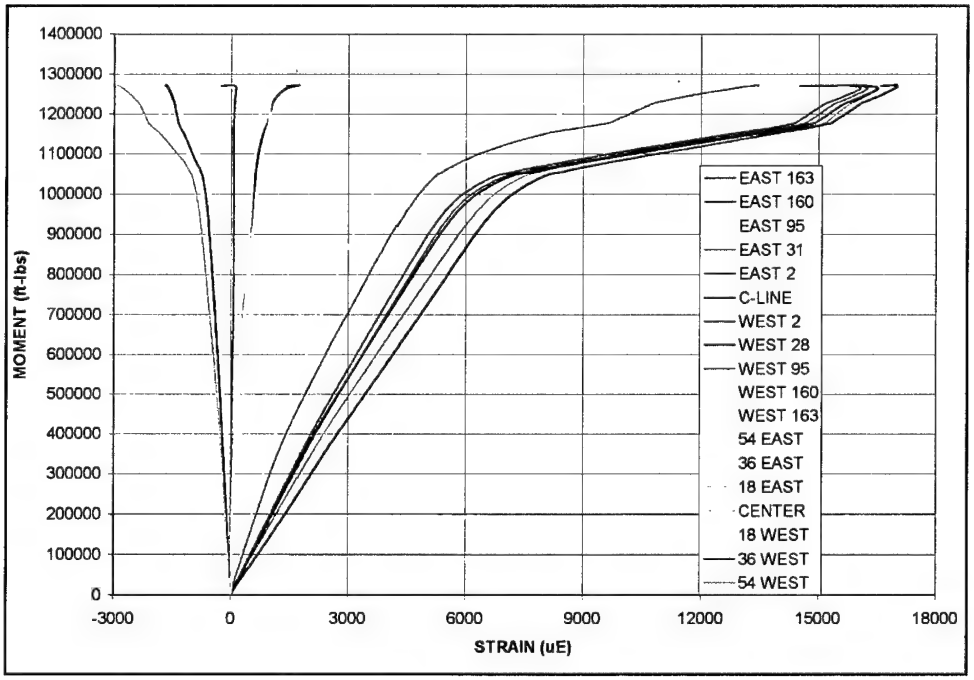

Figure 57. Plot of moment vs strain for Beam A8_Test2

Strain Through Depth Of Section

The plots of strain through the depth of the section provide two useful insights. First, as applied moment increases, concrete in the web cracks and the reinforcing steel yields, driving the neutral axis higher into the flange. The plots clearly show the upward movement of the neutral axis and confirm the predicted behavior. Also, each plot shows the significant increase in strain in the composite strip after yielding of the steel reinforcement. With the steel no longer able to sustain the increase in strain, the strip "picks up" more of the strain and allows the section to accept more moment. The plots confirm the benefit of the strengthening strip (Figures 58-63).

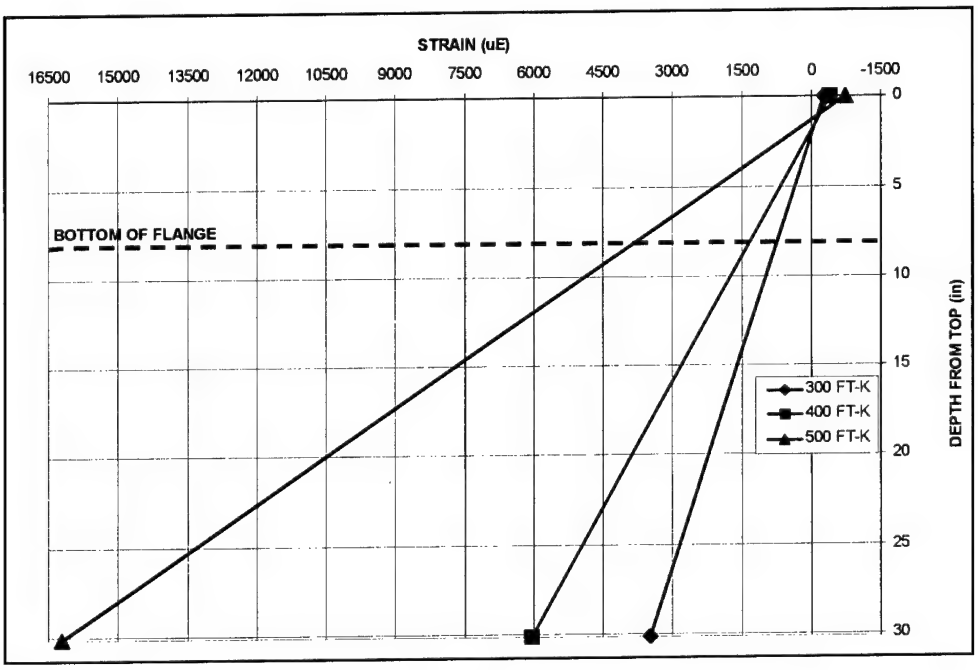

Figure 58. Strain plot for Beam A3_Test1

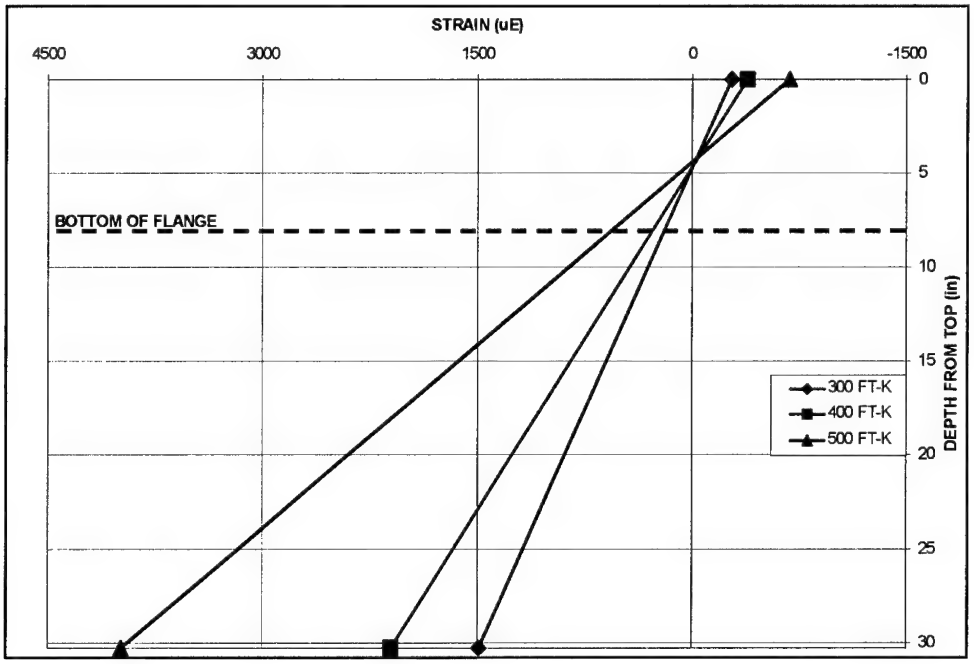

Figure 59. Strain plot for Beam A3_Test2

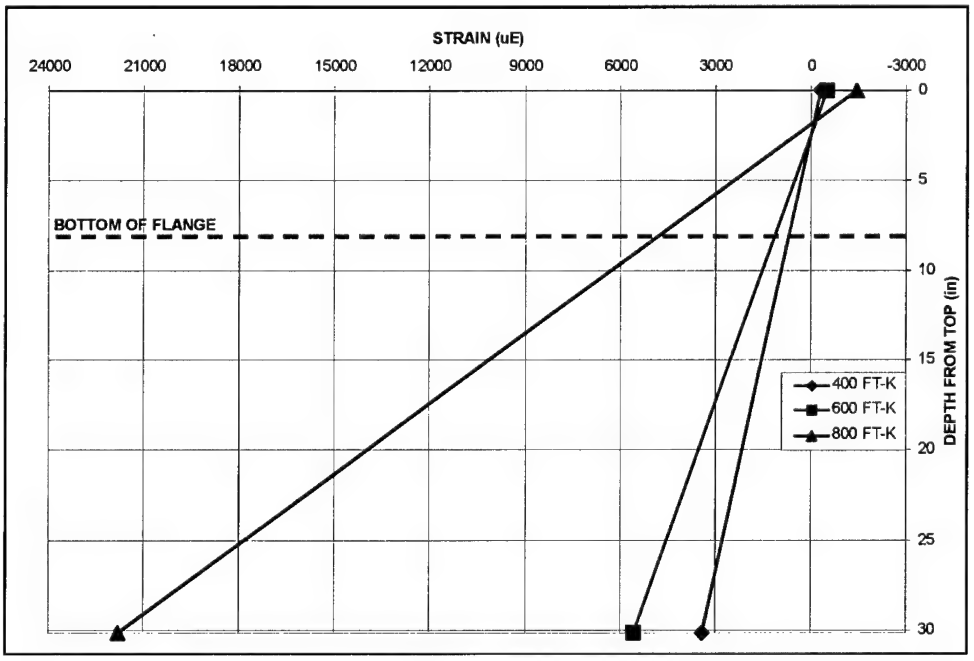

Figure 60. Strain plot for Beam A5_Test1

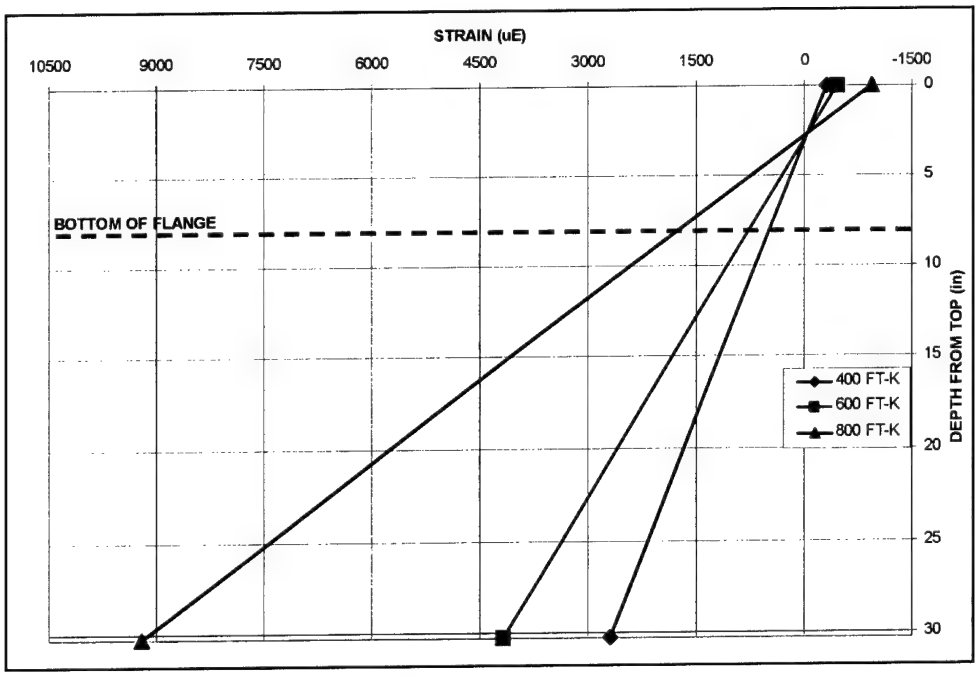

Figure 61. Strain plot for Beam A5_Test2

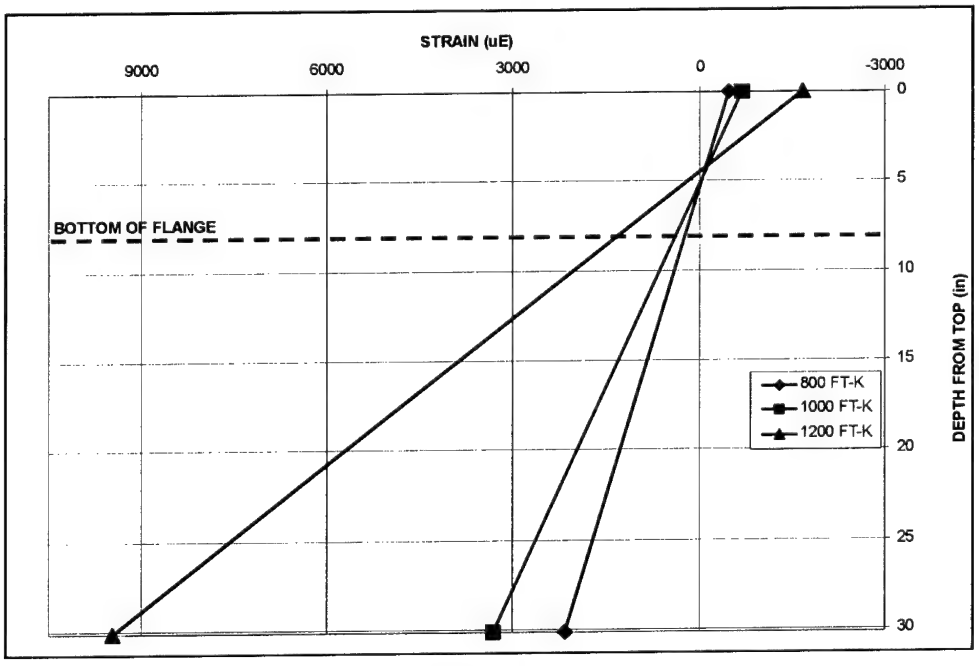

Figure 62. Strain plot for Beam A8_Test1

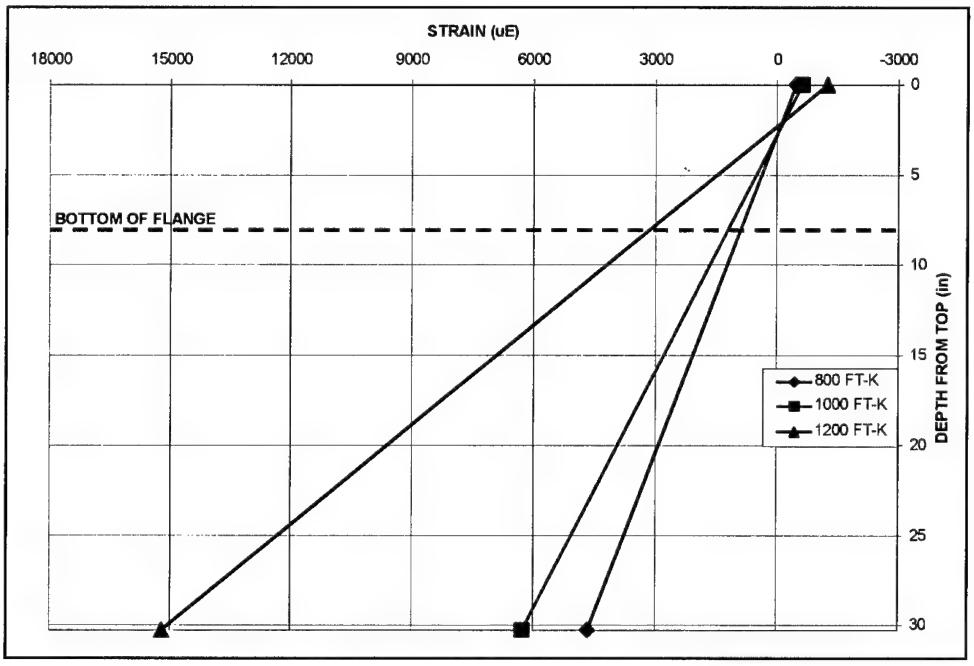

Figure 63. Strain plot for Beam A8_Test2

10 Analytical Modeling of T-Beam Behavior

An analytical model was developed to predict the behavior of reinforced concrete beams strengthened with fiber reinforced polymer (FRP) strips and powder actuated fasteners in order to further understand the factors that effect the strengthening. In addition to predicting the behavior of a strengthened beam, the analytical model can be used in to develop a design procedure for strengthening beams using mechanically fastened FRP strips.

There are three primary models that are typically developed to predict the response of RC beams; strength, moment-curvature, and load-deflection. Strength models predict the ultimate capacity of the section, moment-curvature models predict the behavior of the section through the entire loading regime, and load-deflection models predict the behavior of the entire member throughout the entire loading regime. In this section, moment-deflection is used synonymously with load-deflection.

All three of these models utilize equilibrium, strain compatibility of the cross sections, and the constitutive relations of the materials. Several assumptions were made in this research in developing these analytical models:

a. Plane sections remain plane during bending (MacGregor 1997). This means there exists a linear variation in strain over the cracked concrete cross section, in the concrete, steel reinforcement, and FRP strip. This assumption is supported by strain data obtained during the large scale testing, and is valid even after the reinforcing steel has yielded. This assumption neglects the effect of slip between the steel reinforcing bars and the surrounding concrete and the slip between the FRP strip and the concrete surface.

b. The concrete stress-strain relationship in tension behaves linearly until rupture, and then carries no load. This assumption neglects the tension stiffening effect. Extensive calculations have shown that tension stiffening is not significant in the case of FRP reinforced concrete members (Razaqpur 2000).

c. The FRP strip is modeled as a membrane. It can support axial load but has zero bending stiffness. The height of the FRP strengthening strip is much less than the height of the concrete beam, and therefore has a

negligible bending stiffness compared to the bending stiffness of the reinforced concrete beam.

d. There is uniform stress and strain across the width of the FRP strip. This assumption ignores shear lag and assumes there is no variation in stress across the width of the strip. Small-scale test results show that shear lag can be minimized by using two rows of fasteners across the width of a strengthening strip as opposed to one.

e. The strengthening strip does not affect shear strength. This neglects any increase in shear capacity through dowel action of the strip. Dowel action is usually neglected when determining shear strength of FRP reinforced concrete members (ACI 440F and ACI 440H). It is assumed that the cracks formed from attaching the strip are small enough to maintain aggregate interlock.

f. The fasteners in the shear span transfer the entire load between the concrete and FRP strip. This assumption is supported by the strain distributions obtained during the full scale testing.

g. The fasteners in the shear span transfer the entire load between the concrete and FRP strip. This assumption is supported by the strain distributions obtained during the full scale testing.

Review Of Moment-Curvature Model

A moment-curvature model is used to predict the behavior of a section at any load. An iterative method is used which increases the strain in the top compression fiber of the concrete until the concrete crushes, tensile steel ruptures, or the FRP strip ruptures or detaches. A moment-curvature model can be used instead of a strength model if the section will fail by any mode other than concrete compression.

In the model developed for this research, the steel is assumed to exhibit a bilinear stress-strain behavior. A postyield modulus equal to 1.7 percent of the initial elastic modulus was used (Soroushian and Choi 1991). The concrete in compression is assumed to follow the stress-strain model developed by Park and Paulay (1975), shown schematically in Figure 64. This model is similar to the Hognestad model for concrete in compression (Hognestad 1951), except that Park and Paulay fix ε_o as 0.002 in their model. Hognestad recommends expressing the parabola in region 1 in the form

$$f_c = f_c^{"}\left[2\frac{\varepsilon_c}{\varepsilon_o} - \left(\frac{\varepsilon_c}{\varepsilon_o}\right)^2\right] \qquad (1)$$

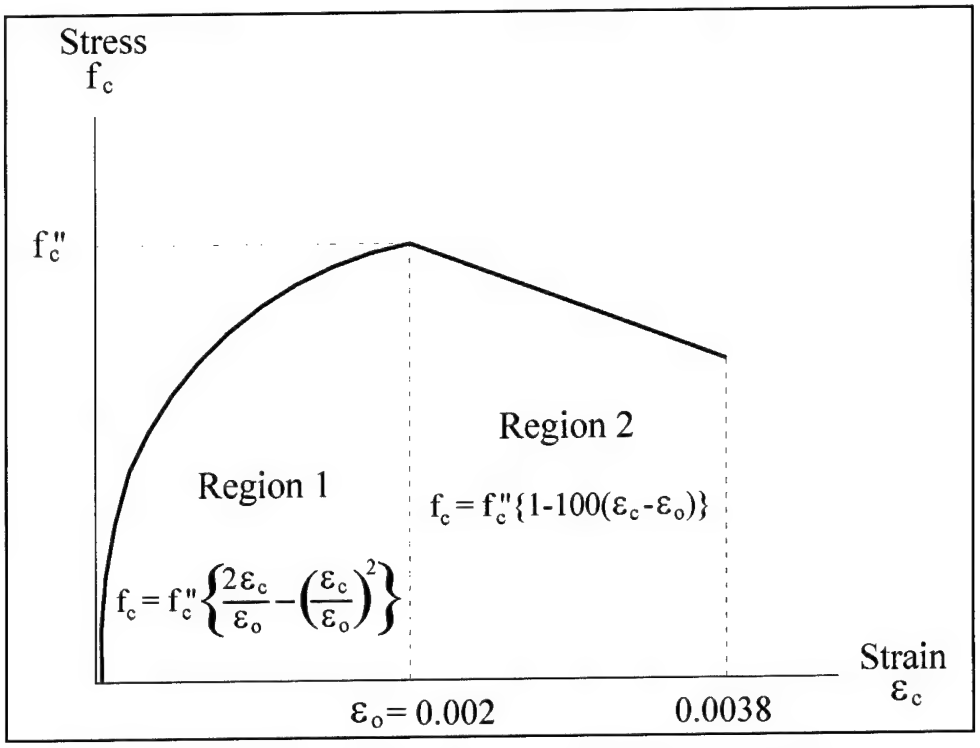

Figure 64. Schematic of concrete stress-strain behavior developed by Park and Paulay (1975)

The linear strain distribution through the cross section is shown in Figure 65. The concrete forces in tension, which are only used before the concrete cracks in tension, are not shown in Figure 65 for clarity. The strain in the compression steel, tensile steel, FRP strengthening strip, and bottom tension fiber in the concrete can be found in terms of the strain in the concrete as follows

$$\varepsilon_{cs} = \frac{\varepsilon_c}{c}(c - d_{cs}) = \varepsilon_c\left(1 - \frac{d_{cs}}{c}\right) \tag{2}$$

$$\varepsilon_s = \frac{\varepsilon_c}{c}(d - c) = \varepsilon_c\left(\frac{d}{c} - 1\right) \tag{3}$$

$$\varepsilon_{con} = \frac{\varepsilon_c}{c}(h - c) = \varepsilon_c\left(\frac{h}{c} - 1\right) \tag{4}$$

$$\varepsilon_{con} = \frac{\varepsilon_c}{c}(h - c) = \varepsilon_c\left(\frac{h}{c} - 1\right) \tag{5}$$

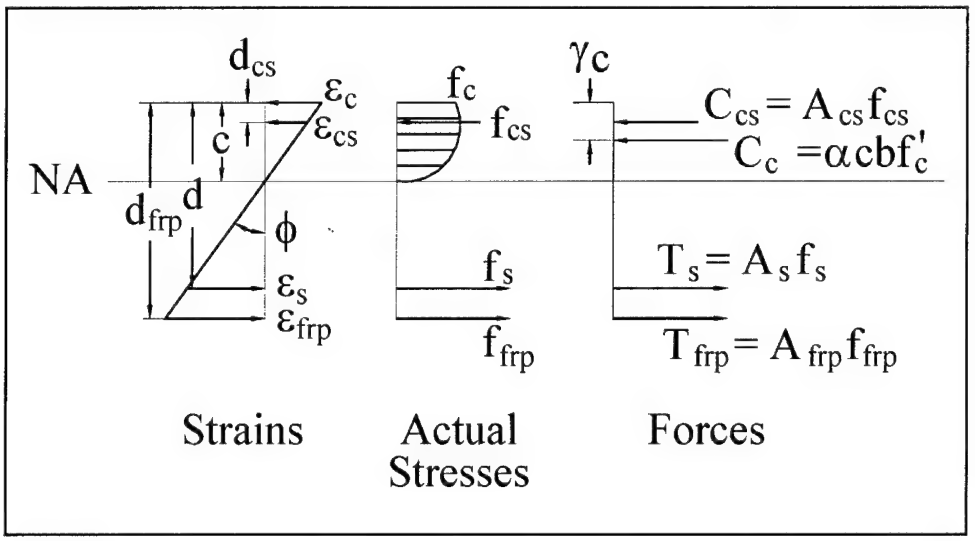

Figure 65. Strains, stresses, and forces used in the moment-curvature model

The corresponding stresses in the cross section under the given linear strain distribution and the corresponding resultant forces are also shown in Figure 65. This is different than a strength model in the location of the concrete compression force, the magnitude of the concrete compression force, and the addition of the compression steel force. The concrete compression force is located using a location factor γ applied to the depth of the neutral axis c. The magnitude is determined using a magnitude factor α. These factors are derived from the Park and Paulay model. These location and magnitude factors are

$$\gamma = \begin{cases} \dfrac{1/3 - 41.7\varepsilon_c}{1 - 166.7\varepsilon_c} & for\ \varepsilon_c \le 0.002 \\ 1 - \dfrac{-25\varepsilon_c^3 + 0.575\varepsilon_c^2 - 0.0000004}{-37.5\varepsilon_c^3 + 1.15\varepsilon_c^2 - 0.000817\varepsilon_c} & for\ 0.002 < \varepsilon_c \le 0.0038 \end{cases} \quad (6)$$

$$\alpha = \begin{cases} -83{,}000\varepsilon_c^2 + 500\varepsilon_c & for\ \varepsilon_c \le 0.002 \\ 1.15 - 37.5\varepsilon_c - \dfrac{0.000817}{\varepsilon_c} & for\ 0.002 < \varepsilon_c \le 0.0038 \end{cases} \quad (7)$$

Applying equilibrium to forces acting on the cross section gives

$$C_c + C_{cs} - T_s - T_{frp} - C_{ct} = 0 \quad (8)$$

Rewriting Equation 8 in terms of stresses gives

$$\alpha c b f_c' + A_{cs} f_{cs} - A_s f_s - A_{frp} f_{frp} - \frac{b}{2}(h-c) f_{con} = 0 \quad (9)$$

Using the stress-strain relationships for steel and FRP, this equation becomes

$$\alpha c b f_c' + A_{cs} E_s \varepsilon_{cs} - A_s E_s \varepsilon_s - A_{frp} E_{frp} \varepsilon_{frp} - \frac{b}{2}(h-c) E_c \varepsilon_{con} = 0 \quad (10)$$

Before the concrete has cracked or the tensile steel has yielded, using Equations 2, 3, 4, and 5, Equation 10 becomes

$$\begin{aligned} &\alpha c b f_c' + A_{cs} E_s \varepsilon_c \left(1 - \frac{d_{cs}}{c}\right) - A_s E_s \varepsilon_c \left(\frac{d}{c} - 1\right) \\ &- A_{frp} E_{frp} \varepsilon_c \left(\frac{d_{frp}}{c} - 1\right) - \frac{b}{2}(h-c) E_c \varepsilon_c \left(\frac{h}{c} - 1\right) = 0 \end{aligned} \quad (11)$$

Once the tensile stress in the extreme bottom tensile fiber of the concrete exceeds the tensile strength of concrete in flexure, the concrete in tension cracks. Once the section is cracked, all concrete below the neutral axis is neglected. The tensile strength of concrete in flexure is typically 15 percent of the compressive strength (Mehta and Monteiro 1993).

After the concrete has cracked in tension, Equation 11 becomes

$$\alpha c b f_c' + A_{cs} E_s \varepsilon_c \left(1 - \frac{d_{cs}}{c}\right) - A_s E_s \varepsilon_c \left(\frac{d}{c} - 1\right) - A_{frp} E_{frp} \varepsilon_c \left(\frac{d_{frp}}{c} - 1\right) = 0 \quad (12)$$

After the tensile steel has yielded, Equation 12 becomes

$$\alpha c b f_c' + A_{cs} E_s \varepsilon_c \left(1 - \frac{d_{cs}}{c}\right) - A_s \left[f_y + E_{pys}\left(\varepsilon_c \left[\frac{d}{c} - 1\right] - \frac{f_y}{E_s}\right)\right] - A_{frp} E_{frp} \varepsilon_c \left(\frac{d_{frp}}{c} - 1\right) = 0 \quad (13)$$

Equations 11, 12, and 13 are quadratic equations in terms of c that can be solved in closed form. The strain in the top compression fiber of the concrete, ε_c, is chosen to be a certain value, and the magnitude factor α is calculated based on the chosen value of ε_c. The depth to the neutral axis can then be found by using either Equation 11, 12 or 13, depending on whether or not the tensile concrete has cracked or if the tensile concrete has cracked and the tensile steel has yielded. The moment on the cross section can be found by taking the sum of moments about the concrete force resultant. Equation 14 is used when the tensile concrete has not cracked, and Equation 15 is used when the tensile concrete has cracked, whether or not the tensile steel has yielded.

$$M_{mc} = A_s f_s (d - \gamma c) + A_{frp} f_{frp} (d_{frp} - \gamma c) + A_{cs} f_{cs} (\gamma c - d_{cs}) + \frac{b}{3} f_{con} (h-c)^2 \quad (14)$$

$$M_{mc} = A_s f_s (d - \gamma c) + A_{frp} f_{frp} (d_{frp} - \gamma c) + A_{cs} f_{cs} (\gamma c - d_{cs}) \quad (15)$$

The corresponding curvature can be found from

$$\phi = \arctan\left(\frac{\varepsilon_c}{c}\right) \quad (16)$$

For any given strain in the top compression fiber of the concrete, the moment-curvature relationship can be found. The entire moment-curvature relationship is found by incrementally increasing the strain in the top fiber until the stress in one of the material components exceeds the ultimate strength of that material. First, Equations 10 and 14 are used to find the depth to the neutral axis and the moment. Once the concrete cracks in tension, Equations 12 and 15 are used. Then once the tensile steel yields Equations 13 and 15 are used. It should be noted that the concrete at the top fiber may be in a state of less stress than concrete lower in the section if the extreme concrete strain is greater than 0.002. For this reason, the maximum compressive strain is used as a limit in the compression concrete, as opposed to a maximum stress, as with the reinforcing steel and FRP strengthening strip. At each strain increment, after the depth to the neutral axis c is found, the stress in the FRP strip is calculated by

$$f_{frp} = E_{frp} \varepsilon_c \left(\frac{d_{frp}}{c} - 1\right) \quad (17)$$

If $f_{frp} \leq f_{yfrp}$, then the FRP strip does not rupture before the concrete crushes at this increment of strain in the top concrete compression fiber.

Modification to Moment-Curvature Model for Fastened Strips

For the new method of attaching the FRP strip to the concrete using mechanical fasteners, the fastened connection between the concrete and the FRP strengthening strip must be checked. It should be noted that predictions for strip delamination, either from the center out or from the end inwards are determined based on member properties, such as number of fasteners, fastener layout, and loading pattern, rather than section properties. The tensile force in the FRP can be calculated using

$$T_{frp} = A_{frp} E_{frp} \varepsilon_c \left(\frac{d_{frp}}{c} - 1\right) \quad (18)$$

The maximum load per fastener is then calculated using

$$P_f = \frac{T_{frp}}{N_s} \quad (19)$$

If the maximum load per fastener P_f exceeds the allowable load per fastener, the section will fail by gross fastener failure. Gross fastener failure occurs when the fasteners cannot transfer the force required from the concrete to the FRP strip.

This strip delamination failure is initiated from the interior of the beam and progresses outward toward one or both of the supports. The model does not differentiate fastener failure by bearing failure in the FRP strip or by concrete pryout failure.

Another failure mode observed during experiments is a strip delamination from the end of the strip. This failure occurs in beams where the strip and the end fasteners are terminated too far from the support. A close up of this region is shown in Figure 66. The section between the end fasteners and the support is unstrengthened, even though the FRP strip continues past the end fasteners and the support. The strip in this region is not connected to the concrete, and does not interact with the section in this region. The section from the end fasteners to the interior of the beam is strengthened, as the FRP strip is attached with fasteners throughout the length.

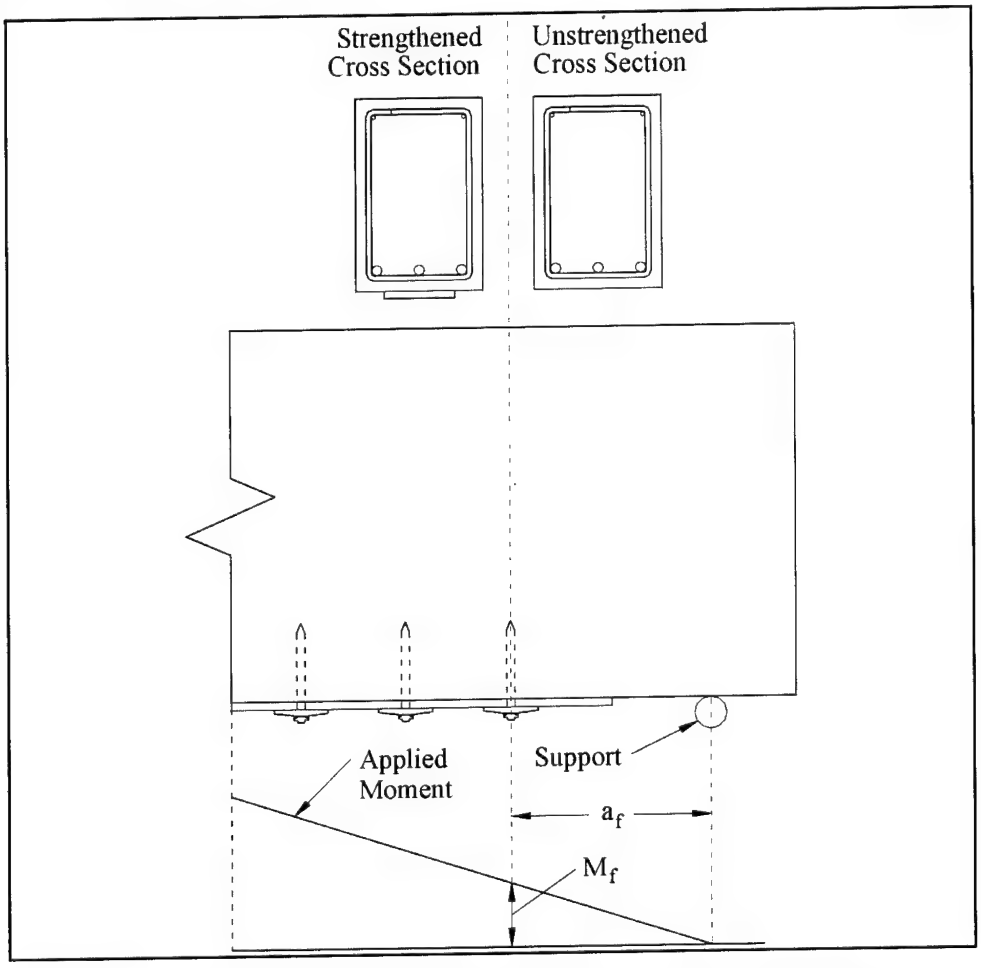

Figure 66. Close-up of end fastener distance, and applied moment diagram

At the location of the end fasteners, a distance a_f from the support, there is an applied moment M_f, caused by the applied load. The farther the end fasteners are from the support, the greater the applied moment M_f at the end fasteners will be. The strengthened section must carry this moment. Under this applied moment,

the tensile force developed in the FRP strip must be transferred to the concrete beam only through the end fasteners. The load per end fastener can be found by

$$P_{ef} = \frac{T_{f,frp}}{N_{ef}} \tag{20}$$

If $P_{ef} \leq F_{efu}$, then end fastener failure will not occur. Currently, the same value is used for both F_{efu} and F_{fu}. The value of F_{efu} is also dependant on the distance the FRP strip extends beyond the last set of fasteners toward the support. A minimum of 50.8 mm (2 in.) has been used in all tests, which has been sufficient to prevent cleavage failure in the FRP strip at the end fasteners. Figure 67 shows the flow chart for the procedure that includes checking for end fastener failure for developing the moment-curvature relationship for a beam.

Moment-Deflection Model

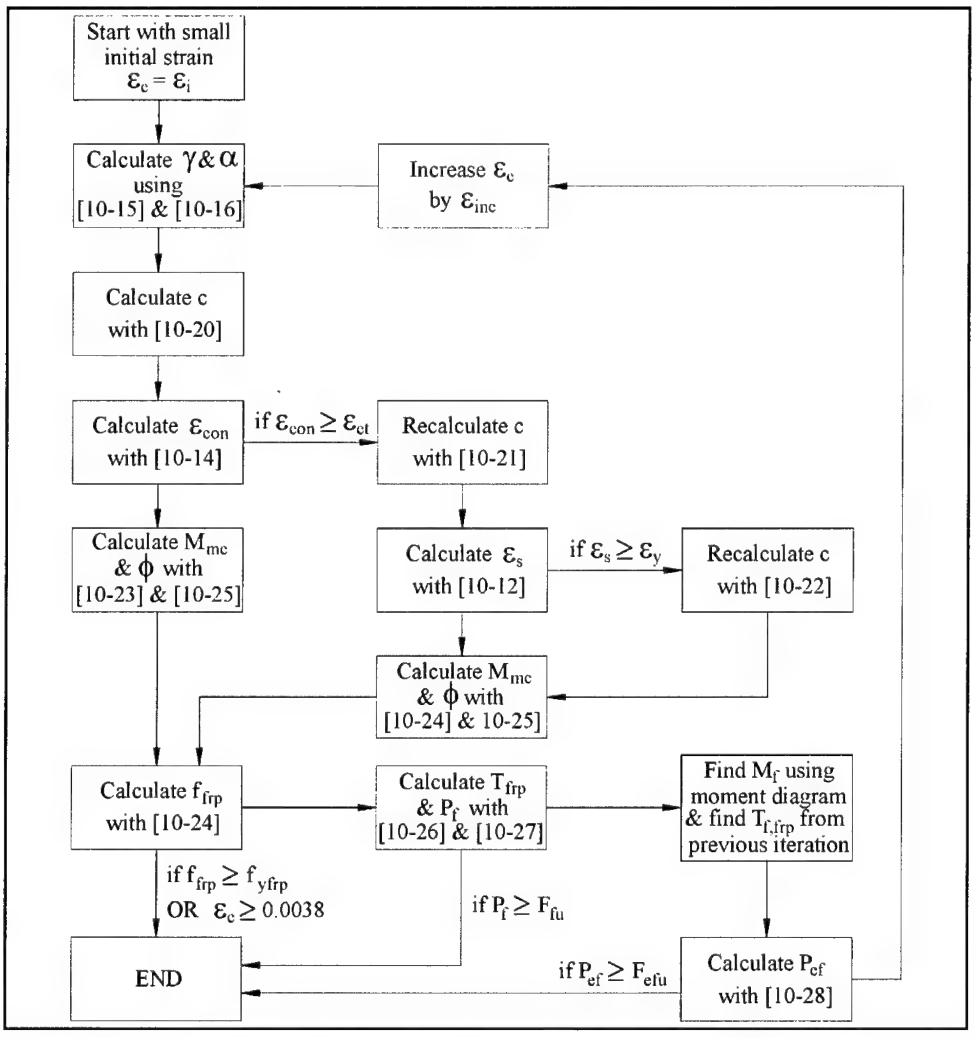

Figure 67. Flow chart showing the procedure that includes checking for end fastener failure for developing the moment-curvature relationship for a beam

A moment-deflection model is used to predict the moment-deflection behavior of a reinforced concrete beam strengthened with an FRP strip and mechanical fasteners. In design, serviceability criteria are given in terms of deflections rather than curvature. In experiments, the deflection is measured rather than the curvature. It is difficult to predict the deflection of reinforced concrete beams. ACI Committee 435 found that deflections calculated using the ACI Code criteria for simply supported beams under controlled laboratory conditions "will be within the range of 20 percent less than to 30 percent more than the calculated value" about 90 percent of the time.

A virtual work approach, similar to the approach used by Razaqpur (2000), can be used to determine the deflection. The basis of the principle of virtual work is

$$W_{ve} = W_{vi} \tag{21}$$

where W_{ve} is the virtual external work, and W_{vi} is the virtual internal work (Kassimali 1999).

In order to apply the principle of virtual work to the beams considered in this research, the moment diagram of the beam was broken up along its length into eight sections, as shown in Figure 68. This analysis only applies to the four point loading considered in this research. The deflection at the center can be written as

$$\delta_c = \sum_{i=1}^{8} \int m_i(x)\, \phi_i(x)\, dx \tag{22}$$

Since the moment diagrams for both the actual two-point loading and the virtual point load are symmetrical about the mid span of the beam, Equation 22 can be rewritten as

$$\delta_c = 2\sum_{i=1}^{4} \int m_i(x)\, \phi_i(x)\, dx \tag{23}$$

Where m_i is the moment at point x along the beam caused by the unit virtual load at the center of the beam, for each section i.

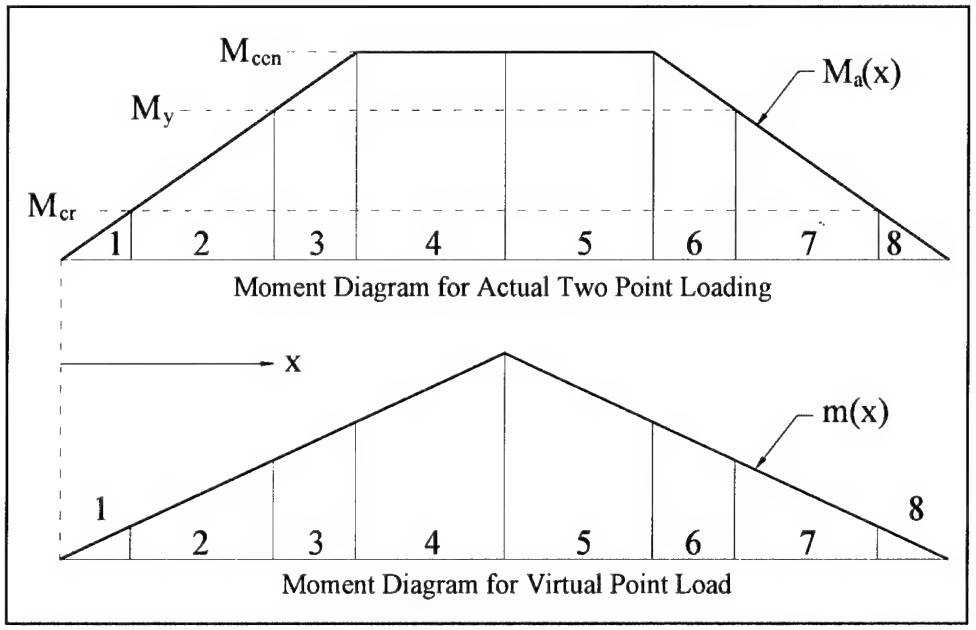

Figure 68. Actual and virtual moment diagrams used in the moment-deflection model

It is assumed that the curvature developed by the moment-curvature model can be expressed in terms of the moment as three quadratic polynomials

$$\phi_{cr}(x) = a_{cr} + b_{cr}[M_a(x)] + c_{cr}[M_a(x)]^2 \quad (24)$$

$$\phi_y(x) = a_y + b_y[M_a(x)] + c_y[M_a(x)]^2 \quad (25)$$

$$\phi_u(x) = a_u + b_u[M_a(x)] + c_u[M_a(x)]^2 \quad (26)$$

Equation 24 is used to fit the curve before the section is cracked; Equation 25 is used to fit the curve between the section cracking and the tensile steel yielding; Equation 26 is used to fit the curve after yield up to ultimate strength. The beam is not cracked in sections 1 and 8, so the coefficients a_{cr}, b_{cr}, and c_{cr} are used for these sections. Sections 2 and 7 are beyond the cracking moment, but below the yield moment, so the coefficients a_y, b_y, and c_y are used for these sections. Sections 3-6 are above yield, so the coefficients a_u, b_u, and c_u are used for these sections.

Figure 68 shows the case where the moment in the center of the beam, M_{cen}, is above yield. The method of virtual work simplifies to 6 sections when M_{cen} is below the yield moment, and simplifies even further to 4 sections when M_{cen} is below the cracking moment. The actual moment is developed based on the length of the beam, location of the two load points, and the applied moment in the center of the beam. This actual moment is then expressed in terms of curvature, using Equations 24, 25, and 26. Thus for a given applied moment in the center of the beam, M_{cen}, a mid span deflection can be calculated utilizing the method of virtual work in unison with the curvature-moment relationship derived from the moment-curvature behavior of the cross section.

Implementation of the Analytical Model

The objective of implementing the analytical model was to automate the analytical theories to develop first the moment-curvature, and then the moment-mid span deflection curves for strengthened and unstrengthened beams.

To automate the analytical model, a computer program was written in the MathCad programming language developed by MathSoft, Inc. (Mathsoft 1999). The first portion of the computer program followed the flow chart previously shown in Figure 67 to develop the moment-curvature curve for the cross section. The second portion used MathCad's built in "linfit" function to fit Equations 22, 23, and 24 to the precracked, preyield, and postyield portions of the moment-curvature data.

In order to prevent a discontinuity when the tensile steel yielded, the Equation 26 was forced through the yield point of the moment-curvature curve with the routine shown in Figure 69. The first line is the sum of the squares to be minimized. The index is over the moment-curvature pairs after and including the yield. The first condition after the "given" sets the sum of the squares of the error to zero, and the second condition forces Equation 26 to pass through the yield point of (ϕ_y, M_y). The final statement finds the three coefficients a_u, b_u, and c_u that provide the minimum error when solving the two conditions. Figure 70 shows the moment-curvature pairs developed by the moment-curvature model in the vicinity of the yield point plotted with Equation 26 and Equation 26 forced through the yield point.

$$SSE\left(a_u, b_u, c_u\right) := \sum_i \left[\phi_i - \left[a_u \cdot \left(m_i\right)^2 + b_u \cdot \left(m_i\right) + c_u \right] \right]^2$$

Given

$$SSE\left(a_u, b_u, c_u\right) = 0$$

$$\phi_y - \left[a_u \cdot \left(M_y\right)^2 + b_u \cdot \left(M_y\right)^2 + c_u \right] = 0$$

$$\begin{pmatrix} a_u \\ b_u \\ c_u \end{pmatrix} := \text{Minerr}\left(a_u, b_u, c_u\right)$$

Figure 69. The MathCad routine used to force Equation 24 through the yield point

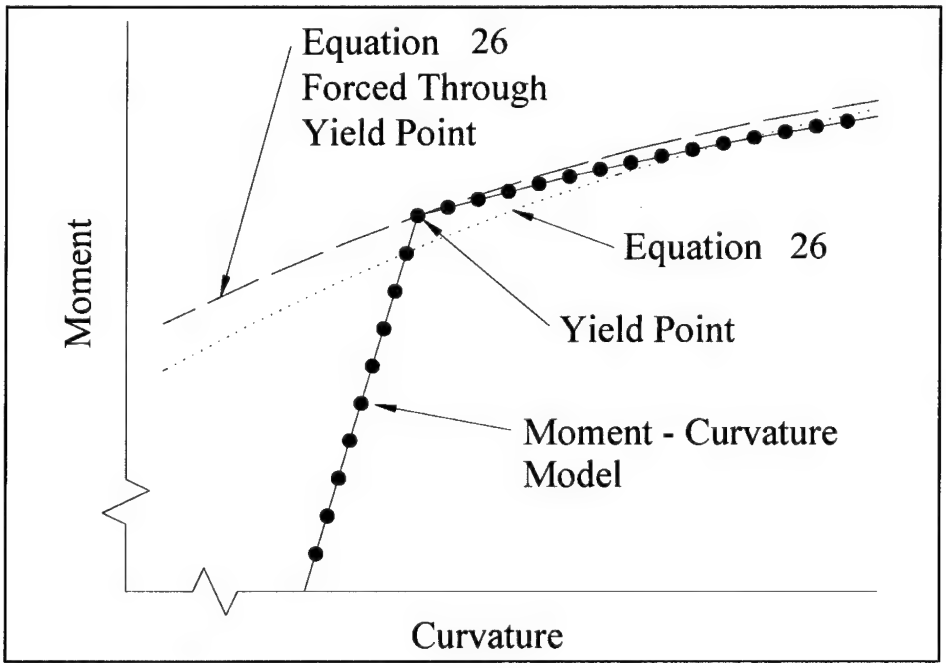

Figure 70. Moment-curvature pairs developed by the moment-curvature model in the vicinity of the yield point plotted with Equation 26 and Equation 26 forced through the yield point

The model then uses Equations 24, 25, and 26 and the equation for $m_i(x)$ developed form the virtual moment diagram in Equation 23 to solve for the deflection at the mid span of the beam. The program provides the following variables at mid span for a beam in four point loading: strain in the top concrete fiber, depth to the neutral axis, stress in the tensile steel, stress in the compression steel, stress in the FRP strip, tensile stress in the bottom concrete fiber, curvature, moment, total load, FRP strength check, gross fastener strength check, tensile steel yield check, vertical displacement, load per end fastener, and end fastener strength check. The output is provided for both a strengthened beam and an unstrengthened beam.

Model Versus T-Beam Experimental Data

The objective of this portion of the research was to compare the analytical predictions to the results of the testing of large T-beams described previously in Chapter 8. Figure 71 shows a cross-section of the T-beam, and Figure 72 is a picture of the T-beam prior to testing.

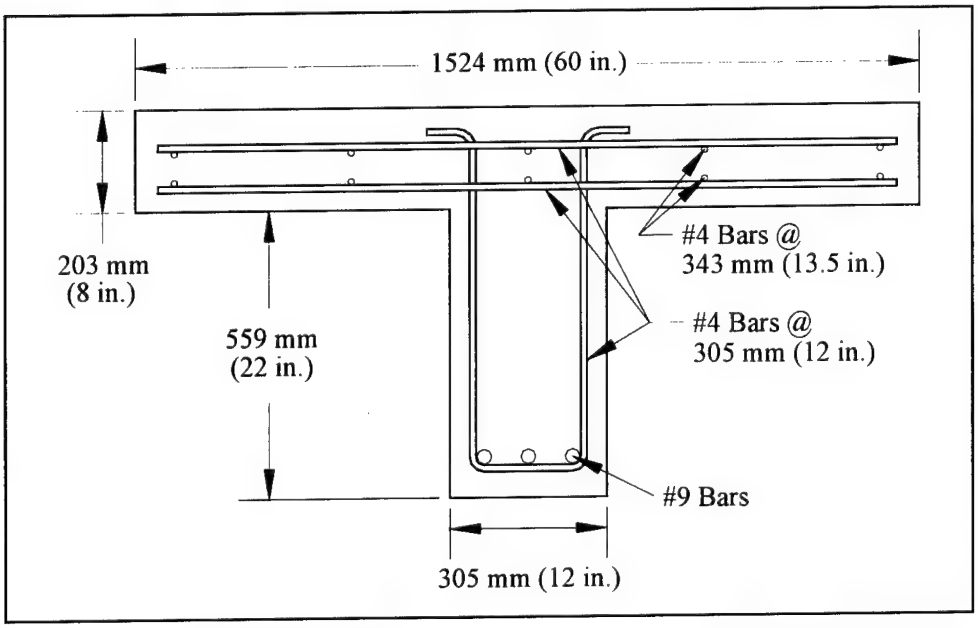

Figure 71. Schematic of the cross section of T-beams

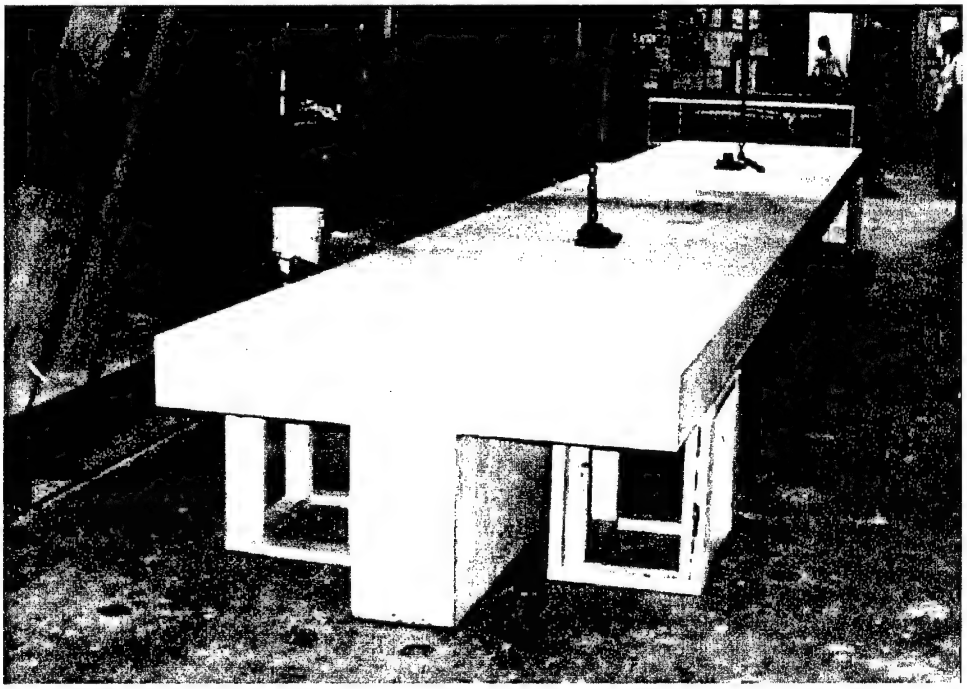

Figure 72. Picture of a T-beam

The beams tests were terminated at an actuator stroke of 6 in. This was the limit of the hydraulic actuators, and occurred before the ultimate strength of all but one the T-beams was reached. For this reason, the yield points are examined, as well as the data at a mid span deflection of 2.5 in., which corresponds to a deflection of approximately L/135, which is a much greater deflection than would be seen in normal usage. AASHTO limits deflections in members having simple or continuous spans to L/800 (Taly 1998).

The experimental and calculated yield moment and yield deflection for the T-beams are compared in Table 10. It can be seen in this table that the yield moment is predicted quite closely, the calculated/actual value ranging from 0.98 to 1.10. The calculated yield deflection is very close for the lighter reinforced A3 beams, ranging from 0.93 to 1.03; however, the calculated yield deflection for the A5 and A8 beams is less than the actual deflection. It appears from Table 10 that the analytical model under predicts the deflections for the more heavily reinforced beams A5 and A8. The under prediction is more for the beams with the heaviest reinforcement.

Table 10. Experimental and Calculated Yield Moment and Yield Deflection for the T-Beams

Beam	Experimental Yield Moment (k-ft)	Calculated Yield Moment (k-ft)	Calc Exp	Experimental Yield Deflection (in.)	Calculated Yield Deflection (in.)	Calc Exp
A3_Control	352	386	1.09	0.95	0.95	1.00
A3_Test1	380	409	1.08	0.95	0.98	1.03
A3_Test2	393	432	1.10	1.05	0.98	0.93
A5_Control	623	611	0.98	1.10	1.05	0.95
A5_Test1	637	634	1.00	1.25	1.06	0.85
A5_Test2	660	658	1.00	1.25	1.06	0.85
A8_Control	950	926	1.02	1.50	1.16	0.77
A8_Test1	960	950	0.99	1.50	1.16	0.77
A8_Test2	993	974	0.98	1.55	1.16	0.75

The experimental and calculated moment at a mid span deflection of 63.5 mm (2.5 in.) of the T-beams is shown in Table 11. It can be seen that the calculated moment predicts the experimental moment closely, the calculated / experimental ranging from 0.97 to 1.16. All nine of the predictions are reasonable. The moment-deflection curves for the control beams are shown in Figure 73, the curves for the beams strengthened with a single strip are shown in Figure 74, and the curves for the beams strengthened with a double thickness strip are shown in Figure 75.

Table 11. Experimental and Calculated Moment at a Mid-Span Deflection of 2.5 in.

Beam	Experimental Moment at 2.5 in., k-ft	Calculated Moment at 2.5 in., k-ft	Calc Exp
A3_Control	423	428	1.01
A3_Test1	484	541	1.12
A3_Test2	538	627	1.16
A5_Control	684	667	0.98
A5_Test1	705	768	1.09
A5_Test2	797	850	1.07
A8_Control	1,030	997	0.97
A8_Test1	1,070	1,090	1.02
A8_Test2	1,110	1,172	1.06

It can be seen in Figures 73, 74, and 75 that the analytical prediction is very close to the actual. The experimental data for beam A5 ends at a deflection of about 51 mm (2 in.) because researchers stopped the test prematurely. In the uncracked region, it is clear that the analytical curves are stiffer than the experimental curves. This is related to the fact that material properties are assumed for concrete are the properties that are acquired from coupon specimens and not directly from the reinforced concrete beams (Arduini et al. 1997).

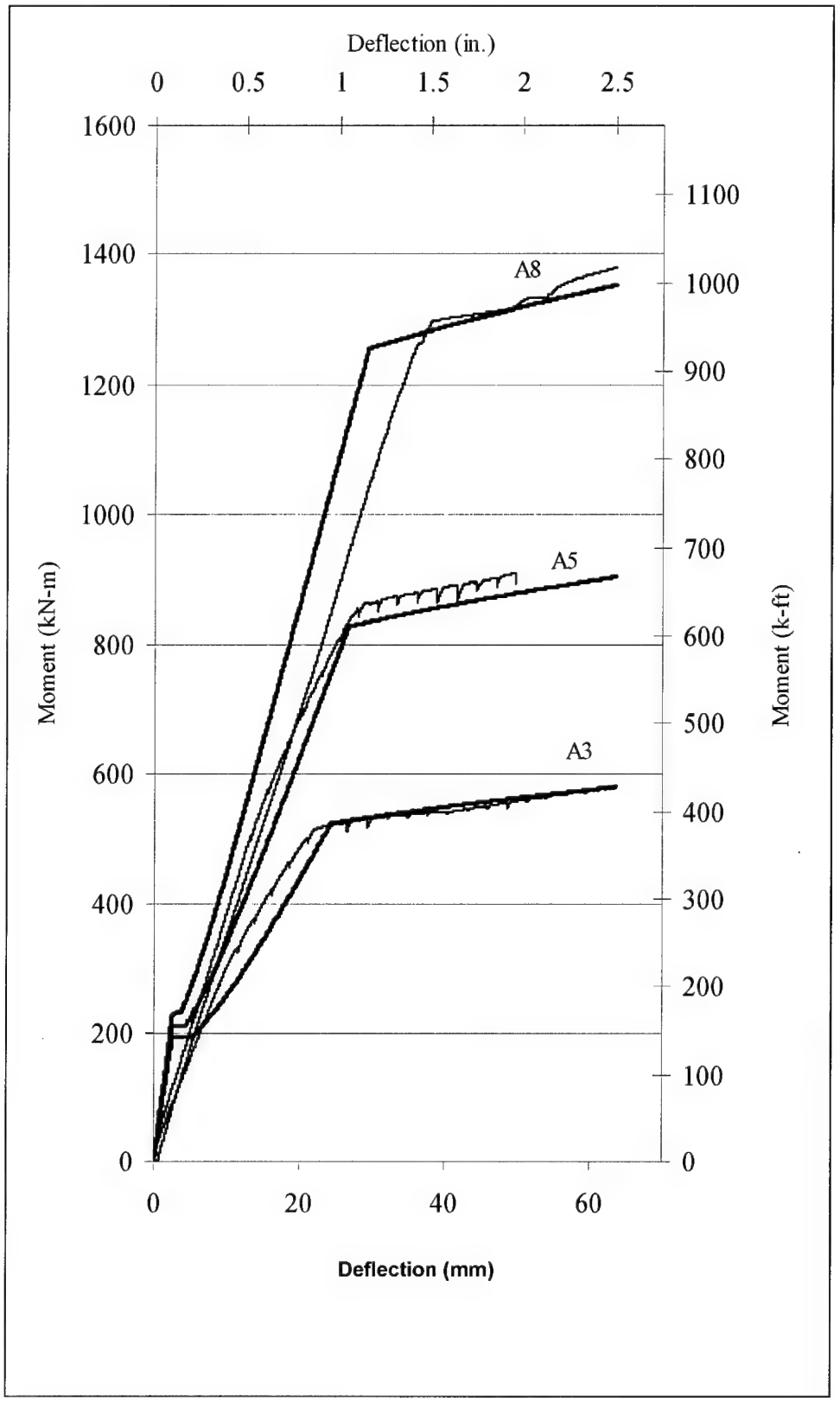

Figure 73. The analytical and experimental moment-deflection curves for the control beams (The predictions are shown bold)

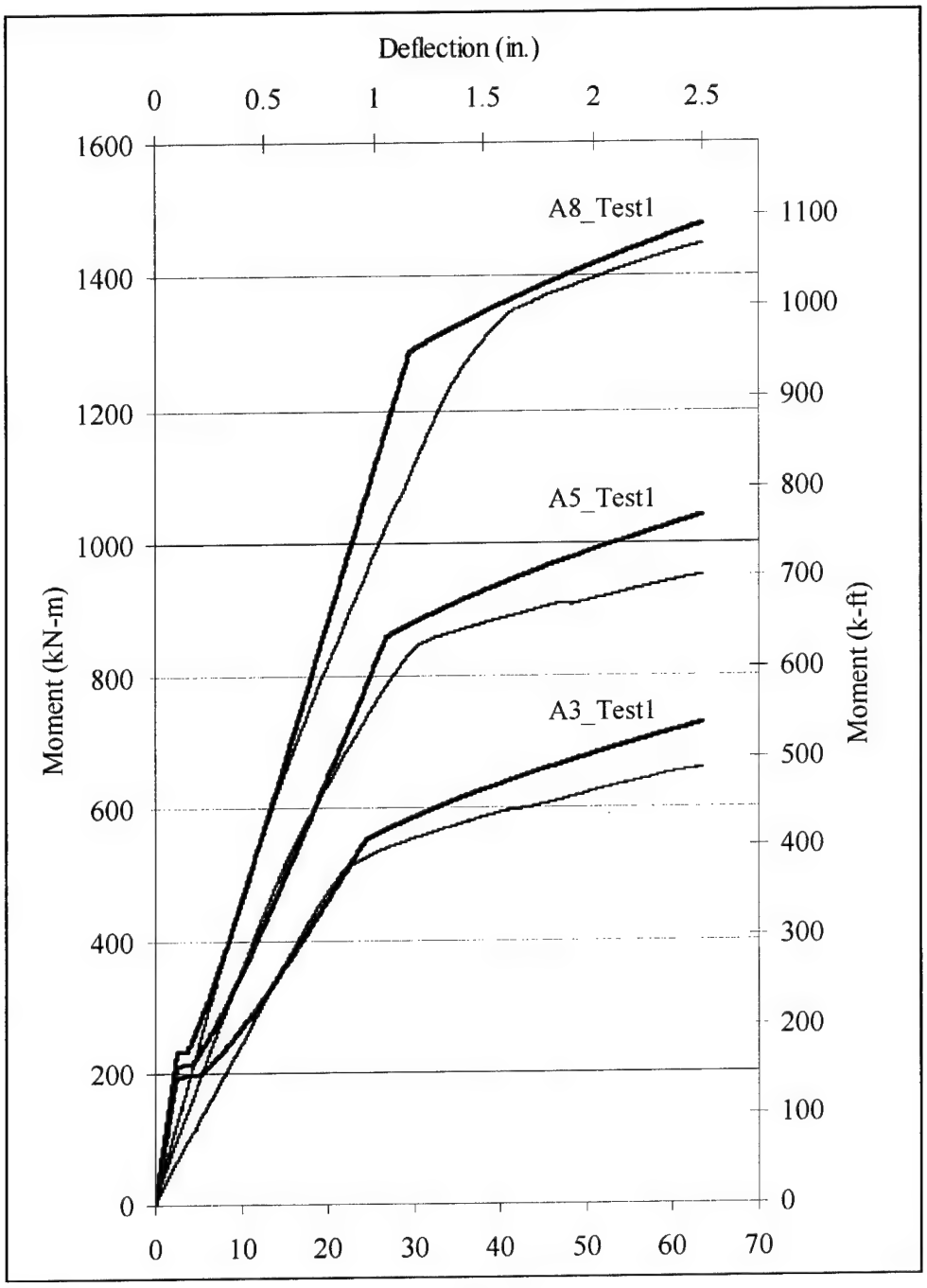

Figure 74. The analytical and experiment moment-deflection curves for the strengthened Beams A3_Test1, A5_Test1, and A8_Test1 (The predictions are shown bold)

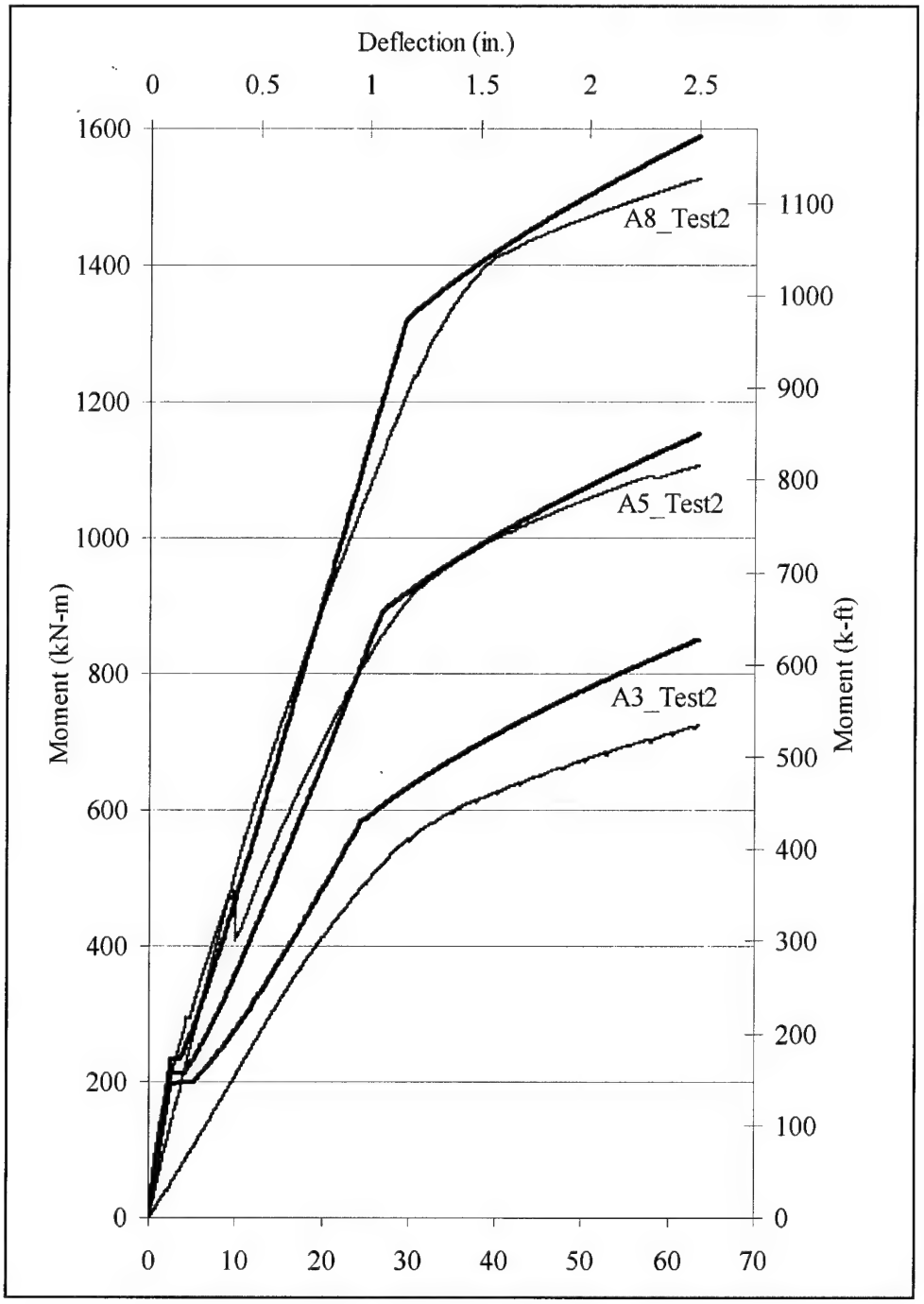

Figure 75. The analytical and experimental moment-deflection curves for the strengthened Beams A3_Test2, A5_Test2, and A8_Test2 (The predictions are shown bold)

The predicted curves for all nine T-beams are shown in Figure 76. It can be seen that the amount in kN-m (k-ft) a single strip strengthens a control beam is the about same for all three control beams; however, this amount is smaller as a percentage of the total strength as the amount of reinforcement in the original control beam increases. This supports the fact that it is more difficult to strengthen heavily reinforced beams. It is also clear from Figure 76 that the stiffness of a control beam increases when a single strip is attached, and increases even more when two strips are attached.

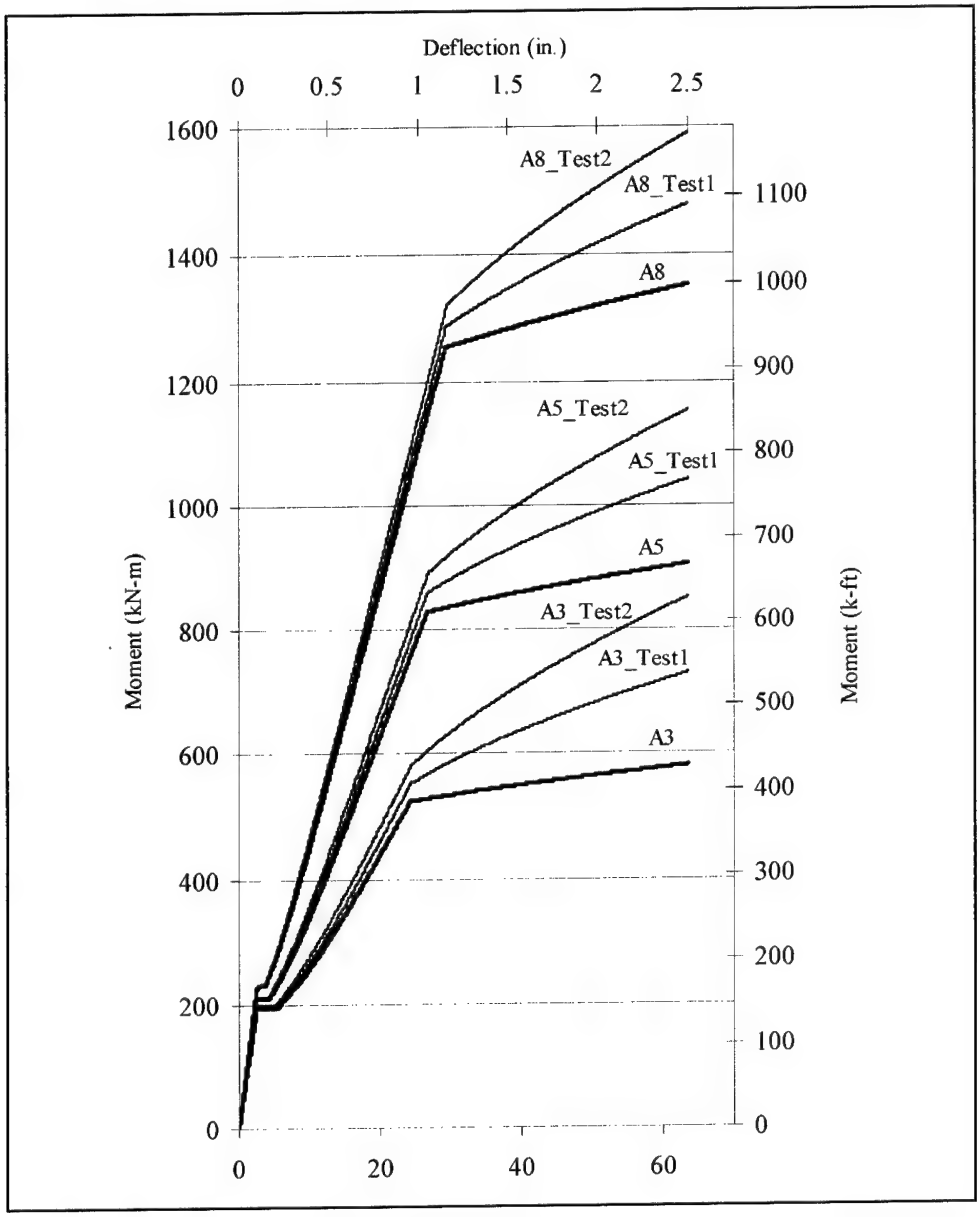

Figure 76. The predicted curves for all nine T-beams

11 Further Investigation of Key Factors Affecting Strengthening

The results from the full-scale T-beam testing prompted researchers to explore some additional issues on large-scale beams. The effects of termination length, size of shear span, and fatigue all came into question after the T-beam testing. As such, ten beams (12 in. x12 in. x 144 in.) were constructed and additional tests conducted. A graphical depiction of the beams' cross-section is shown in Figures 77 and 78. Complete construction details are provided in Appendix B.

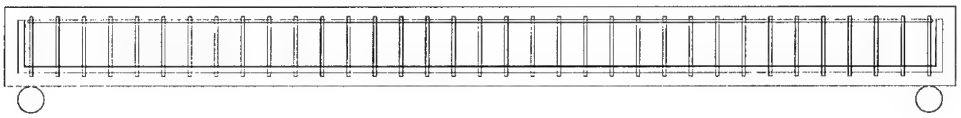

Figure 77. View of reinforcement for large-scale beams

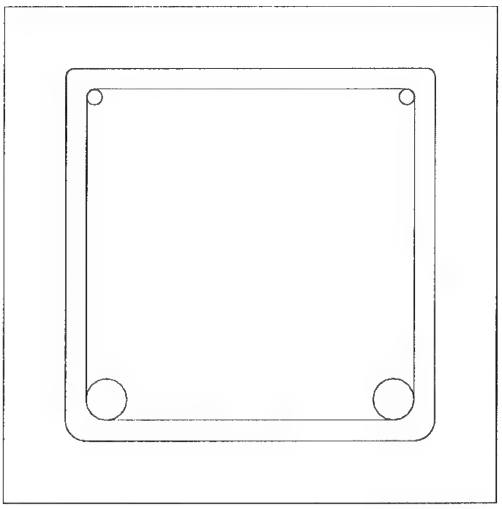

Figure 78. Cross-sectional view of large-scale beams

Materials For Large-Scale Beams

Concrete

A nominal 4000 psi mix from a local vendor was used. The slump for the mix was 2-3 in., and the large aggregate was pea gravel (used to reduce the effects of spalling when fastening the composite strip). The average 28-day compressive strength (based on 6 cylinder tests) was 6480 psi.

Reinforcing Bar

Beams were designed in accordance with ACI 318-99, but the reinforcement ratio was kept constant for all specimens in order to see the impact of other variables (namely termination length and length of shear span). Full construction details are provided in Appendix B, while Table 12 is a summary of the specimens' reinforcement details.

Table 12. Reinforcement Details (Large-Scale)

Beam Type	Type Reinforcement	Size Rebar	Area of Steel ($in.^2$)	A_s/A_{bal}	Yield Strength of Steel, ksi
All Large-Scale	Tension	2 No. 8's	1.58	0.32	60
	Compression	2 No. 3's	0.22	NA	60
	Shear	No. 4 Closed Stirrups @ 4 in. OC	-	-	60

Composite Strengthening Strip

The subsequent testing utilized two different composite strips. The first strip, used on Beams UW3, UW6, UW7, UW8, UW9, and UW10, was the same strip used on the full-scale T-beams. This strip will be referred to as the black strip. The second strip, used on Beams UW2, UW4, and UW5, was pultruded with a gray pigment and did not achieve the same strength as the black strip. This strip will be referred to as the gray strip. Table 13 summarizes the properties of the black strip, while Table 14 summarizes the properties of the gray strip

Table 13. Composite Material Properties - Black Strip

Type Strength	No. of Tests	Average Failure Strength (ksi)	Standard Deviation (ksi)	Coeff of Variance (%)	Modulus of Elasticity (ksi)	Standard Deviation (ksi)	Coeff of Variation (%)
Ultimate	10	107.80	12.70	11.80	8,200	700	8.70
Open-Hole	10	95.00	6.20	6.50	8,200	600	7.80

Table 14. Composite Material Properties - Gray Strip							
Type Strength	No. of Tests	Average Failure Strength (ksi)	Standard Deviation (ksi)	Coeff of Variance (%)	Modulus of Elasticity (ksi)	Standard Deviation (ksi)	Coeff of Variation (%)
Ultimate	9	71.66	7.80	10.88	8,200	750	9.15
Open-Hole	9	52.00	4.50	8.65	8,200	625	7.62

Fasteners

The exact same Hilti fastening system and X-ALH 47 fasteners were used in the full-scale testing. Table 15 reviews the fastener properties.

Table 15. Fastener Properties			
Nomenclature	Intended Use	Length	Shank Diameter
X-ALH 47	High Strength Concrete & High Grade Steel	1.83 in.	0.175 in.

Fabrication Of Beams

University of Wisconsin undergraduate students and research assistants constructed all reinforcement cages and beams in January of 2001. The beams were placed in storage until completion of the full-scale testing at the ERDC in August 2001. Once the full-scale testing data and photographs were analyzed, the objectives were then defined for the ten large-scale beams. The specimen details and intended research purpose are listed in Table 16.

Table 16. Specimen Details (Large-Scale)					
Beam Name	Type Strip	No. of Strips	Fastener Spacing in.	Termination Length, in.	Specimen Purpose
Beam UW1	None	None	-	-	Control
Beam UW2	Gray	1	2	4	Ultimate Strength
Beam UW3	Black	1	2	4	Fatigue
Beam UW4	Gray	1	2	2	Investigate Effect of Short Shear Span
Beam UW5	Gray	1	2	2	Investigate Effect of Short Shear Span
Beam UW6	Black	1	2	4	Investigate Effect of Termination Length
Beam UW7	Black	1	2	10	Investigate Effect of Termination Length
Beam UW8	Black	1	2	12	Investigate Effect of Termination Length
Beam UW9	Black	2	2	4	Determine Impact of Increased Area of Strip
Beam UW10	Black	1	2	4	Fatigue

Attachment Of FRP Composite

The composite strip was attached to the beams in the same manner as listed in Chapter 5 with one exception. Since the beams were small enough to manipulate with a 5-ton overhead crane, researchers "flipped " the beams and attached the strip with the bottom of the beam (tension face) facing skyward. Spalling of the concrete was minimal during the attachment of the strip to the small-scale beams. While there was some cracking, no large chunks of concrete broke away from the beams. Once the strip was in place, researchers "flipped" the beam so the strip was facing down and moved it into position within the testing apparatus.

Testing Of Large-Scale Beams

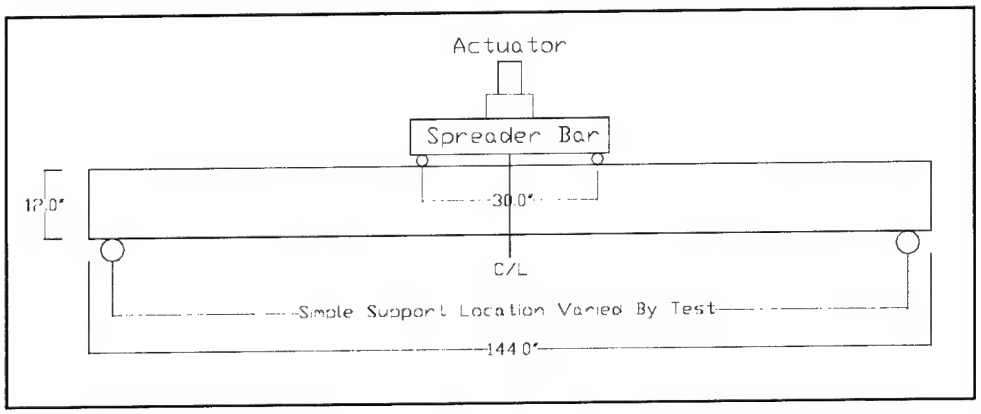

Figure 79. Large-scale test configuration

Strength Tests

All strength tests (Beams UW1, UW2, UW6, UW7, UW8, and UW9) were tested in the configuration shown in Figure 79. The 1,000,000-lb press at the University of Wisconsin was used as the main actuator. The spreader bar distributed the load to two load points and provided four-point bending. All strength tests were conducted in displacement control at a rate of 0.1 in./min. The data acquisition system measured load, stroke, and strain data from three strain gauges. One concrete strain gauge was located on top of the beam at the centerline and measured concrete compressive strain. Two other gauges were on the composite strip at the midspan of the beam and measured the strain in the strip as the specimen deflected. Figure 80 is a picture of the strength test configuration.

Figure 80. Strength and shear span experimental setup

Shear Span Tests

Both shear span investigations were tested in exactly the same manner as the strength tests (Figure 80) except for one difference. Since the purpose of the tests were to determine the effects of a short shear span, researchers moved the simple supports towards the load points and decreased the shear spans of Beams UW4 (27 in. shear spans) and UW5 (37 in. shear spans).

Fatigue Tests

Both fatigue tests (Beams UW3 and UW10) were also tested in the configuration shown in Figure 79. The main actuator in this case, however, was the fifty-five kip actuator located in the University of Wisconsin Structures and Materials Testing Laboratory. The spreader bar distributed the load to two load points and provided four-point bending. Figure 81 shows Beam UW3 in the experimental fixture.

The cyclical loading magnitude were chosen to be 20- to 80 percent of the unstrengthened beam's yield capacity. Since the control yielded at 34,000 lb of total load, the actuator load was cycled from 6800 lb to 27,200 lb at a frequency of 2 Hz. The goal for the test was to complete 2,000,000 cycles and then test the specimens to failure.

The data acquisition system was set up to measure load, stroke, and strain data from three strain gauges (same as above). An initial 10 cycles at 0.1 Hz were run to measure the initial properties of the specimen. Then 200,000 cycles

at the specified 2 Hz were run. Upon completion of the 200,000 cycles, 10 cycles at 0.1 Hz were also applied and the pertinent data recorded. This process was repeated until completion of each test.

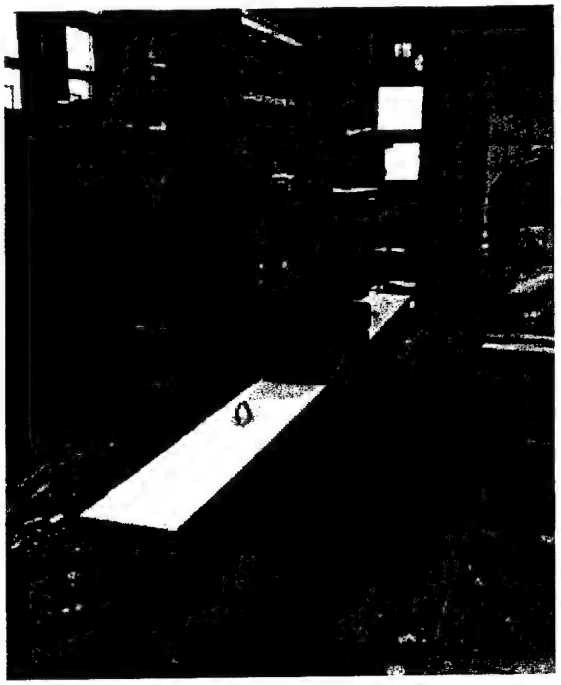

Figure 81. Fatigue test experimental setup

Results Of Large-Scale Beam Tests

Strength Test Results

Table 17 provides a summary of the specimens used to investigate strengthening and the role of termination length in determining the failure mode.

Table 17. Large-Scale Specimen Summary (Strength)

Beam	Type Strip	No. of Strips	Shear Span, in.	Moment Span, in.	No. Fasteners in Shear Span	Termination Length, in.
UW1	-	-	54	30	-	-
UW2	Gray	1	54	30	52	4
UW6	Black	1	51	30	48	4
UW7	Black	1	53	30	44	10
UW8	Black	1	54	30	44	12
UW9	Black	2	54	30	52	4

Table 18 provides the strength test results, and Figure 82 summarizes them graphically. In short, the results indicate an average increase of 10.12 percent in yield capacity and 20.00 percent in ultimate capacity for beams strengthened with one strip. The beam strengthened with a double strip showed an increase of 21.43 percent in yield capacity and 36.84 percent in ultimate capacity. Also, the termination length in beams UW6, UW7, and UW8 were varied to attempt to induce a bearing failure in the strip near the support. While all three beams failed with concrete crushing, Beam UW8 (termination length = 12 in.) displayed signs of a bearing failure. Each beam and its failure mode will be discussed in the following section.

Table 18. Strength Test Results

Beam	Yield Moment (ft-kips)	% Yield Increase (%)	Ultimate Moment (ft-kips)	% Ultimate Moment Increase (%)	Disp @ Failure (in.)	Ductility Ratio @ Failure	Failure Mode
UW1	84	-	95	-	2.05	L/67	Concrete Crushing
UW2	94	11.90	106	11.58	1.42	L/97	Strip Rupture
UW6	92	9.52	116	22.11	1.89	L/97	Concrete Crushing
UW7	92	9.52	116	22.11	1.92	L/71	Concrete Crushing
UW8	92	9.52	118	24.21	2.15	L/64	Concrete Crushing
UW9	102	21.43	130	36.84	2.14	L/64	Delamination

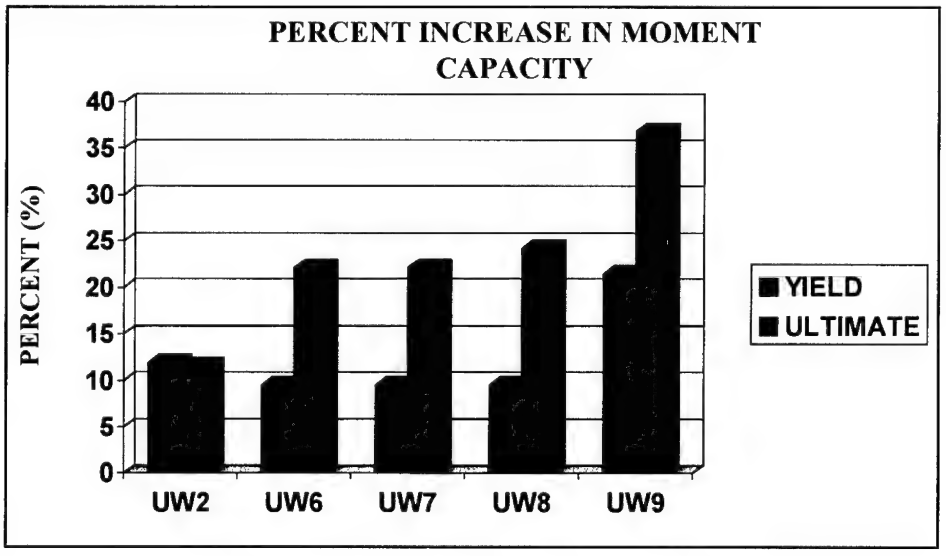

Figure 82. Percent increase in moment capacity for strength tests

Also of interest is the cumulative plot of moment vs deflection for the strength test beams (Figure 83). Each plot is truncated at concrete crushing failure except for the beam with the double strip (UW9), which is truncated at the point of delamination due to gross fastener failure. This cumulative plot reveals not only the increase in post-yield strength, but also shows the increase of postyield stiffness for the strengthened specimens.

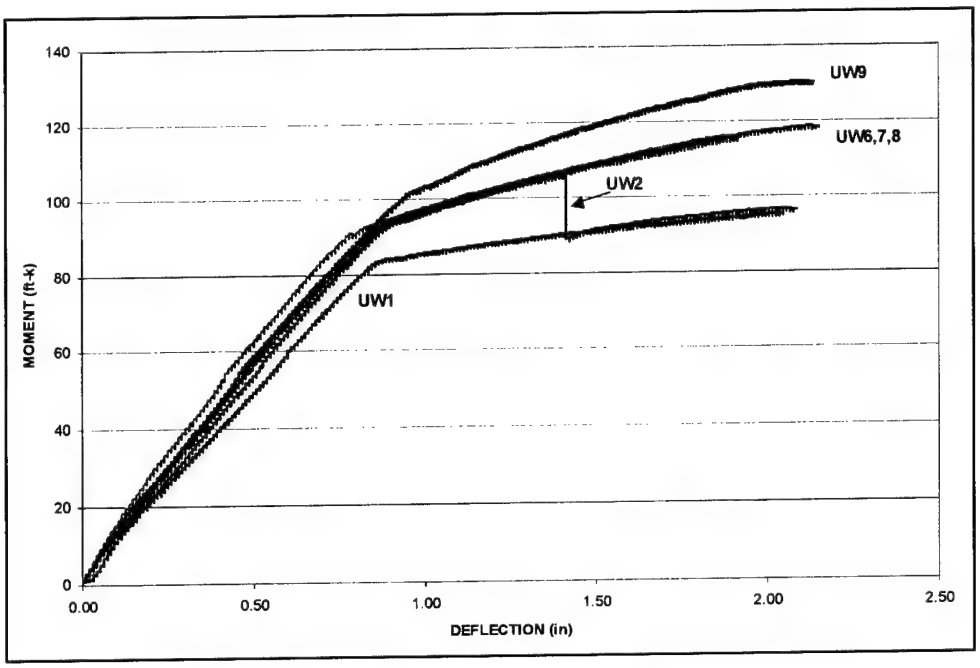

Figure 83. Plot of moment vs deflection for strength tests

Shear Span Test Results

The purpose of the shear span tests was not to examine increased strength capacity. Rather, it was examine whether or not the strengthening system would remain attached while accepting the increased load associated with a shorter shear span. Table 19 summarizes the specimens, while Table 20 indicates that in both cases the strip remained attached for the duration of the test. Also of importance is the load per fastener data for each fastener within the shear span of a specimen. Researchers calculated this result by taking the maximum shear force experienced by the beam and dividing it by the number of fasteners within the shear span. Current modeling assumes a load per fastener of 1,000 lb (Bank et al. 2000). Any loading above this level would result in fastener failure.

Table 19. Large-Scale Specimen Summary (Shear Span)

Beam	Type Strip	No. of Strips	Shear Span (in.)	Moment Span (in.)	No. Fasteners in Shear Span	Termination Length (in.)
UW2	Gray	1	54.0	30.0	52	4
UW5	Gray	1	37.0	30.0	36	2
UW4	Gray	1	27.0	30.0	26	2

Table 20. Shear Span Test Results					
Beam	Max Moment	Strip Strain @ Failure	Strip Force @ Failure	Load per Fastener	Failure Mode
UW2	1,272	0.0063	26,117	502	Strip Rupture
UW5	1,432	0.0059	24,459	686	Strip Rupture
UW4	1,296	0.0043	17,826	679	Strip Rupture

Figure 84 graphically shows the effects of varying the length of the shear span. The beams with the shorter shear spans (Beams UW4 and UW5) have a steeper initial slope (accept more load faster), but are not as ductile and fail at lesser displacements. The plot of moment vs deflection for Beam UW4 is pseudo-plastic. That is, the shape of the post-yield plot is rounded. This shape is attributable to the combination of the short shear span and a span to depth ratio of 2.7 pushing this specimen toward non-linear concrete behavior. The plot of moment vs deflection (Figure 84) for Beam UW5 closely resembles the plot of a beam with a longer shear span (Beam UW2: shear span = 54 in.). The post-yield behavior is linear until the strip ruptured at a moment capacity of 119 ft-kips. The load per fastener for this beam was 679 lb.

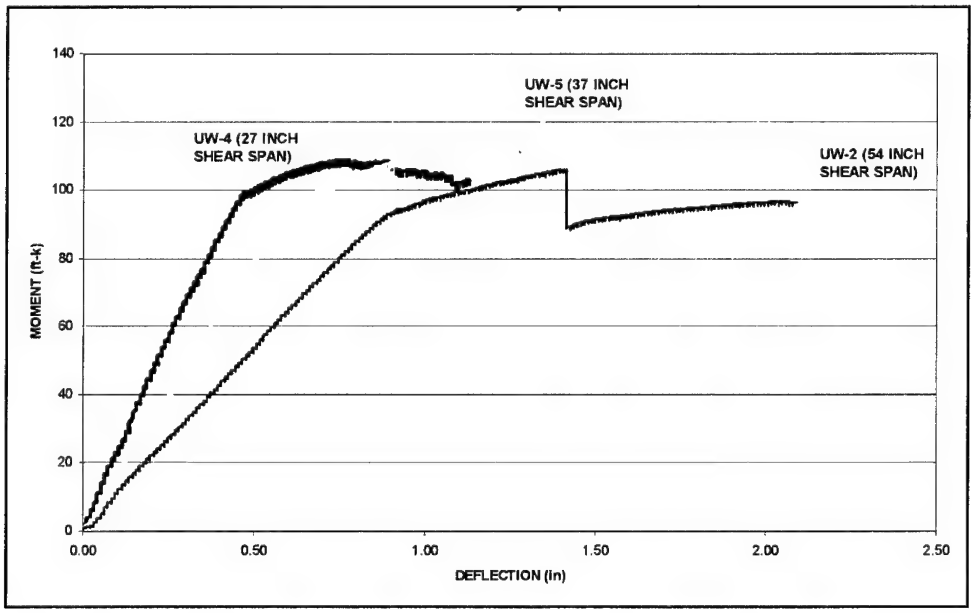

Figure 84. Plot of moment vs deflection for beams of various shear spans

Fatigue Test Results

Table 21 summarizes the physical characteristics of the fatigue beams, while the test results are shown in Table 22. While neither test reached the goal of 2,000,000 cycles, both beams showed promise in that the composite strip and respective fasteners showed no deterioration or signs of wear.

Table 21. Large-Scale Specimen Summary (Fatigue)						
Beam	Type Strip	No. of Strips	Shear Span (in.)	Moment Span (in.)	No. Fasteners in Shear Span	Termination Length (in.)
UW-3	Black	1	54.0	30	52	4
UW-10	Black	1	54.0	30	52	4

Table 22. Fatigue Results		
Beam	Cycles Completed	Failure Mode
UW-3	1,780,000	Fracture of Main Steel Due to Fixture Failure
UW-10	759,000	Fracture of Main Steel Reinforcement

Description Of Failure Modes For Large-Scale Beam Tests

Strength Test Failure Modes

a. *Beam UW1.* The unstrengthened beam failed due to crushing of the concrete in the compression zone. Cracking was predominantly flexural, with a few shear-flexural cracks within the shear span. The failure began in the vicinity of the north load point and proceeded across the constant moment region until it reached the southern load point. Figure 85 shows Beam UW1 after failure.

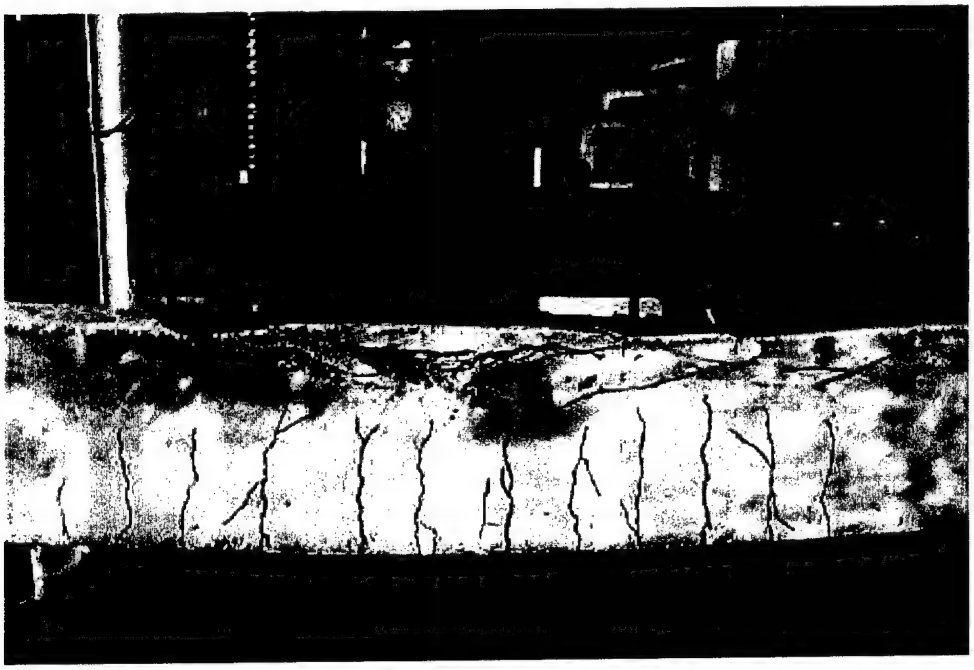

Figure 85. Post-failure of Beam UW1

b. *Beam UW2.* Beam UW2 (shear span = 54 in.) was strengthened with the gray strip and *failed* when the composite strip ruptured in the vicinity of the midspan of the beam. The rupture, caused by the inferior properties of the gray strip, occurred at the location of a flexural crack and appeared as if the strip had been simply cut in two pieces. Figure 86 shows the ruptured gray strip.

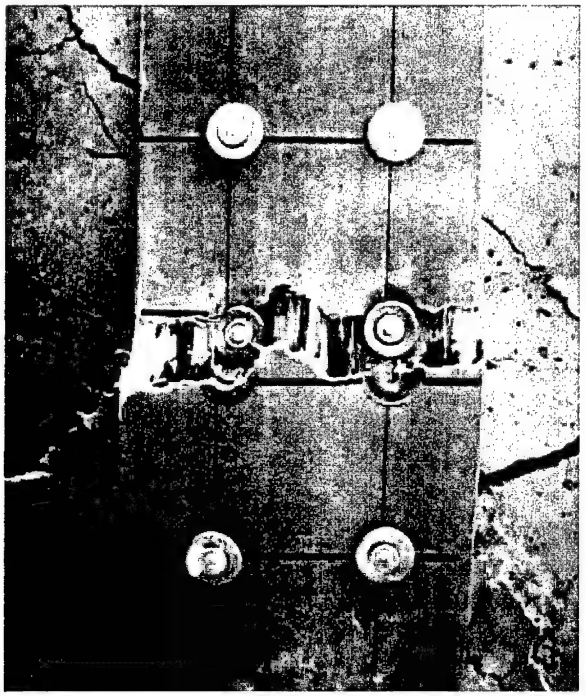

Figure 86. Rupture of gray composite strip on Beam

c. *Beam UW6.* Beam UW6 was strengthened with the black strip such that the termination length of the strip was 4 in. The beam achieved a concrete compression failure well before the composite strip delaminated. Figure 87 shows Beam UW6 after researchers forced strip delamination by continuing the test well past the concrete compression failure.

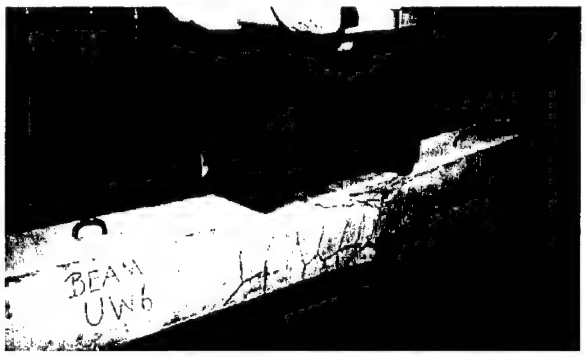

Figure 87. Post-failure of Beam UW6

d. *Beam UW7.* Beam UW7 was strengthened with the black strip such that the termination length of the strip was 10 in. The beam achieved a concrete crushing failure before the strip delaminated. The strip did not show any sign of bearing failure near the ends prior to the concrete crushing failure. Figure 88 shows Beam UW7 after concrete compression failure.

Figure 88. Post-failure of Beam UW7

e. *Beam UW8.* Beam UW8 was strengthened with the black strip such that the termination length of the strip was 12 in. The beam achieved a concrete crushing failure prior to strip delamination. There was however, evidence of a bearing failure in the strip at the south end of the strip. Slight slotting (strip pulling through fasteners) was evident in the first two rows of fasteners nearest the support (Figure 89).

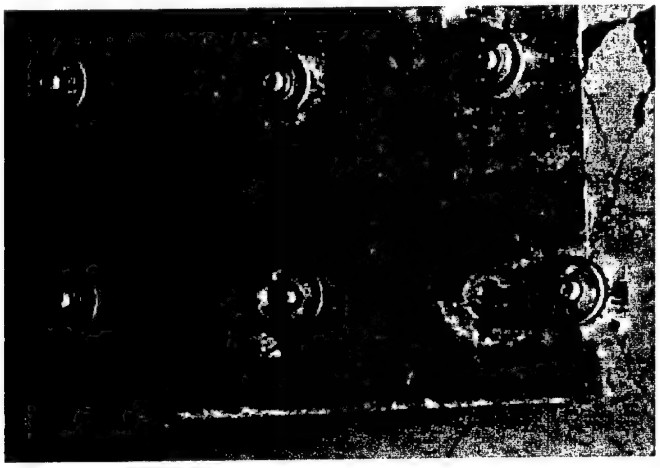

Figure 89. Beginning of bearing failure of black strip on Beam UW8

f. *Beam UW9.* Beam UW9 was strengthened with a double black strip. The termination length of the composite strip was 4 in. The beam failed due to the strip delaminating from the centerline towards the support. Figure 90 shows the gross fastener failure of the strengthening system on Beam UW9.

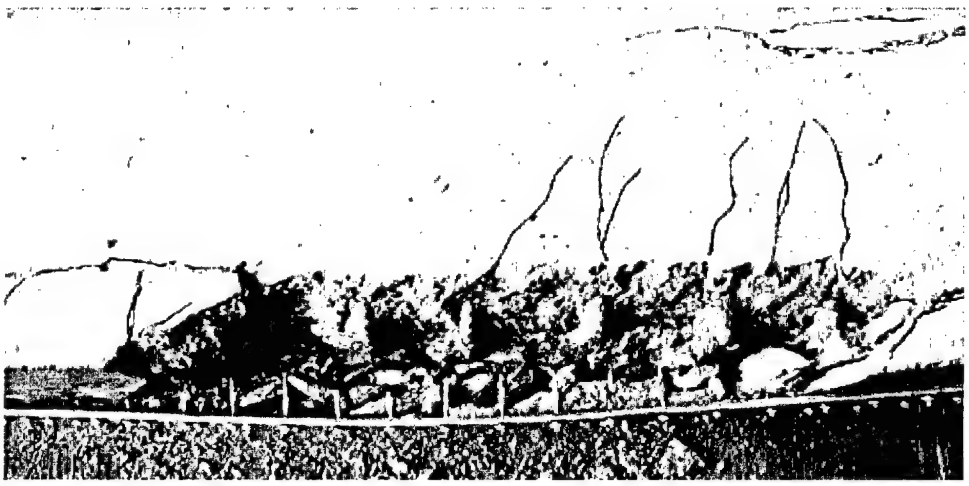

Figure 90. Gross fastener failure of Beam UW9

Shear Span Test Failure Modes

a. *Beam UW4.* Beam UW4 was strengthened with the gray strip, but the roller supports were moved towards the midspan to provide a 27-in.-shear span. The beam failed when the gray strip ruptured. Figure 91 shows the condition of Beam UW4 after strip delamination (well after concrete crushing failure).

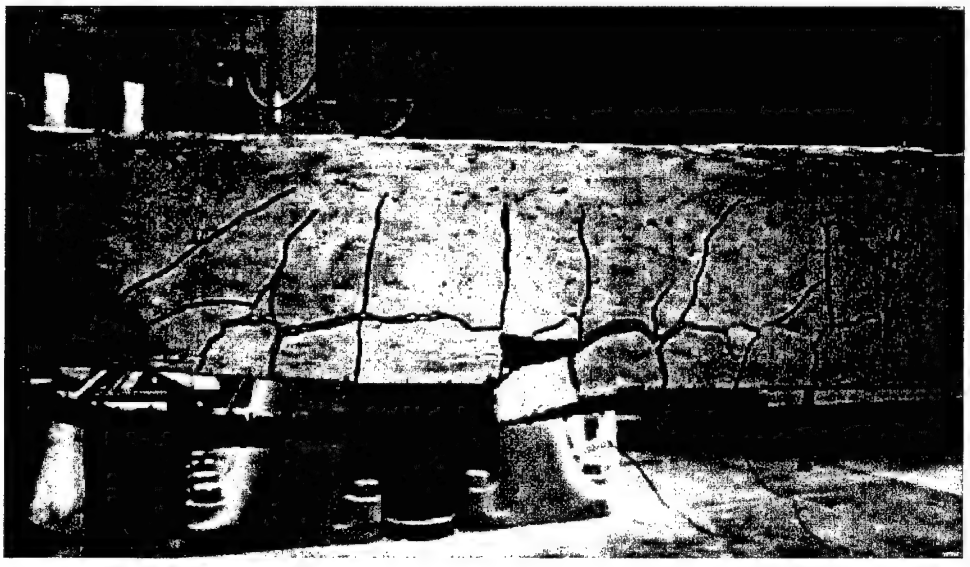

Figure 91. After concrete crushing failure of UW4 Beam

b. *Beam UW5.* Beam UW5 was strengthened with the gray strip, but the roller supports were moved towards the midspan to provide a 37-in. shear span. The gray strip ruptured (Figure 92) prior to a concrete compressive failure, but the beam failed in compression soon thereafter.

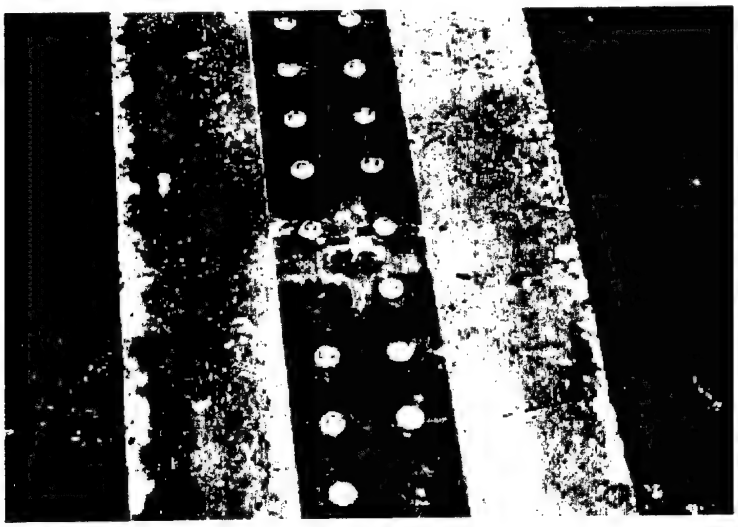

Figure 92. Rupture of gray strip on Beam UW5

Fatigue Test Failure Modes

a. *Beam UW3.* Beam UW3 was strengthened with the black strip and cycled from 6,800 lb to 27,200 lb at a frequency of 2 Hz. The rollers supporting the beam translated at 1,780,000 cycles and crashed the beam against the load frame. The beam was damaged to the point where it could no longer accept any load. Up until that point, the beam had not experienced any loss of stiffness (Figure 93), and the composite strip had no visible signs of wear or degradation. All fasteners were intact and firmly imbedded in the concrete. A manual check with pliers revealed no loose fasteners.

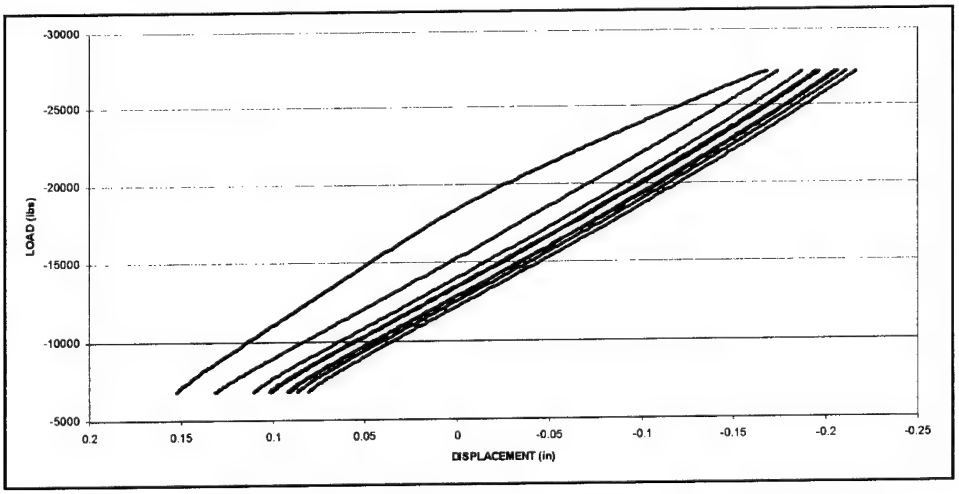

Figure 93. Plot of relative stiffness for Beam UW3 (Every 200,000 cycles)

b. *Beam UW10.* Beam UW10 was strengthened with the black strip and cycled from 6,800 lb to 27,200 lb at a frequency of 2 Hz. Researchers constructed special bracing to insure there was no support translation during testing. The beam failed after 759,000 cycles at a large flexural crack within the constant moment region. Upon inspection of the crack, researchers discovered that both main reinforcing bars (tension) had fractured in the plane of the large flexural crack. This fracture is shown in Figure 94. Although the beam failed, the composite strip and all fasteners were intact and showed no visible signs of damage.

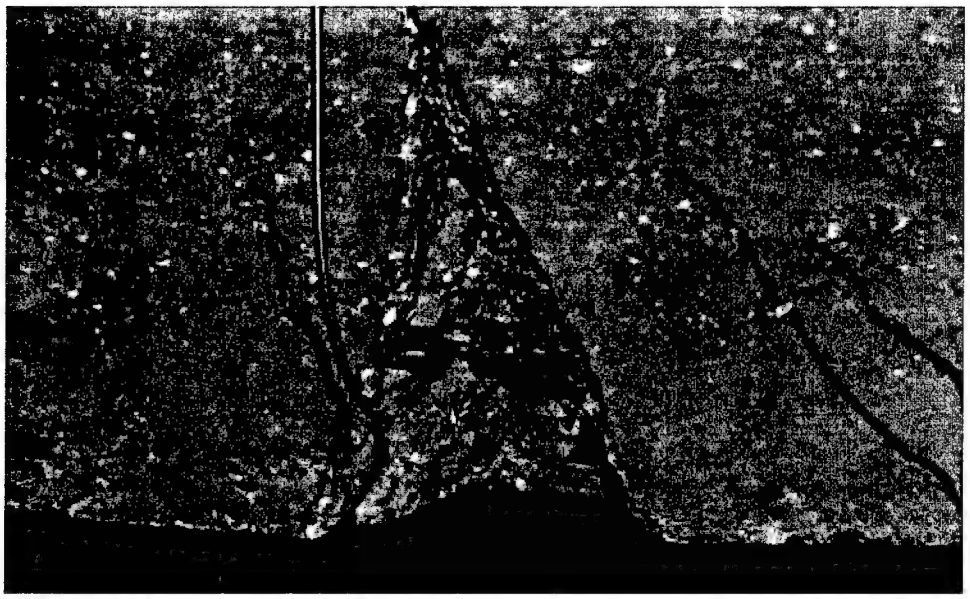

Figure 94. Fractured tensile reinforcement in Beam UW10

c. *Fatigue Beams Tested To Ultimate.* Although both fatigue beams were damaged and failed during cyclic loading, researchers tested the beams in four-point bending until the composite strip failed. This was significant in that since the steel rebar had fractured during the fatigue testing, the composite strip would now be carrying the entire tensile load. The result of the testing was a failure mode that researchers had never previously encountered. While all fasteners remained intact, the strip split longitudinally along the line of fasteners over the length of the strip. Figures 95 and 96 show this new failure mode.

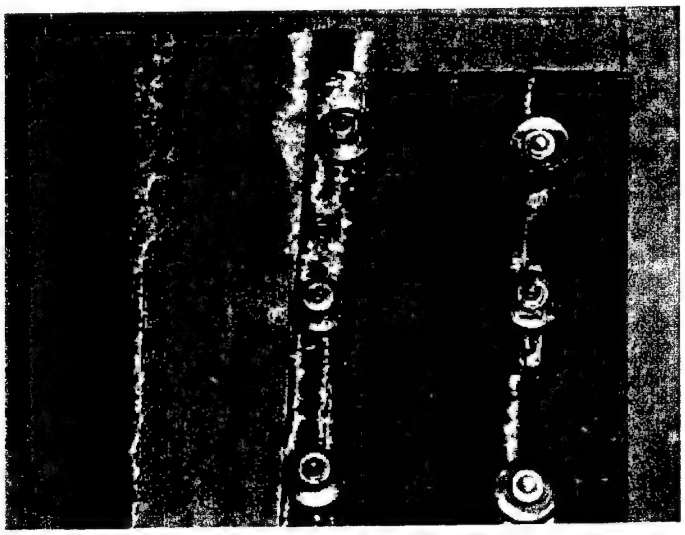

Figure 95. Longitudinal splitting of black strip on Beam UW10 (Near support)

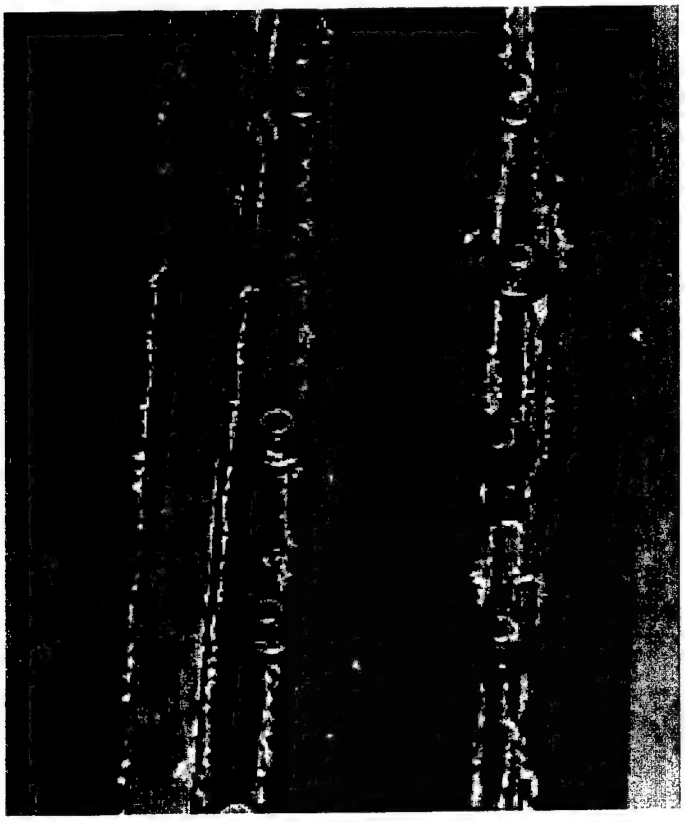

Figure 96. Longitudinal splitting of black strip on Beam UW10 (Near midspan)

12 Conclusions

The series of tests conducted on both full-scale T-beams and large-scale reinforced concrete beams strengthened with powder-actuated fasteners and composite strips leads to the following conclusions:

a. *Strengthening Method:* The method of strengthening reinforced concrete beams with powder-actuated fasteners and composite materials is viable for full-scale reinforced concrete beams. With only minimal training, researchers were able to retrofit a 29 ft beam in just 5.0 man-hours. While the concrete did spall during the fastening procedure, it did not lead to any premature failures during testing. Increases in postyield moment capacity for the T-beams ranged from 3.88 percent to 27.19 percent, and moment capacity at yield increased in between 1.05 percent and 11.65 percent.

b. *Termination Length and Failure Modes:* The termination length (the distance from the simple support to the first row of fasteners) plays a role in the way a strengthened beam fails. If the termination length is too large, the strip fails in bearing and delaminates from the support towards the midspan of the beam (outside in). On the other hand, if the termination length is small, the strip fails via gross fastener failure and delaminates from the midspan of the beam towards the supports (inside out).

c. *Short Shear Span:* Tests on Beams UW4 and UW5 confirm that the fastened method is capable of increasing the strength of beams with short shear spans. While you cannot compare the short shear spans to the control beam because of the differences in experimental set-up, the load per fastener for UW4 and UW5 remained below the load of 1000 lb for design and analysis as cited in the report of work conducted during the second year of research (Bank et al. 2000). The plot of moment vs displacement for the short shear span beams resembled the behavior of the longer shear span beams, with Beam UW4 acting in a non-linear fashion due to its span to depth ratio of 2.7.

d. *Fatigue:* The strengthening system performs well under cyclic loading. In both tests, the composite strip showed no signs of degradation, and all fasteners remained embedded in the concrete. There was no loss of stiffness in either trial, and deflections remained consistent.

e. *Analytical Model:* The analytical model was created to predict the moment-deflection behavior of a beam strengthened with a mechanically fastened FRP strip, and to further examine the factors that affect the behavior of a strengthened beam. The following conclusions were made in this portion of the research:

(1) The load per fastener can be checked in the strength model; however, the limiting aspect of the strength model is that it can only be used when the beam fails in concrete compression. This is because the strength model uses the Whitney stress block, which is only valid at concrete compression failure.

(2) Two checks must be added to the model to develop the moment-curvature relationship for a beam with a fastened FRP strip. One check is to insure the load per fastener in each moment span does not exceed the fastened connection strength, and the second is to insure that the load on the end fasteners does not exceed the fastened connection strength.

(3) The moment-deflection behavior of a reinforced concrete beam strengthened with a mechanically fastened FRP strip can be calculated using a virtual work approach. The analytical model predicts the moment-deflection behavior of the T-beam experiments and the large-scale beam experiments reasonably well.

(4) Failure modes were modeled; however, more exact values for the material and connections need to be developed for input in to the model. The value for connections on gross, or the "average" strength of a single connection, needs to be investigated with more in depth experiments. The strength for end fasteners, by pairs or singly, also needs to be studied in depth in order to more accurately predict the failure mode of the strengthened beams.

(5) The number of fasteners in the shear span must be great enough to develop the required forces in the FRP strip, or the strip will delaminate by gross fastener failure.

(6) The farther away from the support that the end fasteners are located, the greater the moment must be transferred to the FRP strip by the end fasteners. This is called end fastener failure.

(7) Initial cracking is not modeled in the analytical model, which may cause the model to over predict the strength of beams that experience initial cracking upon strip attachment, as seen in the large-scale beam experiment comparisons.

(8) A thicker FRP strip may be less beneficial for load redistribution at lower load levels, as seen in the difference between the experimental results and the predicted results.

13 Recommendations for Future Work

The study has indicated that the powder-actuated fastener and composite material strengthening method is viable for large-scale beams and real-world applications. In order to continue to develop and refine the method, the following recommendations are made:

a. Continue to refine application process. Focus on making composite strip easier to manipulate and position along beam. Two men were able to attach the strip while lying on their backs on stable ground. Military applications will not allow for such sterile conditions. Being able to keep hands free and work with less material handling equipment will allow soldiers to apply the system quicker in any environment.

b. Conduct material testing on full-width (4-in.) coupons to refine composite material properties. Composite material strengths are currently based on a 1-in.-wide coupon with a central hole. Work must be done to better approximate the 4-in.-wide strip with pairs of holes in series.

c. Conduct additional fatigue testing on full-scale specimens. Cycle load between 20 percent and 40 percent of unstrengthened beam yield capacity in order to prevent the premature failure of the tensile steel. Upon completion of two million cycles, test beams to failure and note the mode of failure.

d. Conduct in-place testing of strengthening method on an existing bridge. In order to consider this application valid, it must be tested on an existing structure.

e. Conduct material testing on fastened strip to further refine bearing capacity of composite strip. To date, the bearing strength of the composite strip (unattached) has not been determined. Completing such experiments will provide insight into the failure mode of the composite and lead to better analytical predictions.

f. Investigate effects of environment on strengthened beams. Focus on fastener corrosion and strip degradation. The fasteners are steel, and the composite strip has high carbon content. There is a possibility of interaction between the two that would lead to the corrosion of the fasteners and premature failure of the strengthened member.

g. Develop quality control specifications for the composite strips used for strengthening in order to guarantee minimum strength of strip and of load per fastener.

REFERENCES

American Concrete Institute Committee 318. (1999). "Building code requirements for structural concrete (318-99) and commentary (318R-99)," Farmington Hills, MI.

American Concrete Institute Committee 435. (1972). "Variability of deflections of simply supported reinforced concrete beams," *ACI Journal63*, Proceedings 63, 29-35.

American Concrete Institute Committee 440F. (2001). "Guide for the design and construction of externally bonded FRP systems for strengthening concrete structures," (Pending publication), Detroit, MI.

American Concrete Institute Committee 440H. (2001). "Guide for the design and construction of concrete reinforced with FRP bars (ACI 440.1R-01)," Farmington Hills, MI.

Arduini, M., and Nanni, A. (1997). "Behavior of Precracked RC beams strengthened with carbon FRP sheets," *ASCE Journal of Composites for Construction*, 1(2), 63-70.

Bank, L.C., and Lamanna, A.J. "Final Report: Rapid repair of concrete structures using composite materials and power actuated fastening systems," (unpublished), ERDC under Contract No. DACA39-99-K-0001.

Bank, L.C., Lamanna, A.J., Ray, J.C., Velazquez, G.I. (2000). "Final report: rapid strengthening of full-sized concrete beams with powder actuated fastening systems and composite materials," (unpublished) ERDC.

Emmons, P. H., Vaysburg, A. M., and Thomas, J. (1998). "Strengthening of concrete structures, part II, advanced composites," *ACI Concrete International* 20(4), 56-60.

Hilti. (2001). *North american product technical guide*, Hilti, Inc., Tulsa, OK.

Hognestad, E. (1951). "A study of combined bending and axial load in reinforced concrete members," *Bulletin No. 399*, Engineering Experiment Station, University of Illinois, Urbana.

Kassimali, A. (1999). *Structural analysis*, 2nd ed., PWS Publishing Co., Boston, MA.

Lamanna, A.J., Bank, L.C., and Scott, D.W. (2001a). "Rapid strengthening of RC beams using powder actuated fasteners and FRP strips," Proceedings of the *5th International Symposium of FRP in Reinforced Concrete Structures*, Cambridge, UK, July 16-18 2001a, 398-397.

Lamanna, A.J., Bank, L.C., and Scott, D.W. (2001b). "Flexural strengthening of RC beams using fasteners and FRP strips," *ACI Structures Journal* 98(3), 368-376.

MacGregor, James G. (1999). *Reinforced Concrete: Mechanics and Design*, 3rd ed., Prentice Hall, Upper Saddle River, NJ.

Mathsoft. (1999). *User's Guide: Mathcad 2000*, MathSoft, Inc., Cambridge, MA.

Mehta, P. K., and Monteiro, P. J. M. (1993). *Concrete: Microstructure, Properties, and Materials*, 2nd ed., McGraw Hill, New York, NY.

Park, R., and Paulay, T. (1975). *Reinforced Concrete Structures*, John Wiley and Sons, New York, NY.

Ray, J.C., Scott, D.W., Lamanna, A.J., and Bank, L.C. (2001a). "Flexural behavior of reinforced concrete members strengthened using mechanically fastened fiber reinforced polymer plates," *Army Science Conference*, Baltimore MD, Dec 11-13.

Ray, J.C., Velazquez, G.I., Lamanna, A.J., and Bank, L.C. (2001b). "Rapidly installed fiber-reinforced polymer (FRP) plates for upgrade of reinforced concrete bridges," *High Performance Materials in Bridges and Buildings*, Koha, HI.

Razaqpur, A. G., Svecova, D., and Cheung, M. S. (2000). "Rational method for calculating deflection of fiber-reinforced polymer reinforced beams," *ACI Structural Journal* 97(1), 175-184.

Soroushian, P., and Choi, K. B. (1991). "Analytical evaluation of straight bar anchorage design in exterior joints," *ACI Structural Journal* 88(2), 161-168.

Taly, N. (1998). *Design of Modern Highway Bridges*, McGraw-Hill, New York, NY.

Appendix A
T-Beam Construction Drawings

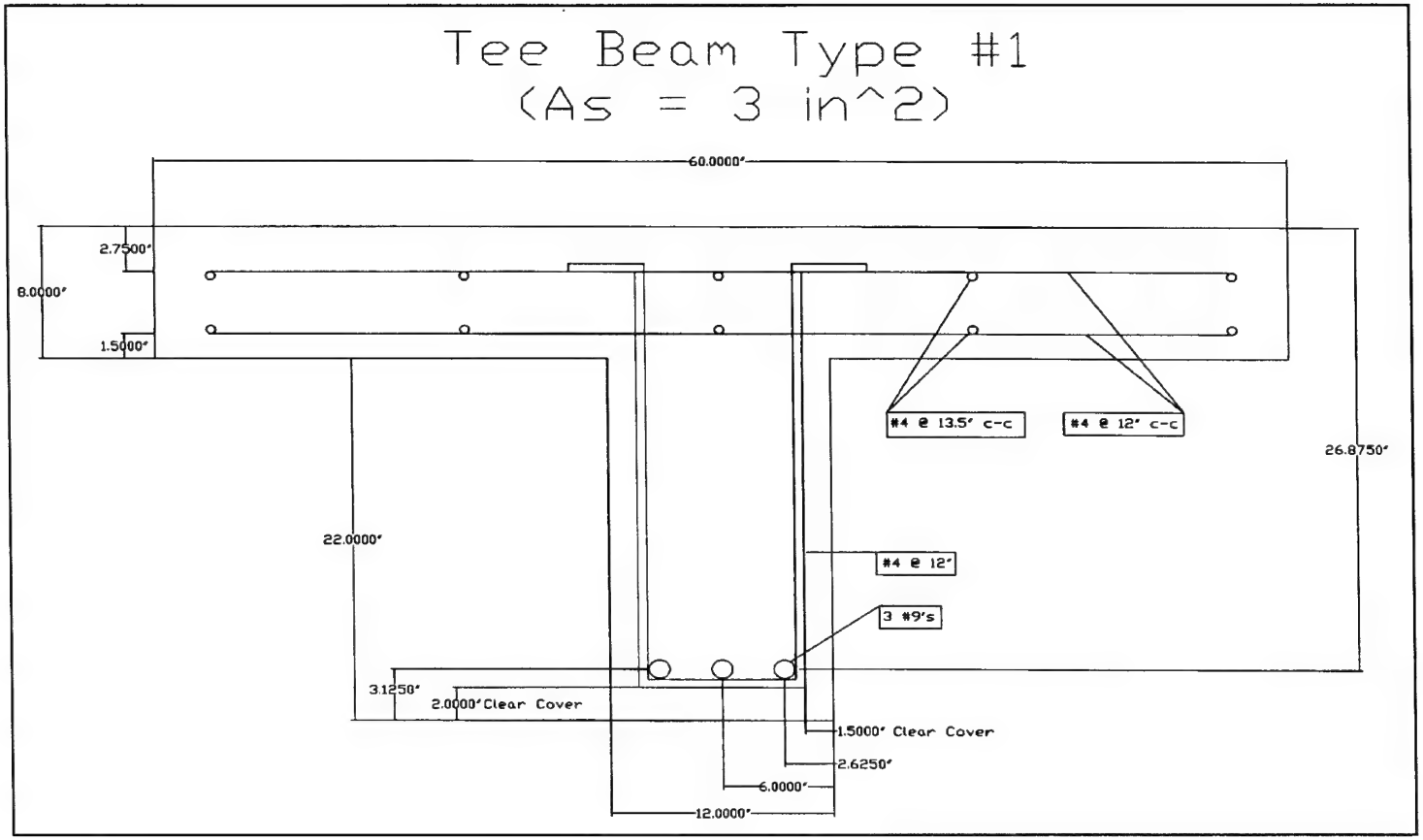

Figure A1. Construction drawing – A3 family of beams

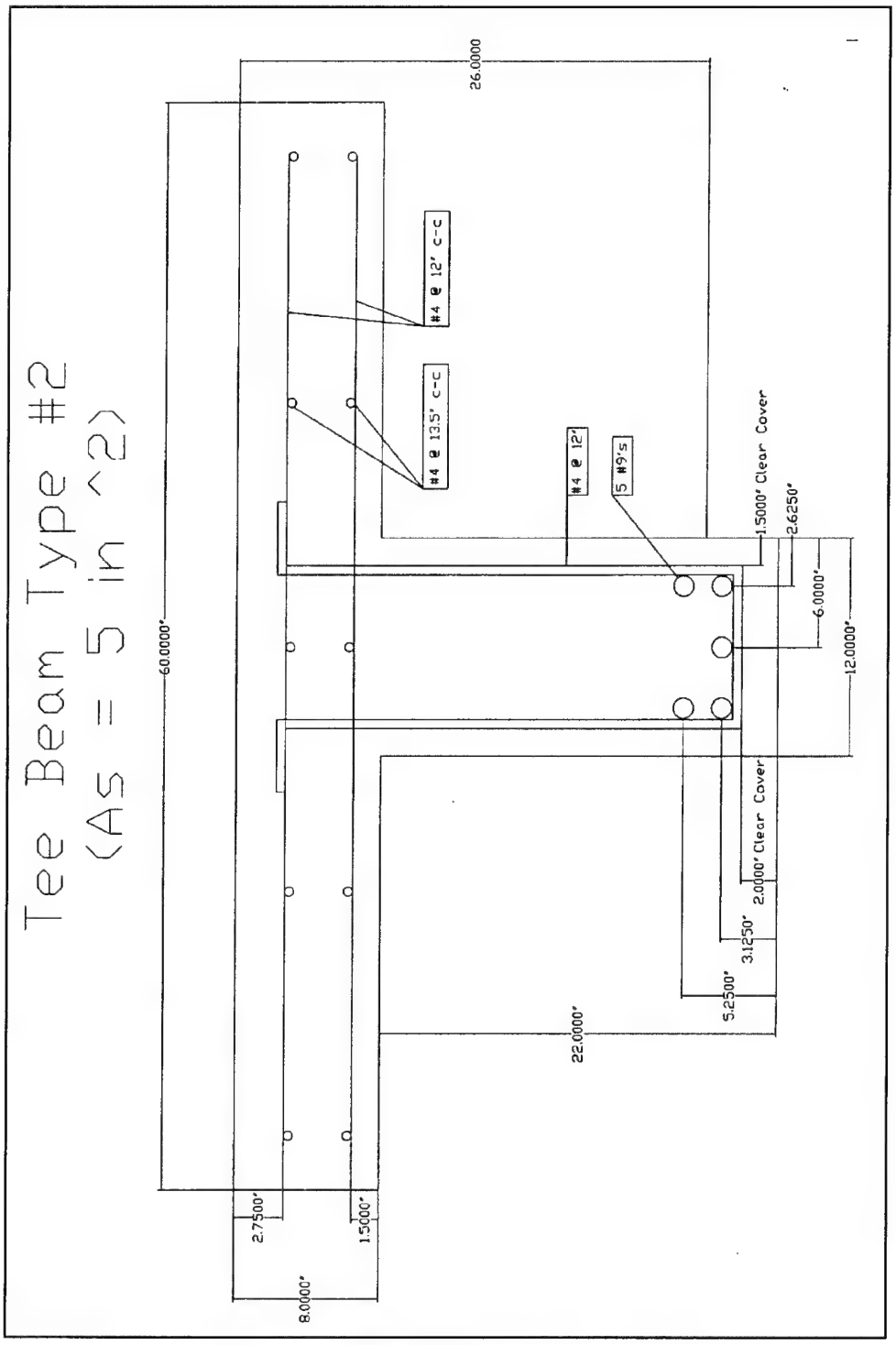

Figure A2. Construction drawing – A5 family of beams

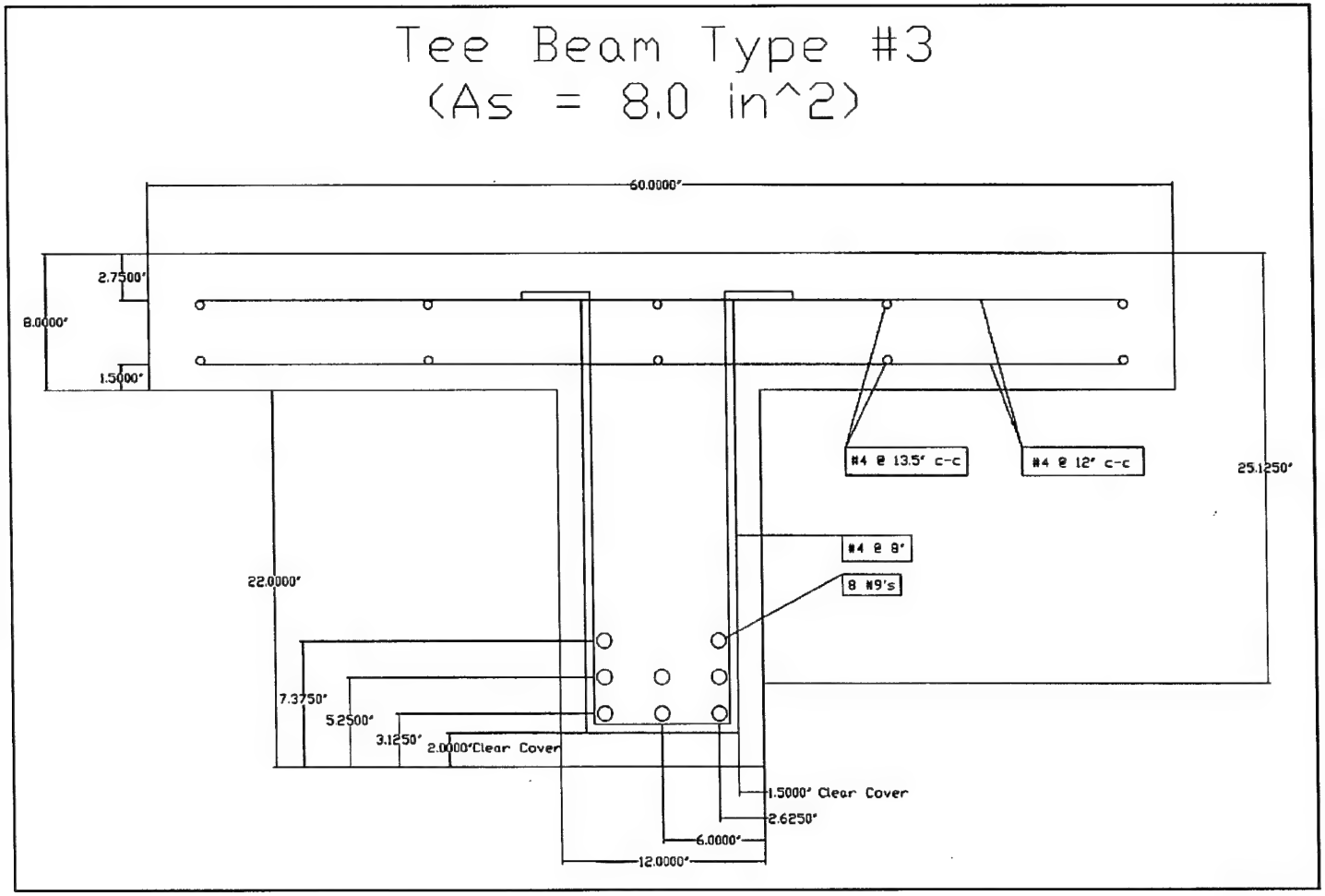

Figure A3. Construction drawing – A8 family of beams

Appendix B
Large-Scale Beam Construction Drawings

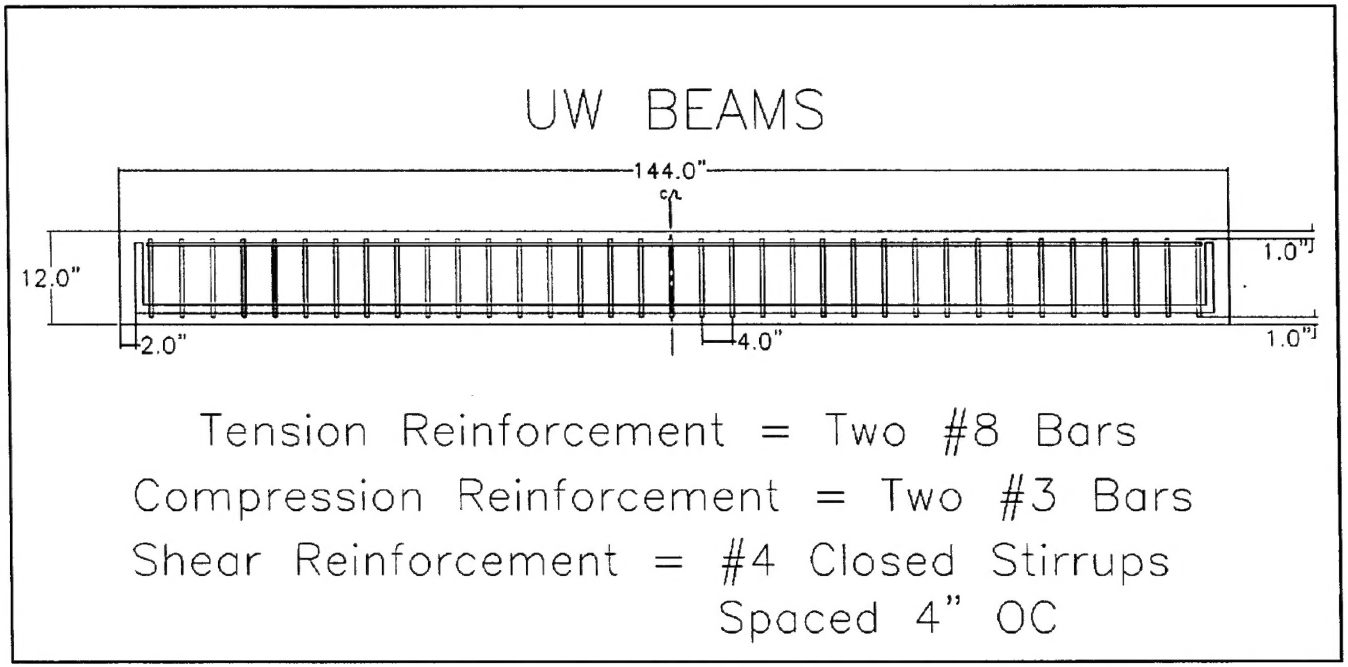

Figure B1. Construction drawing – large - scale beam - side view

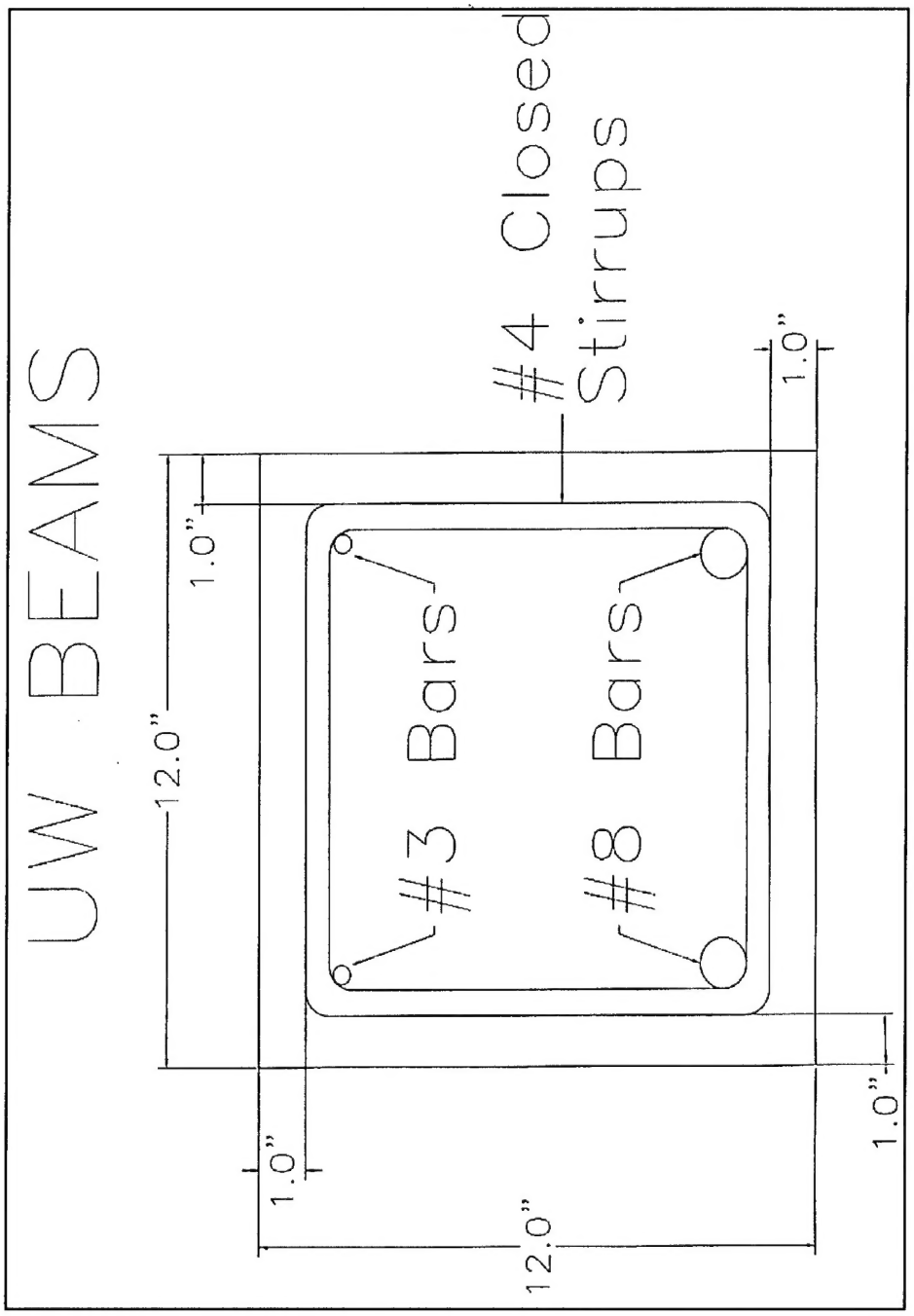

Figure B2. Construction drawings – large-scale beams

REPORT DOCUMENTATION PAGE

Form Approved
OMB No. 0704-0188

1. REPORT DATE *(DD-MM-YYYY)*	2. REPORT TYPE	3. DATES COVERED *(From - To)*
July 2002	Final report	

4. TITLE AND SUBTITLE

Rapid Strengthening of Full-Sized Concrete Beams with Powder-Actuated Fastening Systems and Fiber-Reinforced Polymer (FRP) Composite Materials

5a. CONTRACT NUMBER

5b. GRANT NUMBER

5c. PROGRAM ELEMENT NUMBER

6. AUTHOR(S)

Lawrence C. Bank, David T. Borowicz, Anthony J. Lamanna,
James C. Ray, Gerardo I. Velázquez

5d. PROJECT NUMBER

5e. TASK NUMBER

5f. WORK UNIT NUMBER

7. PERFORMING ORGANIZATION NAME(S) AND ADDRESS(ES)

Department of Civil and Environmental Engineering
University of Wisconsin-Madison
Madison, WI 53706;

U.S. Army Engineer Research and Development Center
Geotechnical and Structures Laboratory
3909 Halls Ferry Road
Vicksburg, MS 39180-6199

8. PERFORMING ORGANIZATION REPORT NUMBER

ERDC/GSL TR-02-12

9. SPONSORING / MONITORING AGENCY NAME(S) AND ADDRESS(ES)

U.S. Army Corps of Engineers
Washington, DC 20314-1000

10. SPONSOR/MONITOR'S ACRONYM(S)

11. SPONSOR/MONITOR'S REPORT NUMBER(S)

12. DISTRIBUTION / AVAILABILITY STATEMENT

Approved for public release; distribution is unlimited.

13. SUPPLEMENTARY NOTES

14. ABSTRACT

A research study was conducted to determine if the method of retrofitting reinforced concrete beams with powder-actuated fasteners and composite materials was applicable to full-scale flexural members. The work was conducted in the third year of an ongoing study. This report details the experimental and analytical work completed during the course of a 12-month investigation at the University of Wisconsin-Madison and a 1-month period of experimental testing at the United States Army Research and Development Center (ERDC), Vicksburg, Mississippi. The primary objective of the study was to determine the applicability of the strengthening method to full-scale concrete T-beams similar to those found on bridges within the continental United States. Secondary objectives include expanding the current analytical model, investigating the effects of span ratios, investigating the effects of termination lengths, and studying retrofitted beam behavior under fatigue loading. Nine full-scale T-beams were cast and tested at the ERDC. The results of these tests were analyzed and compared to the expanded analytical model. The test results compared favorably to the analytical predictions. Ten large-scale beams were cast and tested at the University of Wisconsin-Madison, Structures and Materials Testing Laboratory, to investigate the secondary objectives of the study. Overall, the research study showed that the strengthening method is applicable to full-scale T-beams; the strengthening effect is comparable to traditional bonded methods; termination length impacts the failure mode of the strengthened beam; the method can be applied to members with short shear spans; and cyclic loading does not degrade the strengthening system.

15. SUBJECT TERMS

Beam retrofit; Bridge retrofit; Fiber reinforced polymetric; FRP plates
Beam upgrade; Bridge upgrade; FRP; Mechanical fasteners

16. SECURITY CLASSIFICATION OF:			17. LIMITATION OF ABSTRACT	18. NUMBER OF PAGES	19a. NAME OF RESPONSIBLE PERSON James C. Ray
a. REPORT	b. ABSTRACT	c. THIS PAGE			19b. TELEPHONE NUMBER *(include area code)*
UNCLASSIFIED	UNCLASSIFIED	UNCLASSIFIED		110	(601) 634-3839